

ผลของพารามิเตอร์ในการสังเคราะห์และการเติมโลหะตัวที่สองต่อสมบัติทางกายภาพและทางเคมีของเส้นใย

ไททานเนียม (IV) ออกไซด์ขนาดนาโนจากการปั่นเส้นใยด้วยไฟฟ้าสถิต



นายจิรพงษ์ วัฒนารุณ

สถาบันวิทยบริการ

วิทยานิพนธ์นี้เป็นส่วนหนึ่งของการศึกษาตามหลักสูตรปริญญาวิศวกรรมศาสตรมหาบัณฑิต

สาขาวิชาวิศวกรรมเคมี ภาควิชาวิศวกรรมเคมี

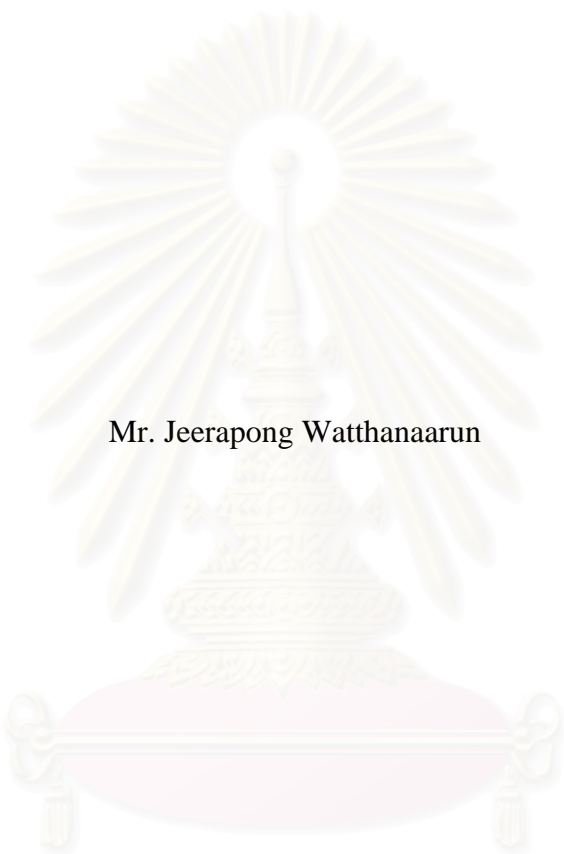
คณะวิศวกรรมศาสตร์ จุฬาลงกรณ์มหาวิทยาลัย

ปีการศึกษา 2547

ISBN 974-53-1662-8

ลิขสิทธิ์ของจุฬาลงกรณ์มหาวิทยาลัย

EFFECTS OF SYNTHESIS PARAMETERS AND SECONDARY METAL  
DOPING ON PHYSICAL AND CHEMICAL PROPERTIES OF THE  
ELECTROSPUN TITANIUM (IV) OXIDE NANOFIBERS



Mr. Jeerapong Watthanaarun

สถาบันวิทยบริการ  
จุฬาลงกรณ์มหาวิทยาลัย

A Thesis Submitted in Partial Fulfilment of the Requirements  
for the Degree of Master of Engineering in Chemical Engineering

Department of Chemical Engineering

Faculty of Engineering

Chulalongkorn University

Academic Year 2004

ISBN 974-53-1662-8

Thesis Title            EFFECTS OF SYNTHESIS PARAMETERS AND  
SECONDARY METAL DOPING ON PHYSICAL AND  
CHEMICAL PROPERTIES OF THE ELECTROSPUN  
TITANIUM (IV) OXIDE NANOFIBERS

By                         Mr. Jeerapong Watthanaarun

Field of study         Chemical Engineering

Thesis Advisor        Varong Pavarajarn, Ph.D

Thesis Co-advisor    Assistant Professor Pitt Supaphol, Ph.D

---

Accepted by the Faculty of Engineering, Chulalongkorn University in Partial  
Fulfillment of the Requirements for the Master's Degree

.....Dean of the Faculty of Engineering  
(Professor Direk Lavansiri, Ph.D)

#### THESIS COMMITTEE

.....Chairman  
(Associate Professor Suttichai Assabumrungrat, Ph.D )

.....Thesis Advisor  
(Varong Pavarajarn, Ph.D)

.....Thesis Co-advisor  
(Assistant Professor Pitt Supaphol, Ph.D)

.....Member  
(Associate Professor Siriporn Damrongsakkul, Ph.D)

.....Member  
(Akawat Sirisuk, Ph.D)

จิรพงษ์ วัฒนารุณ : ผลของพารามิเตอร์ในการสังเคราะห์และการเติมโลหะตัวที่สองต่อสมบัติทางกายภาพและทางเคมีของเส้นใยไททาเนียม (iv) ออกไซด์ขนาดนาโนจากการปั่นเส้นใยด้วยไฟฟ้าสถิต (EFFECTS OF SYNTHESIS PARAMETERS AND SECONDARY METAL DOPING ON PHYSICAL AND CHEMICAL PROPERTIES OF THE ELECTROSPUN TITANIUM (IV) OXIDE NANOFIBERS) อ. ที่ปรึกษา : ดร. วรงค์ ปวราจารย์, อ. ที่ปรึกษาร่วม : ผศ. ดร. พิชญ์ ศุภผล, 130 หน้า. ISBN 974-53-1662-8

เทคนิคโซล-เจลและการปั่นเส้นใยด้วยไฟฟ้าสถิตได้ถูกใช้ร่วมกันเพื่อผลิตเส้นใยคอมโพสิตขนาดนาโนของไททาเนียม (iv) ออกไซด์กับพอลิไวนิลไพโรลิโดนจากสารละลายที่ประกอบด้วยพอลิไวนิลไพโรลิโดนและไททาเนียมเตตระไฮดรอกไซด์ เส้นผ่านศูนย์กลางเฉลี่ยของเส้นใยคอมโพสิตที่ได้อยู่ในช่วง 145 ถึง 350 นาโนเมตร เมื่อเพิ่มความเข้มข้นของพอลิไวนิลไพโรลิโดน เส้นผ่านศูนย์กลางของเส้นใยเพิ่มขึ้น โดยมีการกระจายตัวของขนาดที่กว้างมากขึ้น การเพิ่มความเข้มข้นไฟฟ้าส่งผลให้เส้นผ่านศูนย์กลางของเส้นใยลดลงแต่มีการกระจายตัวของขนาดที่แคบลง การเผาเส้นใยคอมโพสิตเหล่านี้ในอากาศที่อุณหภูมิ 500 องศาเซลเซียสส่งผลให้ได้เส้นใยอนาเทสไททาเนียมขนาดนาโนที่มีรูโกล์ปะปนอยู่ในปริมาณเล็กน้อย ความเป็นผลึกและปริมาณรูโกล์ของเส้นใยไททาเนียมเพิ่มขึ้น ในขณะที่เส้นผ่านศูนย์กลางลดลงเมื่ออุณหภูมิการเผาในอากาศสูงขึ้น การเติมซิลิกอนลงไปบนเส้นใยไททาเนียมทำให้ขนาดเส้นผ่านศูนย์กลางของเส้นใยลดลง ในขณะที่ความเป็นผลึก พื้นที่ผิว และความร้อนของเส้นใยเพิ่มขึ้น ในท้ายที่สุดการเติมซิลิกอนเข้าไปบนเส้นใยไททาเนียมส่งผลให้ได้ความว่องไวของการเร่งปฏิกิริยาดูด้วยแสงในการสลายตัวของเมทิลีนบลูที่มีค่าสูงขึ้น

|                                |                                     |
|--------------------------------|-------------------------------------|
| ภาควิชา.....วิศวกรรมเคมี.....  | ลายมือชื่อนิสิต.....                |
| สาขาวิชา.....วิศวกรรมเคมี..... | ลายมือชื่ออาจารย์ที่ปรึกษา.....     |
| ปีการศึกษา.....2547.....       | ลายมือชื่ออาจารย์ที่ปรึกษาร่วม..... |

# # 4670266821 : MAJOR CHEMICAL ENGINEERING

KEY WORD: TITANIA / ELECTROSPINNING / NANOFIBERS / DOPING

JEERAPONG WATTHANAARUN : EFFECTS OF SYNTHESIS PARAMETERS AND SECONDARY METAL DOPING ON PHYSICAL AND CHEMICAL PROPERTIES OF THE ELECTROSPUN TITANIUM (IV) OXIDE NANOFIBERS.

THESIS ADVISOR : VARONG PAVARAJARN, Ph.D, THESIS CO-ADVISOR : ASSISTANT PROFESSOR PITT SUPAPHOL, Ph.D , 130 pp. ISBN 974-53-1662-8

Sol-gel and electrospinning techniques are incorporated to produce titanium (IV) oxide/polyvinylpyrrolidone (PVP) composite nanofibers from solution containing PVP and titanium tetraisopropoxide. The average diameters of the obtained composite fibers are in the range of 145 to 350 nm. When concentration is increased, fiber diameter increases with broader size distribution. Increasing electric field strength results in a decrease in fiber diameter but more narrow size distribution. Calcination of the composite fibers at 500°C results in anatase titania nanofibers with a trace amount of rutile. The crystallinity and rutile content of all titania fibers are increased, while the average fiber diameter is decreased, with an increase in the calcination temperature. Silicon doping in titania fibers reduces the fiber diameter, while increases crystallinity, surface area, and thermal stability of fibers. Finally, the addition of silicon results in enhanced photocatalytic activity of methylene blue decomposition.

สถาบันวิทยบริการ  
จุฬาลงกรณ์มหาวิทยาลัย

|   |                             |
|---|-----------------------------|
| Department.....Chemical Engineering.....  | Student's signature.....    |
| Field of study...Chemical Engineering.... | Advisor's signature.....    |
| Academic year.....2004.....               | Co-advisor's signature..... |

## ACKNOWLEDGEMENTS

The author would like to express his greatest gratitude to his advisor, Dr. Varong Pavarajarn, and his co-advisor, Assistant Professor Dr. Pitt Supaphol for their invaluable guidance throughout this study. In addition, I would also grateful to thank to Associate Professor Dr. Suttichai Assabumrungrat, as the chairman, Associate Professor Dr. Siriporn Damrongsakkul and Dr. Akawat Sirisuk, members of the thesis committee for their kind cooperation.

Many thanks for kind suggestions and useful help to many friends in the Research Center on Catalysis and Catalytic Reaction Engineering who always provide the encouragement and co-operate along the thesis study.

The author wish to acknowledge partial supports recieved from the Graduate School, Chulalongkorn University and the Nation Research Council of Thailand.

Finally, I would like to express my deep thanks to my parents for their financially support and encouragement, and to my girlfriend, Rawipa, for her encouragement and love.

สถาบันวิทยบริการ  
จุฬาลงกรณ์มหาวิทยาลัย

# CONTENTS

| Subject  | Page |
|--|------|
| ABSTRACT (THAI).....   | iv   |
| ABSTRACT (ENGLISH).....  | v    |
| ACKNOWLEDGEMENTS.....  | vi   |
| CONTENTS.....  | vii  |
| LIST OF TABLES.....  | ix   |
| LIST OF FIGURES.....   | x    |
| CHAPTER  |      |
| I INTRODUCTION.....  | 1    |
| II THEORY AND LITERATURE SURVEY.....                                 | 6    |
| 2.1 Physical and Chemical Properties of Titanium (IV) Oxide.....     | 6    |
| 2.2 Sol-Gel Process.....   | 8    |
| 2.3 Electrospinning Process.....                                     | 12   |
| 2.3.1 Background.....  | 12   |
| 2.3.2 Mechanism of Electrospinning Process.....                      | 17   |
| 2.3.2.1 Jet initiation and diameter of a single jet.....             | 18   |
| 2.3.2.2 Bending instability and elongation of the jet.....           | 20   |
| 2.3.3 Applications of Electrospinning.....                           | 25   |
| 2.4 Photocatalytic Process.....                                      | 26   |
| III EXPERIMENTAL.....  | 31   |
| 3.1 Materials.....   | 31   |
| 3.2 Electrospinning Apparatus.....                                   | 31   |
| 3.3 Procedures.....  | 33   |
| 3.3.1 Spinning Solution Preparation.....                             | 33   |
| 3.3.2 Spinning of the TiO <sub>2</sub> /PVP Composite Fibers.....    | 33   |
| 3.3.3 Calcination of the TiO <sub>2</sub> /PVP Composite Fibers..... | 34   |
| 3.3.4 Photocatalytic Activity Evaluation.....                        | 34   |
| 3.4 Samples Characterizations.....                                   | 34   |
| 3.4.1 Scanning Electron Microscopy (SEM).....                        | 34   |
| 3.4.2 X-ray Diffractometry (XRD).....                                | 35   |

| <b>Subject</b>   | <b>Page</b> |
|--|-------------|
| 3.4.3 Fourier Transform Infrared Spectroscopy (FTIR).....          | 35          |
| 3.4.4 Thermogravimetric and Differential Thermal Analysis (TG-DTA) | 35          |
| 3.4.5 Surface Area Measurement.....                                | 35          |
| 3.4.6 UV-Vis Spectrophotometry.....                                | 36          |
| <b>IV RESULTS AND DISCUSSION.....</b>                              | <b>37</b>   |
| 4.1 Effects of Electrospinning Conditions on As-spun Fibers.....   | 37          |
| 4.1.1 Effects of PVP Concentration.....                            | 37          |
| 4.1.2 Effect of Applied Electric Field Strength.....               | 40          |
| 4.2 Properties of Titania Nanofibers.....                          | 47          |
| 4.2.1 Thermal Analysis.....  | 47          |
| 4.2.2 Morphology of Titania Fibers.....                            | 48          |
| 4.2.3 X-ray Diffraction Analysis.....                              | 52          |
| 4.2.4 FT-IR Analysis.....  | 52          |
| 4.3 Effect of Silicon as Secondary Metal Dopant.....               | 55          |
| 4.3.1 Properties of Silicon-Doped Titania Fibers.....              | 55          |
| 4.3.2 Morphology of Silicon-Doped Titania Fibers.....              | 60          |
| 4.3.3 Thermal Stability of Silicon-Doped Titania Fibers.....       | 67          |
| 4.3.4 Photocatalytic Activity.....                                 | 73          |
| <b>V CONCLUSIONS AND RECOMMENDATIONS.....</b>                      | <b>81</b>   |
| 5.1 Conclusions.....   | 81          |
| 5.2 Recommendations.....   | 81          |
| <b>REFERENCES.....</b>   | <b>83</b>   |
| <b>APPENDICES.....</b>   | <b>92</b>   |
| <b>APPENDIX A LIST OF PUBLICATIONS.....</b>                        | <b>93</b>   |
| <b>VITA.....</b>   | <b>130</b>  |

## LIST OF TABLES

| Table  | Page |
|--|------|
| 2.1 Crystallographic properties of anatase, brookite, and rutile.....  | 7    |
| 4.1 BET surface area of undoped and silicon-doped titania nanofibers<br>at different calcination temperature.....        | 68   |
| 4.2 Percent of rutile phase of undoped and silicon-doped titania nanofibers<br>at different calcination temperature..... | 68   |



สถาบันวิทยบริการ  
จุฬาลงกรณ์มหาวิทยาลัย

## LIST OF FIGURES

| Figure | Page  |
|--------|---|
| 2.1    | Schematic representation of the electrospinning process..... 17   |
| 2.2    | Photographs of the pendent droplet and jet, near the time the jet was ejected.. 18  |
| 2.3    | (a) Magnified image of the shape of the jet near the spoon.<br>(b) Schematic drawing of a jet flowing from a hole in the bowl<br>of a spoon. The jet is separated from the spoon for clarity..... 19  |
| 2.4    | The development of the second cycle of bending instability.<br>The time interval between these two images was 15 ms.<br>The camera shutter speed was 0.25 ms..... 21  |
| 2.5    | Images of electrospinning jet with different exposure times.<br>(a), (b), and (c), shutter speed was 1.0 ms. The spots in (d)<br>are artifacts produced by a faceted reflector used in the illuminating system.. 24   |
| 2.6    | Primary steps in the photoelectrochemical mechanism..... 28   |
| 3.1    | Experimental set up for electrospinning process..... 32   |
| 4.1    | SEM images of pre-calcined as-spun fibers from spinning solutions<br>containing (a) 7, (b) 9, (c) 13, and (d) 15 wt.% PVP solution.<br>The applied electric field strength was 9 kV/7cm..... 38   |
| 4.2    | Frequency distribution of fiber diameters of<br>pre-calcined as-spun fibers from spinning solution containing<br>7, (b) 10, (c) 13, and (d) 15 wt.% PVP..... 39   |
| 4.3    | Diameters of pre-calcined as-spun fibers as a function of PVP concentration.. 40  |
| 4.4    | SEM images of pre-calcined as-spun fibers from spinning solution<br>containing 13 wt.% PVP solution under different applied electric field<br>strengths: (a) 9, (b) 11.25, (c) 15, (d) 18.75, and (e) 22.5 kV. The distance<br>between the injection orifice and the collector was kept at 7 cm..... 41 |
| 4.5    | Frequency distribution of fiber diameters of pre-calcined<br>as-spun fibers using applied electric potential of: (a) 9,<br>(a) 11.25, (c) 15, (d) 18.75, and (e) 22.5 kV/7 cm..... 42   |

## Figure

|             |   |    |
|-------------|---|----|
| <b>4.6</b>  | SEM images of pre-calcined as-spun fibers<br>across the collection distance of (a) 7, (b) 10, and (c) 13 cm.<br>The PVP concentration of the spinning solution was 13wt.%<br>and the applied electric potential was 15 kV.....  | 44 |
| <b>4.7</b>  | Frequency distribution of fiber diameters of pre-calcined as-spun fibers<br>using the collection distance of: (a) 7, (b) 10, and (c) 13 cm.....   | 45 |
| <b>4.8</b>  | Diameters of pre-calcined as-spun fibers as a function of<br>(a) applied electric potential (across a fixed collection distance of<br>7 cm) and (b) collection distance.....  | 46 |
| <b>4.9</b>  | TGA-DTA thermodiagram for the undoped TiO <sub>2</sub> nanofibers.....  | 47 |
| <b>4.10</b> | SEM images of fibers calcined at different temperature:<br>(a) as-spun fibers, (b) calcined at 500°C, (c) calcined at 600°C, and<br>(d) calcined at 800°C. The PVP concentration of the spinning solution<br>was 13 wt.% and the applied electric field strength was 15 kV/7 cm.....                          | 49 |
| <b>4.11</b> | Frequency distribution of fiber diameters of titania fibers calcined<br>at different temperatures : (a) pre-calcined as-spun fibers, (b) 500°C,<br>(c) 600°C, and (d) 800°C.....  | 50 |
| <b>4.12</b> | Diameters of calcined titania fibers as a function of calcination temperature..   | 51 |
| <b>4.13</b> | EDX spectrum and elemental analysis result of titania fiber.....  | 51 |
| <b>4.14</b> | XRD patterns of pre-calcined as-spun fibers (a) and titania fibers<br>calcined at temperature of: (b) 500, (c) 600, and (d) 800 °C,<br>comparing with the reference titania (e). The PVP concentration<br>of the spinning solution was 13 wt.% and the applied electric field<br>strength was 15 kV/7 cm..... | 53 |
| <b>4.15</b> | FT-IR spectra of pre-calcined as-spun fibers (a) and titania fibers<br>calcined at temperature of: (b) 500, (c) 600, and (d) 800°C,<br>comparing with the reference titania (e).....  | 54 |
| <b>4.16</b> | DTA thermodiagram for TiO <sub>2</sub> nanofibers: (a) undoped, (b) doped<br>with 1 wt.% TEOS, and (c) doped with 2 wt.% TEOS.....  | 56 |
| <b>4.17</b> | FT-IR spectra of titania fibers calcined at 500°C with different silicon<br>content: (a) undoped, (b) 1 wt.% TEOS, and (c) 2 wt.% TEOS.....   | 57 |

|             |  |    |
|-------------|--|----|
| <b>4.18</b> | FT-IR spectra of titania fibers calcined at 600°C with different silicon content: (a) undoped, (b) 1 wt.% TEOS, and (c) 2 wt.% TEOS.....                                   | 58 |
| <b>4.19</b> | FT-IR spectra of titania fibers calcined at 800°C with different silicon content: (a) undoped, (b) 1 wt.% TEOS, and (c) 2 wt.% TEOS.....                                   | 59 |
| <b>4.20</b> | SEM images and frequency distribution of fiber diameters of pre-calcined as spun fibers: (a) undoped, (b) doped with 1 wt.% TEOS, and (c) doped with 2 wt.% TEOS.....      | 61 |
| <b>4.21</b> | SEM images and frequency distribution of fiber diameters of titania fibers calcined at 500°C: (a) undoped, (b) doped with 1 wt.% TEOS, and (c) doped with 2 wt.% TEOS..... | 62 |
| <b>4.22</b> | SEM images and frequency distribution of fiber diameters of titania fibers calcined at 600°C: (a) undoped, (b) doped with 1 wt.% TEOS, and (c) doped with 2 wt.% TEOS..... | 63 |
| <b>4.23</b> | SEM images and frequency distribution of fiber diameters of titania fibers calcined at 800°C: (a) undoped, (b) doped with 1 wt.% TEOS, and (c) doped with 2 wt.% TEOS..... | 64 |
| <b>4.24</b> | Average diameters of as-spun and calcined titania fibers doping with various amount of silicon.....  | 65 |
| <b>4.25</b> | EDX spectrum and elemental analysis results of titania fibers doped with: (a) 1 wt.% TEOS and (b) 2 wt.% TEOS.....   | 66 |
| <b>4.26</b> | TEM images of titania fibers calcined at 500°C: (a) undoped and (b) doped with 2 wt.% TEOS.....  | 69 |
| <b>4.27</b> | SAED images of titania fibers calcined at 500°C: (a) undoped and (b) doped with 2 wt.% TEOS.....   | 69 |
| <b>4.28</b> | XRD patterns of titania fibers calcined at 500°C with different silicon content: (a) undoped, (b) 1 wt.% TEOS, and (c) 2 wt.% TEOS.....                                    | 70 |
| <b>4.29</b> | XRD patterns of titania fibers calcined at 600°C with different silicon content: (a) undoped, (b) 1 wt.% TEOS, and (c) 2 wt.% TEOS.....                                    | 71 |
| <b>4.30</b> | XRD patterns of titania fibers calcined at 800°C with different silicon content: (a) undoped, (b) 1 wt.% TEOS, and (c) 2 wt.% TEOS.....                                    | 72 |

**Figure****Page**

|  |    |
|--|----|
| <b>4.31</b> Degradation of methylene blue solution on titania fibers photocatalysts<br>(in flake form) calcined at 500°C with different silicon content<br>under UV irradiation.....                         | 74 |
| <b>4.32</b> Degradation of methylene blue solution on titania fibers photocatalysts<br>(in flake form) calcined at 600°C with different silicon content<br>under UV irradiation.....                         | 75 |
| <b>4.33</b> Degradation of methylene blue solution on titania fibers photocatalysts<br>(in flake form) calcined at 800°C with different silicon content<br>under UV irradiation.....                         | 76 |
| <b>4.34</b> Degradation of methylene blue solution on titania fibers photocatalysts<br>(packed with 3x3 stainless steel mesh) calcined at 500°C with different<br>silicon content under UV irradiation.....  | 77 |
| <b>4.35</b> Degradation of methylene blue solution on titania fibers photocatalysts<br>(packed with 3x3 stainless steel mesh) calcined at 500°C with different<br>silicon content under solar radiation..... | 79 |
| <b>4.36</b> Degradation of methylene blue solution on titania fibers photocatalysts<br>(in flake form) calcined at 500°C with different silicon content<br>under solar radiation.....                        | 80 |

# CHAPTER I

## INTRODUCTION

Titanium (IV) oxide or titania ( $\text{TiO}_2$ ) is one of the most common materials that suits many applications. It has been known to be an excellent catalyst in the field of photocatalysis. Titania is a wide bandgap semiconductor with many interesting properties, such as transparency to visible light, high refractive index and low absorption coefficient. Other than these properties, its eminent capability of photocatalytic decomposition of organic materials has come to utilization in the environmental applications, i.e. organic pollutant treatment (Kwon et al. 2004). Generally, large surface area is required for catalyst. Since the catalyst is usually used at high temperature, high thermal stability, as well as large surface area, is also important. Titania is also commercially very important as a white pigment because of its maximum light scattering with virtually no absorption. It is also nontoxic, chemically inert, and considered as dielectric ceramic material due to its high dielectric constant. Recently, it has been suggested that monodispersed oxide powders are preferable to ceramic raw materials (Kominami et al. 1999).

Titania is known to have several natural polymorphs, i.e. rutile, anatase and brookite. Rutile is thermodynamically stable, especially at high temperature, while anatase is metastable at high temperature (both belong to the tetragonal crystal system). Brookite, which has a structure belong to the orthorhombic crystal system is formed only under hydrothermal conditions or usually found only in minerals (Keesmann 1966). Anatase titania has been used as catalyst for photodecomposition and solar energy conversion, because of its high photoactivity (Kamat and Dimitrijevic 1990; Fox and Dulay 1993; Larson and Falconer 1994; Herrmann et al. 1997; Fujishima et al. 1999a). On the other hand, rutile titania has been used as white pigment materials, because of its good scattering effect, which protects materials from ultraviolet light. Anatase titania has been reported to be unstable at high temperature. However its transformation temperature has been reported in a wide range (Zzanderna et al. 1958; Yogarasimhan and Rao 1962), depending upon its the grain size,

impurities, composition, nature of the dopant, amount of dopant, and processing technique (Fujishima et al. 1999a; Hirano et al. 2002).

Nanocrystalline and nanocomposite materials, characterized by an ultra fine grain size (<50 nm), are subject of current interest because of their unusual magnetic, optical and electronic properties. It has been reported that nanometer-sized particles have different physical and chemical properties from bulk materials. Their catalytic activity is expected to be enhanced not only because of their increased surface area, but also because of the change of surface properties such as surface defect (Popielaski 1998; Payakgul 2002).

The particle size of nanocrystalline titanium (IV) oxide plays an important role in the physical and chemical behavior because the specific surface area, the chemical stability, and the chemical reactivity of the materials are all highly correlated with particle size. It has been shown that the adsorption of organic compounds to the surface of nanocrystalline anatase is particle-size-dependent. Therefore, the particle size is one of the crucial factors in photocatalytic decomposition activity (Zhang et al. 2001).

Titania can be synthesized by various techniques, such as precipitation (Kim et al. 1999), chemical vapor deposition (Ding et al. 2000), hydrothermal method (Yang et al. 2001), and glycothermal method (Iwamoto et al. 2000). Another common technique that can result in titania with extremely high surface area is sol-gel method (Dagan and Tomkiewicz 1994; Zaharescu et al. 1997; Jung and Park. 1999; Jung and Park 2000; Cheng et al. 2003). The method basically consists of many steps, i.e. hydrolysis of alkoxide to form sol, gelation, gel-aging, drying and thermal stabilization. Each step can be manipulated to obtain product with specific characteristic, such as narrow pore size distribution and narrow particle size distribution (Montoya et al. 1992). However, titania obtained usually contains certain amount of amorphous phase, in which their surface area decrease drastically during calcination (Fujishima et al. 1999a; Payakgul 2002).

Anatase is an unstable polymorph of titania. Phase transformation from anatase to rutile, the less chemically active polymorph, takes place at temperatures as

low as 300°C. However, the transformation temperature strongly depends upon how titania is synthesized (Jung and Park. 1999). Anatase titania that transforms to rutile at high temperature is considered having good thermal stability. In catalytic application, large surface area and reasonably good thermal stability is often desired. Therefore, many studies have been devoted to improve the thermal stability of titania using additives such as silicon (Iwamoto et al. 2000) and aluminum (Lee et al. 2004). Furthermore, it has been also reported that the addition of the secondary metal dopant can enhance the photocatalytic activity of the resulting titania. Anatase/silica composite nanoparticles exhibit much better photocatalytic activity than that of the pure anatase (Yoshinaka et al. 1997; Viswanath and Ramasamy 1998; Jung and Park. 1999; Iwamoto et al. 2000; Jung and Park 2000; Soult et al. 2002; Cheng et al. 2003; Hong et al. 2003; Oh et al. 2003; Hirano and Ota 2004).

In this research, the sol-gel method is combined with electrospinning technique to produce titania nanofibers. Electrospinning technique is a relatively simple and versatile method for fabricating nanofibers. In typical electrospinning process, a droplet of the polymer solution held by its surface tension at the end of a capillary tube is subjected to an electric field. Charge is induced on the liquid surface by electric field. As the intensity of the electric field is increased, the hemispherical surface of the solution at the tip of the capillary tube elongates to form a conical shape known as the Taylor cone. When the electric field reaches a critical value at which the repulsive electric force overcomes the surface tension force, a charged jet of the solution is ejected from the tip of the Taylor cone. Since this jet is charged, its trajectory can be controlled by the electric field. As the jet travels in air, the solvent evaporates, leaving a charged polymer fiber behind which lays itself randomly on a collecting metal screen. Thus, continuous fibers are laid to form a non-woven fabric (Jayesh and Reneker 1995). In the continuous-feeding mode, the number of fibers can be formed within short period of time, as short as a few seconds. Those fibers are often collected on the surface of a conductor to form non-woven mats that have high surface areas and relatively small pore sizes.

In the past several decades, more than 20 different types of organic polymers have been successfully processed as ultrathin fibers using the electrospinning

technique, with typical examples including various engineering plastics, biopolymer, and electronically conductive polymer (Jayesh and Reneker 1995; Li and Xia 2003). Amorphous titania nanofibers have also been preliminarily produced by electrospinning technique from titanium isopropoxide mixed with acetic acid and high molecular weight polyvinylpyrrolidone (Li and Xia 2003). Although nanocrystalline titanium (IV) dioxide particles have shown many beneficial features, handling of such small particles in some applications such as in photocatalytic applications, is difficult. Fibers consisting of nanocrystalline titania can be advantageous. However, nanocrystalline titania undergoes phase transformation and grain growth at relatively low temperature, which limits its application at high temperature. In order to improve the thermal and physical properties of titania fibers, the doping of titania fibers with secondary metal is studied. This research intends to investigate the production of titania nanofibers in more detail as well as their properties and applications.

Objectives of the research :

1. Study the effects of solution, spinning conditions, and calcination conditions on morphological appearance, crystal structure as well as physical and chemical properties of the resulting titania fibers.
2. Study the effects of the secondary metals doping on the thermal stability of the resulting titania fibers.
3. Study the activity of the resulting titania fibers by using photocatalytic decomposition of methylene blue.

The present study is arranged as follows:

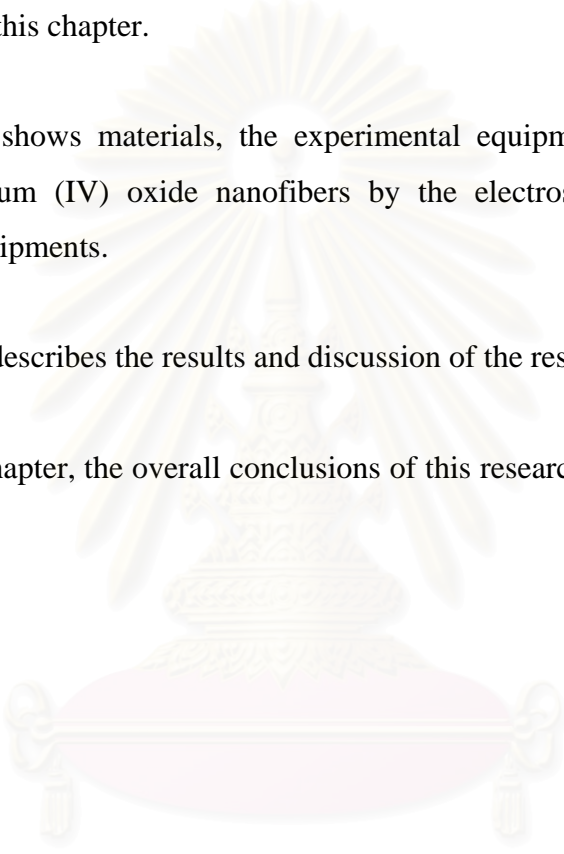
Chapter I is the introduction of this work.

Chapter II describes the basic theory about titania such as the general properties of titania, sol-gel process, electrospinning process and photocatalytic process. Furthermore, literature survey of the previous works related to this research is also presented in this chapter.

Chapter III shows materials, the experimental equipments, the preparation procedure of titanium (IV) oxide nanofibers by the electrospinning process and characterization equipments.

Chapter IV describes the results and discussion of the research.

In the last chapter, the overall conclusions of this research and future work are given.



สถาบันวิทยบริการ  
จุฬาลงกรณ์มหาวิทยาลัย

## CHAPTER II

### THEORY AND LITERATURE SURVEY

It has been recognized that titanium (Ti) can form a large number of compounds by coordination with other substances such as hydrogen, nitrogen, boron, carbon, and oxygen. Titania is the most important form of titanium compound commercially available. Physical and chemical properties of titania as well as its various preparation procedures have been long studied.

#### 2.1 Physical and Chemical Properties of Titanium (IV) Oxide

Titanium (IV) oxide occurs naturally in three crystalline forms: anatase which tends to be more stable at low temperature, brookite which is usually found only in minerals, and rutile which is thermally stable form of titania and thus is sometimes found in igneous rocks. The three forms of titanium (IV) oxide have been successfully prepared artificially. However, only rutile has been obtained in the form of transparent large single crystal. A summary of the crystallographic properties of all forms are given in Table 2.1.

The important commercial forms of titanium (IV) oxide are anatase and rutile. Both of them are tetragonal. Anatase occurs usually in near-regular octahedral, while rutile forms slender prismatic crystals, which are frequently twinned. Therefore, they are both anisotropic. Their physical properties, e.g. refractive index, vary according to the direction relative to the crystal axes. However, in most applications, the distinction between crystallographic direction is lost because of the random orientation in large number of small particles.

Phase transformation from anatase to rutile is accompanied by the evolution of ca. 12.6 kJ/mol (3.01 kcal/mol). Nevertheless, the rate of transformation is greatly affected by temperature and the presence of other substances which may either

catalyze or inhibit the transformation. The anatase-to-rutile transformation is not reversible since Gibb's free energy for the change is always negative (Othmer 1999).

Table 2.1 Crystallographic properties of anatase, brookite, and rutile(Othmer 1999).

|                               | Anatase  | Brookite   | Rutile   |
|-------------------------------|--|--|--|
| Crystal structure             | Tetragonal                                       | Orthorombic                                      | Tetragonal                                       |
| Density, [g/cm <sup>3</sup> ] | 3.9  | 4.0  | 4.23   |
| Hardness, [Mohs scale]        | 5.5 - 6  | 5.5 - 6  | 7 - 7.5  |
| Unit cell                     | D <sub>4h</sub> <sup>19</sup> .4TiO <sub>2</sub> | D <sub>2h</sub> <sup>15</sup> .8TiO <sub>2</sub> | D <sub>4h</sub> <sup>12</sup> .3TiO <sub>2</sub> |
| Lattice parameters, [nm]      |  |  |  |
| <i>a</i>                      | 0.3758   | 0.9166   | 0.4584   |
| <i>b</i>                      |  | 0.5436   |  |
| <i>c</i>                      | 0.9514   | 0.5135   | 2.953  |

Titanium (IV) oxide is thermally stable (melting point of 1855°C) and has high resistance to chemical attack. When it is severely heated under vacuum, there is a chance of slight loss in oxygen atom that results in a change in composition to TiO<sub>1.97</sub>. The product is dark blue but can be reverted to the original white color when it is heated in air (Fujishima et al. 1999a; Payakgul 2002).

In 2000, Iwamoto and coworkers (2000) synthesized silica-modified titania with various silica contents by the reaction of titanium tetraisopropoxide (TTIP) and tetraethyl orthosilicate (TEOS) in 1,4-butanediol. The products possessed significantly large surface area with small crystallite size, and exhibited remarkable thermal stability. They described that the presence of Si in the titania lattice contributed to the deceleration of the grain growth of anatase and the suppression of anatase-rutile transformation (Iwamoto et al. 2000). Jung and Park (1999) prepared silica-embedded titania particles by sol-gel process. They observed that the added silicon formed segregated amorphous silica and embedded into anatase titania matrix. Surface area and defects were increased with increasing the silica content. The increase of thermal stability, which was successfully accomplished by embedding amorphous silica into titania matrix, resulted in suppressing the phase transformation from anatase to rutile (Jung and Park. 1999; Jung and Park 2000).

In 2003, Hong and coworkers (2003) prepared nanosized  $\text{TiO}_2/\text{SiO}_2$  particles in the microemulsion. They observed that the titania/silica mixture had high thermal stability, which resulted in the suppression of phase transformation from anatase to rutile. In addition, this high thermal stability made it possible to calcine the  $\text{TiO}_2/\text{SiO}_2$  particles at higher temperature without forming the rutile phase to prepare high crystalline particles by reducing the bulk defect (Hong et al. 2003).

## 2.2 Sol-Gel Process

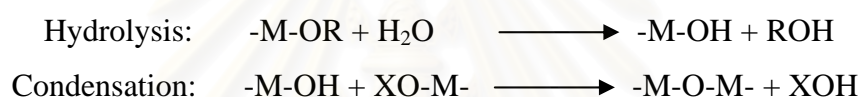
The sol-gel process involves the formation of sol followed by gelation. Sol, which is suspension of solid particles with size ranging from 1 nm to 1 micron in liquid, can be obtained by hydrolysis and partial condensation of a precursor such as inorganic salt or metal alkoxide. Further condensation of sol particles into a three-dimensional network produces gel, which is a diphasic material with a solids encapsulating solvent. Alternatively, gel can be produced by destabilizing the solution of preformed sols. In either case, the materials are referred as aquasol (or aquagel) if water is used as a solvent, and alcosol (or alcogel) if alcohol is used. The encapsulated liquid can be removed from gel by either evaporative drying or drying with supercritical extraction (supercritical drying in short).

The single most important characteristic of the sol-gel preparation of catalytic materials is its ease of control that translates into the following advantages:

- (i) the ability to maintain high purity (because of purity of starting materials);
- (ii) the ability to change physical characteristics such as pore size distribution and pore volume;
- (iii) the ability to vary compositional homogeneity at a molecular level;
- (iv) the ability to prepare samples at low temperatures;
- (v) the ability to introduce several components in a single step;
- (vi) the ability to produce samples in different physical forms.

The four key steps to convert a precursor to a particular product via sol-gel preparation are; formation of gel, aging of gel, removal of solvent, and heat treatment. The versatility of this preparative approach lies in the number of parameters that can be manipulated in each of these steps.

The precursor in sol-gel preparation can either be a metal salt/alkoxide dissolved in an appropriate solvent or a stable colloidal suspension of preformed sols. Metal alkoxides have been most extensively used because they are commercially available in high purity and their solution chemistry has been well documented. At its simplest level, sol-gel chemistry with metal alkoxides can be described in terms of two classes of reactions:



where X can be either H or R (an alkyl group).

Such description oversimplifies the overall process because it does not correctly represent the molecular formula of intermediates as well as end products, nor does it depict the simultaneous occurrence of the two reactions. However, this oversimplification captures the key phenomenological idea that a three-dimensional gel network comes from the condensation of partially hydrolyzed species. Any parameters affecting either or both of these reactions are thus likely to impact on the properties of the product. In fact, the important variables are the reactive rates of hydrolysis and condensation, which have been pointed out.

Because hydrolysis and condensation are both nucleophilic displacement reactions, the reactivity of metal alkoxides depends on the positive partial charge of the metal atom and its coordination number. For example, TEOS, which has small positive partial charge on silicon, is the least reactive among the common alkoxides. In general, the longer and bulkier the alkoxide group attached to a particular metal atom, the less reactive that precursor is in hydrolysis and condensation. Changing the

type of precursor and/or its concentration are thus effective means to control the reaction rates.

The amount of water used in sol-gel preparation and the rate by which it is added into the system also influence gel characteristics. The former is usually expressed in terms of the hydrolysis ratio  $h$ , defined as the moles of water per mole of metal alkoxide,  $M(OR)_m$ . There are three specific regions of interest:

- (i)  $h < 1$ : An infinite network seldom forms due to low functionality of the precursor towards condensation. Because there are few M-OH groups for cross-linking, gelation or precipitation can not occur when there is no local excess of water.
- (ii)  $1 < h < m$ : Polymeric gels can form.
- (iii)  $h < m$ : Cross-linked polymers, particulate gels, or precipitates can form when an excess of water is added to the alkoxides.

For given amount of water, another level of control comes from the rate of addition. Common approaches to slowly add water into the system are: using a micropipette, absorbing moisture from a controlled humidity environment, and generating water in the solution with another chemical reaction.

Two other important sol-gel parameters are temperature and solvent. Both hot and cold plates are commercially available, which can be used to increase and decrease the reaction rate, respectively. Varying the temperature is most effective when it can alter the relative rate of competing reactions. Solvent can change the nature of an alkoxide precursor through solvent exchange or affect the condensation reaction directly. It is also possible to prepare gel without solvent as long as another mean, such as ultrasound irradiation, is used to homogenize an otherwise immiscible alkoxide/water mixture.

Using preformed sols instead of metal alkoxides as precursors is an attractive alternative in sol-gel preparation because recent advances in inorganic colloidal dispersions allow some control over the characteristic of the starting sols. Colloidal

suspension of sol particles is often stabilized (i.e. prevented from flocculation) by pH adjustment. Thus, pH of the solution, which can be changed by the addition of either acid or base, is the single most important parameter in obtaining gel from preformed sols. Other parameters that influence gel quality are size and concentration of the starting sol particles.

For any of the sol-gel parameters discussed so far, its effect on gel properties can often be observed by an experimental parameter known as gel time. Gel time is defined as the time that the solution undergoes rapid rise in viscosity which is corresponding to the transition from viscous fluid to elastic gel. At the gel point, the solid phase forms a continuous structure that reflects the formation and branching of particles under specific growth condition. This particular phase is important because it is the genesis of structural evolution that takes place in all subsequent processing steps (Ertl et al. 1999).

In 1998, Viswanath and Ramasamy (1998) prepared titania-silica nanocomposite system with well-dispersed  $\text{TiO}_2$  particles in the glassy matrix by the sol-gel method. The Si-O-Ti bonded glassy matrix acts as an anti-sintering agent which controls the growth of the  $\text{TiO}_2$  particles. Also, this glassy medium stabilizes the anatase phase at high temperature (Viswanath and Ramasamy 1998). In 2004, Kwon and coworkers (2004) have fabricated titania nano-crystal thin films on glass, polycarbonate, polymethyl methacrylate, and aluminum via sol-gel process using different alkoxide precursors. Unlike the conventional sol-gel process, no heat treatment was required to obtain nano-sized crystals of  $\text{TiO}_2$ . All the specimens possessed nano-sized (<10 nm) crystals of anatase phase with very tiny brookite phase. As the thickness of the film increased, the effect of the substrate diminished in terms of photocatalytic decomposition of methyleneblue solution. Appropriate heat treatment can tailor the surface microstructure in such a way that photocatalytic decomposition of methylene blue solution was achieved by heat treatment at  $400^\circ\text{C}$ , which was ascribed to the enlarged surface area upon morphological change of the surface (Kwon et al. 2004).

## 2.3 Electrospinning Process

### 2.3.1 Background

Electrospinning is a straightforward method to produce polymer nanofibers. When the electrical force at the surface of a polymer solution or polymer melt overcomes the surface tension, a charged jet is ejected. The jet extends in a straight line for a certain distance, and then bends and follows a looping and spiraling path. The electrical forces elongate the jet thousands or even millions of times and the jet becomes very thin. Ultimately the solvent evaporates, or the melt solidifies, resulting in very long fibers, often in the form of a non-woven fabric.

The electrospinning process produces fibers with diameter in the range of one or two orders of magnitude smaller than those of conventional textile fibers. The small diameter provides large surface area to mass ratio, in the range from  $10 \text{ m}^2/\text{g}$  (when the diameter is around 500 nm) to  $1000 \text{ m}^2/\text{g}$  (when the fiber diameter is around 50 nm). The equipment required for electrospinning is simple and only a small amount of polymer sample is needed to produce nanofibers.

Polymer nanofibers are being used, or finding uses, in filtration, protective clothing, and biomedical applications including wound dressings and drug delivery systems. Other possible uses include solar sails, light sails, and mirrors for using in space. Nanofibers offer advantages for the application of pesticides to plants, as structural elements in artificial organs, as supports for enzymes or catalysts that can promote chemical reactions, and in reinforced composites. Ceramic or carbon nanofibers made from polymeric precursors extend nanofiber applications to uses involving high temperature and high modulus. The electrospinning process can incorporate particles such as pigments or carbon black particles into nanofibers. Flexible fibers are needed on a scale commensurate with micro or nano-electrical mechanical and optical systems. The use of electrical forces may lead to new ways to fabricate micro or nano scale devices.

The electrostatic spray related literatures contain many helpful insights into the electrospinning process. Lord Rayleigh (1882) studied the instabilities that occur

in electrically charged liquid droplets. He showed, over 100 years ago, that when the electrostatic force overcame the surface tension, a liquid jet was created (Rayleigh 1882). Zeleny considered the role of surface instability in electrical discharges from droplets. He published a series of papers around 1910 on discharges from charged droplets falling in electric fields, and showed that, when the discharge began, the theoretical relations for surface instability were satisfied (Zeleny 1914; Zeleny 1915; Zeleny 1917; Zeleny 1935). In 1952, Vonnegut and Neubauer (1952) produced uniform streams of highly charged droplets with diameters of around 0.1 mm, by applying potentials of 5 to 10 kilovolts to liquids flowing from capillary tubes. Their experiment proved that monodisperse aerosols with a particle radius of a micron or less could be formed from the pendent droplet at the end of the pipette. The diameter of the droplet was sensitive to the applied potential (Vonnegut and Neubauer 1952). Wachtel and coworkers (1962) prepared emulsion particles using an electrostatic method to make a monodispersed emulsion of oil in water. The diameter of the emulsion particles was in the range from 0.5 to 1.6 microns (Wachtel and LaMer 1962). In the 1960's, Taylor studied the disintegration of water droplets in an electrical field. His theoretical papers demonstrated that a conical interface, with a semi-angle close to  $49.3^\circ$ , was the limiting stable shape (Taylor 1964; Taylor 1965; Taylor 1966; Taylor 1969).

Electrospinning of solutions of macromolecules can be traced back to 1934, when Formhals invented a process for making polymer fibers by using electrostatic force. Fibers were formed from a solution of cellulose acetate. The potential difference required depended on properties of the spinning solution such as molecular weight and viscosity. Formhals obtained a series of patents on his electrospinning inventions (Formhals 1934; Formhals 1937; Formhals 1939a; Formhals 1939b; Formhals 1940a; Formhals 1940b; Formhals 1944).

Gladding and Simons improved the electrospinning apparatus and produced more stable fibers. They used movable devices such as a continuous belt for collecting the fibers (Gladding 1939; Simons 1966). Later, Bornat patented another electrospinning apparatus that produced a removable sheath on a rotating mandrel. The basic principles were similar to previous patents. He determined that the tubular

product obtained by electrospinning polyurethane materials in this way could be used for synthetic blood vessels and urinary ducts (Bornat 1982; Bornat 1987).

In 1971, electrospinning of acrylic fibers was described by Baumgarten (1971). Acrylic polymers were electrospun from dimethylformamide solution into fibers with diameters less than 1 micron. A stainless steel capillary tube was used to suspend the droplets of polymer solution and the electrospun fibers were collected on a grounded metal screen. Baumgarten observed relationships between fiber diameter, jet length, solution viscosity, feed rate of the solution and the composition of the surrounding gas (Baumgarten 1971).

In 1981, Manley and Larrondo (1981) reported that continuous fibers of polyethylene and polypropylene could be electrospun from the melt, without mechanical forces. A drop of molten polymer was formed at the end of a capillary. A molten polymer jet was formed when a high electric field was established at the surface of the polymer. The jet became thinner and then solidified into a continuous fiber. The polymer molecules in the fiber were oriented by an amount similar to that found in conventional as-spun textile fibers before being drawn. The fiber diameter depended on the electric field, the operating temperature and the viscosity of the sample. The electrospun fibers were characterized by X-ray diffraction and mechanical testing. As either the applied electric field or the take-up velocity was increased, the diffraction rings became arcs, showing that the molecules were elongated along the fiber axis (Larrondo and Manley 1981a; Larrondo and Manley 1981b; Larrondo and Manley 1981c).

Reneker and coworkers (Doshi and Reneker 1995; Srinivasan and Reneker 1995; Reneker and Chun 1996; Fang and Reneker 1997; Chun et al. 1999; Fong et al. 1999a; Fong et al. 1999b; Fong and Reneker 1999; Kim and Reneker 1999; Kim et al. 1999; Kim and Reneker 1999a) made further contributions to understanding the electrospinning process and characterizing the electrospun nanofibers in recent years. Doshi and Reneker (1995) made electrospun nanofibers, from water soluble poly(ethylene oxide), with diameters of 0.05 to 5 microns. They described the electrospinning process, the processing conditions, fiber morphology and some possible uses of electrospun fibers (Doshi and Reneker 1995). Srinivasan and Reneker

(1995) electrospun a liquid crystal polyaramid, poly (aniline), each from solution in sulfuric acid. They observed electron diffraction patterns of the polyaramid nanofibers, both as spun and after annealing at 400°C (Srinivasan and Reneker 1995). Reneker and Chun (1996) used transmission electron microscopy, scanning electron microscopy and atomic force microscopy to characterize electrospun fibers of poly (ethylene terephthalate) (Reneker and Chun 1996). Fang and Reneker (1997) electrospun DNA into nanofibers, some of which were beaded (Fang and Reneker 1997). Polybenzimidazole nanofibers were electrospun by Kim and Reneker (1999 a,b), who also studied the reinforcing effects of these nanofibers in an epoxy matrix and in a rubber matrix (Kim and Reneker 1999a; Kim and Reneker 1999b). Fong et al (1999) described the electrospinning of beaded nanofibers (Fong et al. 1999b). They also studied the morphology of phase separation in electrospun nanofibers of a styrene-butadiene-styrene tri-block copolymer (Fong and Reneker 1999). Elastomeric nanofibers were made from this thermo-elastic copolymer. The smallest fibers of this tri-block copolymer had diameters around 3 nm. Reneker and coworker also made carbon nanofibers, from polymers or pitch. The resulting carbon nanofibers had diameters of from 50 to 500 nm. The morphology ranged from highly oriented, crystalline, nanofibers to very porous ones with high values of surface area per unit mass (Chun et al. 1999; Fong et al. 1999a).

In 2003, Li and Xia (2003) studied fabrication of titania nanofibers by electrospinning with controllable diameters and porous structures. When ethanol solution containing both poly(vinyl pyrrolidone) (PVP,  $M_w \sim 1,300,00$ ) and titanium tetraisopropoxide was injected through a needle under strong electrical field, composite nanofibers made of PVP and amorphous  $TiO_2$  were formed as a result of electrostatic jetting. These nanofibers could be subsequently converted into fibers of anatase titania without changing their morphology via calcination in air at 500°C. The average diameter of these ceramic nanofibers could be controlled in the range from 20 to 200 nm. It was found that, after calcined at 500°C, the nanofibers remained in continuous structure with their average diameter reduced. This size reduction could be accounted by the loss of PVP from the nanofibers and the crystallization of titania. They also reported the followings: the nanofibers increased in diameter as the PVP concentration was increased, thinner nanofibers were obtained when the strength (E) of the electric field was increased, faster feeding rate of PVP solution often resulted in

thicker fibers, the use of titanium tetraisopropoxide at lower concentration led to the formation of thinner ceramic nanofibers. Furthermore, it was suggested that the electrospinning procedure could be extended to provide a generic route to nanofibers made of other oxides such as  $\text{SnO}_2$ ,  $\text{SiO}_2$ ,  $\text{Al}_2\text{O}_3$ , and  $\text{ZrO}_2$  (Li and Xia 2003).

In 2004, Viswanathamurthi and coworkers (2004) have been prepared nano to sub-micron fibers of ruthenium doped titanium dioxide/poly(vinylacetate) hybrid by electrospinning method. Pure ceramic metal oxide fibers were obtained by high temperature calcination of the organic-inorganic hybrid fibers. It was observed that the diameter of as-synthesized titania fibers was slightly increased by the addition of ruthenium. However there was no change in the diameter of ruthenium-doped fibers with the increase in ruthenium content. The surface of the fibers obtained was smooth and uniform. The fibers calcined at  $600^\circ\text{C}$  contained only anatase phase of titanium dioxide and metallic ruthenium, while the fibers calcined at  $800^\circ\text{C}$  showed the presence of rutile in addition to those two phases. When the ruthenium content was increased, the fibers were no longer straight and some of fibers are broken. Moreover, the fiber surface showed shrinkage and roughness. It was seen that the surface of high ruthenium content fibers appeared smooth and porous. The porosity increased with the increase in ruthenium content. The fiber calcined at  $1000^\circ\text{C}$  showed only rutile and metallic ruthenium. At this stage no change in fiber morphology with respect to ruthenium content was observed. They found that the porous and polycrystalline structure of the electrospun fibers provided a surface area to volume ratio roughly 1-2 orders of magnitude higher than that has been known for continuous thin films (Viswanathamurthi et al. 2004).

In 2004, Madhugiri and coworkers (2004) have prepared electrospun mesoporous titanium dioxide fibers. The fibers contained anatase crystallized in the pore walls which transformed to rutile upon the calcination above  $800^\circ\text{C}$ . The electrospun fibers (calcination at  $600^\circ\text{C}$ , surface area  $32 \text{ m}^2/\text{g}$ ) were evaluated for the photodecomposition of phenol and formic acid comparing with two different commercial  $\text{TiO}_2$  samples (Degussa P25, surface area  $50 \text{ m}^2/\text{g}$  and Hombikat UV 100, surface area  $334 \text{ m}^2/\text{g}$ ). It was found that the photocatalytic properties of the calcined  $\text{TiO}_2$  fibers fell well below those of commercial catalysts. Nevertheless, they

suggested that there were several parameters including fiber size and porosity that can be tuned to improve reactivity (Madhugiri et al. 2004).

### 2.3.2 Mechanism of Electrospinning Process

Electrospinning process involves polymer science, applied physics, fluid mechanics, electrical engineering, mechanical engineering, chemical engineering, material engineering and rheology. Many parameters, including the electric field, solution viscosity, resistivity, surface tension, charge carried by the jet and relaxation time can affect the process. A comprehensive mathematical model of this process was developed by Reneker et al (Reneker et al. 2000).

The electrospinning process consists of three stages: (1) jet initiation and the extension of the jet along a straight line; (2) the growth of a bending instability and the further elongation of the jet, which allows the jet to become very long and thin while it follows a looping and spiraling path; (3) solidification of the jet into nanofibers. A schematic drawing of the electrospinning process is shown in Figure 2.1.

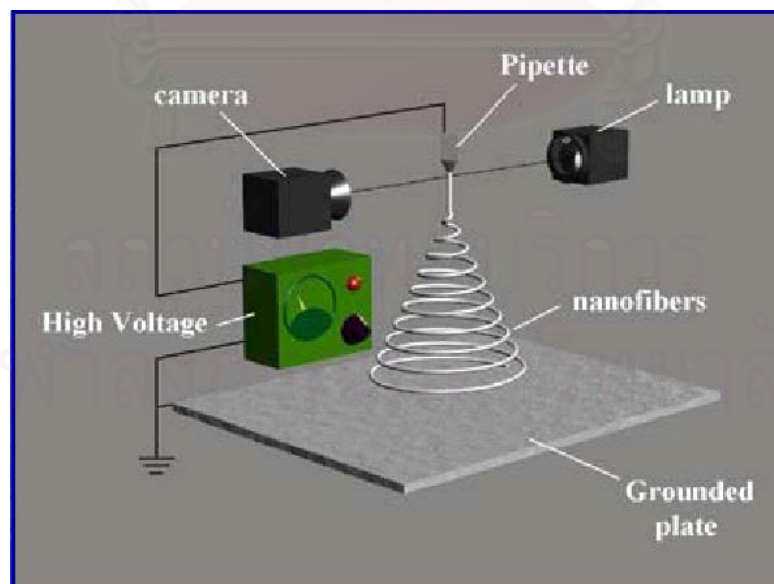


Figure 2.1 Schematic representation of the electrospinning process.

### 2.3.2.1 Jet initiation and diameter of a single jet

In a typical experiment, a pendent droplet of polymer solution is supported by surface tension at the tip of the spinneret. When the electrical potential difference between the spinneret and the grounded collector is increased, the motion of ions through the liquid charges the surface of the liquid. The electrical forces at the surface overcome the forces associated with surface tension. A liquid jet emerges from a conical protrusion that formed on the surface of the pendant droplet. The jet is electrically charged. It carries away the ions that are attracted to the surface when the potential is applied. Increasing the potential increases both the charge density on the jet and the flow rate of the jet.

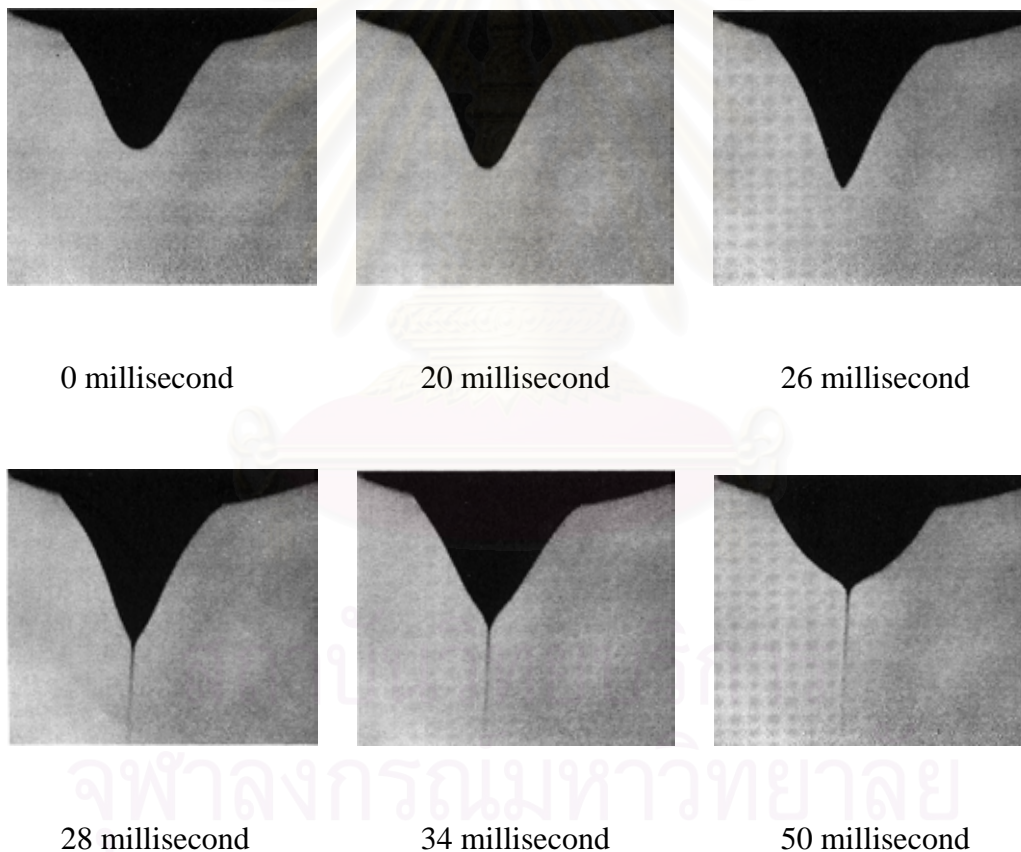


Figure 2.2 Photographs of the pendent droplet and jet, near the time the jet was ejected.

Figure 2.2 shows a sequence of droplet shapes taken at a frame rate of 500 frames per second and a shutter speed 2 ms (Salem 2001). A 3.0% solution of polyethylene oxide in water was used. The solution flowed through a hole, with diameter of 300 microns, in the bottom of a bowl of a metal spoon. The electric field along the axis of the jet was 0.5 kV/cm. The length of the horizontal edge of each of the images was 1.0 mm. When the semi-vertex angle of the droplet was around  $22.5^\circ$ , the electric force was high enough to overcome both surface tension and viscoelastic forces, and a fluid jet was ejected. Jet diameters near the droplet were in the range from 20  $\mu\text{m}$  to 100  $\mu\text{m}$ . After the charged jet was ejected, the conical protrusion relaxed to a rounded shape, reaching a steady shape in a few milliseconds. A jet can also be initiated, at a lower potential, by mechanically pulling a jet out of the pendent droplet, since the voltage required for initiation was higher than that required for maintaining the jet flow.

The observed semi-vertex angle as the jet emerged from the droplet was less than the  $49.3^\circ$  that Taylor calculated (Taylor 1964; Taylor 1965; Taylor 1966; Taylor 1969). Sometimes the jet current and the shape of the droplet pulsated while the applied voltage was constant. A steady current was associated with a droplet that had a constant shape.

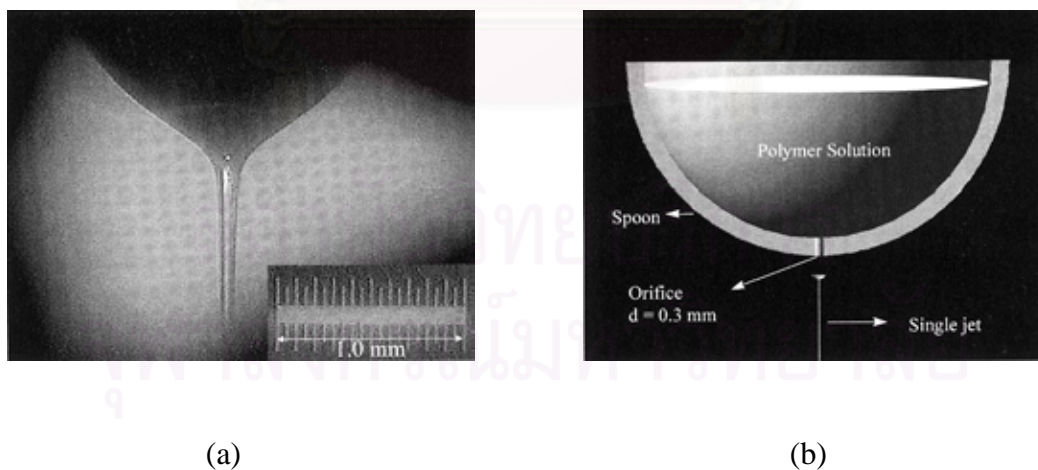


Figure 2.3 (a) Magnified image of the shape of the jet near the spoon. (b) Schematic drawing of a jet flowing from a hole in the bowl of a spoon. The jet is separated from the spoon for clarity.

The jet diameter decreases with the distance from the orifice. Higher electric fields and a lower surface tension coefficient favor the formation of a thicker jet. Addition of salt (NaCl) to the solution, with other parameters held constant, reduces the diameter of the jet. Increasing the viscosity of the solution does not always increase the diameter. The largest jet diameter occurs when the solution viscosity is in a medium range. Both higher and lower viscosity favors a thinner jet.

#### *2.3.2.2 Bending instability and elongation of the Jet*

After initiation, the path of the jet is straight for a certain distance. Then, an electrically driven bending instability grows at the bottom end of the straight segment. The bending allows large elongation to occur in small region of space. The electrically driven bending instability occurs in self-similar cycles. Each cycle has three steps and is smaller in scale than the preceding cycle.

The three steps in each cycle are:

Step 1. A smooth segment that is straight or slightly curved suddenly develops an array of bends.

Step 2. As the segment of the jet in each bend elongates, the linear array of bends becomes a series of spiraling loops with growing diameters.

Step 3. As the perimeter of each loop increases, the cross-sectional diameter of the jet forming the loop gets smaller, and the conditions for Step 1 are established everywhere along the loop.

After the first cycle, the axis of a particular segment might lie in any direction. The continuous elongation of each segment is most strongly influenced by the repulsion between the charges carried by adjacent segment of the jet. The externally applied field, acting on the charged jet, causes the entire jet to drift toward the collector, which is maintained at an attractive potential.

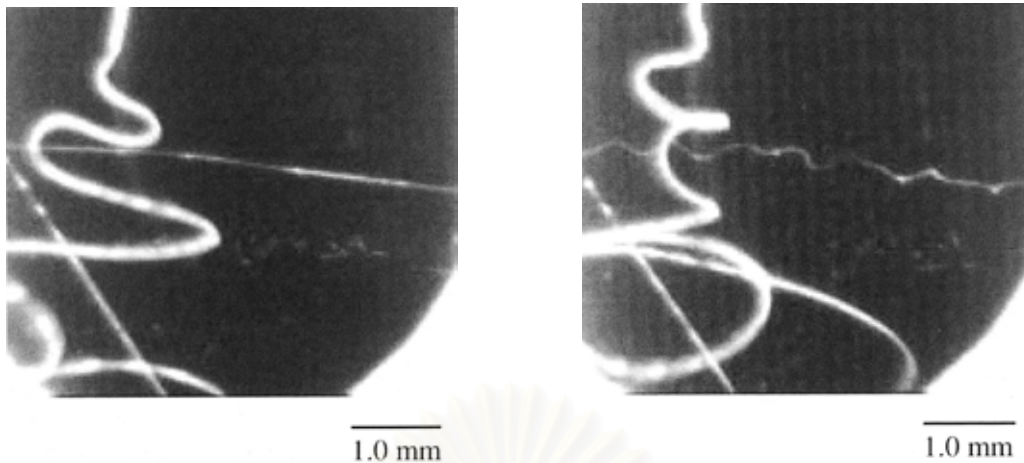


Figure 2.4 The development of the second cycle of bending instability. The time interval between these two images was 15 ms. The camera shutter speed was 0.25 ms.

Figure 2.4 shows two cycles of bending instability. The jet enters the image near the end of the straight segment, where the first electrically driven bending instability produces an array of helical bends. While the jet runs continuously, it shifts through a series of similar but changing paths. Most loop moves downward at a velocity of about 1 m/s, but some loops with larger diameter remain in the field of view for long time. The slightly curved thin segment that runs horizontally across the left image in Figure 2.4 is part of such loop that remain in view for over 15 ms. This segment is smooth until, in a time interval of only one ms, the bends and loops shown in the right image of Figure 2.4 are developed. During this 15 ms period, many bends and loops of the first cycle of bending instability are formed and move downward through the field of view. The diameter of every segment of the jet becomes smaller, and the length of every segment increases. The loops grow larger. Bending instabilities are developed and grow.

It is often possible to follow the evolution of the shape of segments, such as those shown in the right part of Figure 2.4, back to the time at which they enter the upper left corner of the image, by stepping backward in time through the image files created by the electronic camera. It is more difficult to follow the evolution of the jet into the third cycle of bending because the images of the path become fainter as the jet

becomes thinner, and soon they are ambiguous. The elongation and the associated thinning of the jet continue as long as the charge on the jet supplies enough force to overcome the surface tension and viscoelastic forces. Meanwhile, the elongational viscosity increases as the solvent evaporates and eventually the elongation is stopped. Details of the evolution of the solidification process remain to be investigated.

The “area reduction ratio”, which is defined as the ratio of the cross-sectional area of the upper end of a segment to the cross-sectional area at the lower end of the same segment, is equal to the draw ratio if the volume of material in the segment is conserved. Consider a jet, with a 6% concentration of polymer in a volatile solvent, which transforms from a jet diameter of 50  $\mu\text{m}$  to a dry nanofiber with relatively large diameter of 0.5  $\mu\text{m}$ . The area reduction ratio is  $2500/0.25 = 10000$ . The drying process accounts for a factor of 16, and the elongation of the initial straight part of the jet contributes an additional factor of 5. The remaining area reduction ratio, 125, occurs in the parts of the jet affected by the bending instabilities (Salem 2001).

Many nanofibers as thin as 0.05  $\mu\text{m}$  (50 nm) in diameter have been observed. The corresponding total area reduction ratio is 1,000,000, for an initial jet diameter of 50  $\mu\text{m}$ . If, as above, evaporation of solvent contributes to a factor of 16 and the elongation of the straight segment contributes a factor of 5, in this case, the bending and looping part of the jet provide the remaining the factor of 12,500 to the area reduction ratio.

While 12,500 is a high area reduction ratio, it occurs as many segments of the jet are drawn in different directions at the same time, in expanding loops. If the jet is drawn in a straight line to a ratio of 12,500, the velocity required at the nanofiber end of the jet would be much faster than the speed of sound in most solids. The actual path achieves very high elongation without such an unreasonably high velocity.

The longitudinal strain rate could be estimated as follows, by using the area reduction ratio and the time of flight. The time that a typical segment of the jet is in flight ( $\delta t = 0.2$  s) could be estimated as the distance between the pendent droplet and the collector (20 cm) divided by the downward velocity of the jet (1 m/s). The longitudinal strain rate was  $\delta\zeta / (\delta t \cdot \zeta)$  where  $\zeta$  is the initial segment length, and  $\delta\zeta$  is

the growth in length. The draw ratio  $\delta\zeta/\zeta$  is around 125 to 12,500, assuming that there is no solvent loss, so that the longitudinal strain rate is around 625 to 62500  $\text{s}^{-1}$  for the two cases described above.

Theory has suggested that the transformation from a random coil to an elongated macromolecule occurs when the strain rate multiplied by the conformational relaxation time of the molecule is greater than 0.5 (De Gennes 1974; Smith and Chu 1998). If the relaxation time of the polymer solution is longer than 0.01 s, which is a conservative estimation, the macromolecules are expected to be elongated and axially oriented during electrospinning.

Before high frame-rate, short exposure time cameras were available, visual observations and video images (30 frames per second) of electrically driven jets were interpreted as evidence for a process that splayed the primary jet into many smaller jets. The splaying jets were supposed to emerge from the region at the end of the straight segment. Figure 2.5(a) and 2.5(b) show images from video frames with an exposure time of 16.7 ms (Salem 2001). The jet path was illuminated with a single bright incandescent light that projected a narrow beam through the path of the jet. Figure 2.5c shows a jet similar to that shown in Figure 2.5a, illuminated with light from a broader source, and photographed at 30 frames per second. A shorter exposure time of 1 ms was used. Several loops were visible. The parts of the jet closer to the beginning of the bending instability appeared only as bright, short and unconnected lines. Specular reflections of the narrow beam of light, off nearly horizontal segment of downward moving loop, were shown to be the cause of these bright spots. In Figure 2.5a, similar spots moved downward during the longer exposure and created the lines that are prominent.

At 30 frames per second, for any particular frame, the preceding and the following frames showed loops and spirals in completely different positions. After the illumination was broadened and made brighter, and a high frame rate electronic camera was used, it was obvious that the envelope cone was occupied by a long, looping, spiraling, continuous, and gradually thinner jet as shown in Figure 2.5d.

Although the elongation of the jet during the bending instability is considered as the major cause for the decrease in the diameter of the jet in experiments described in this paper, splitting and splaying of the jet have been observed in some experiments with other materials. These processes provide viable alternative mechanisms for the production of nanofibers.

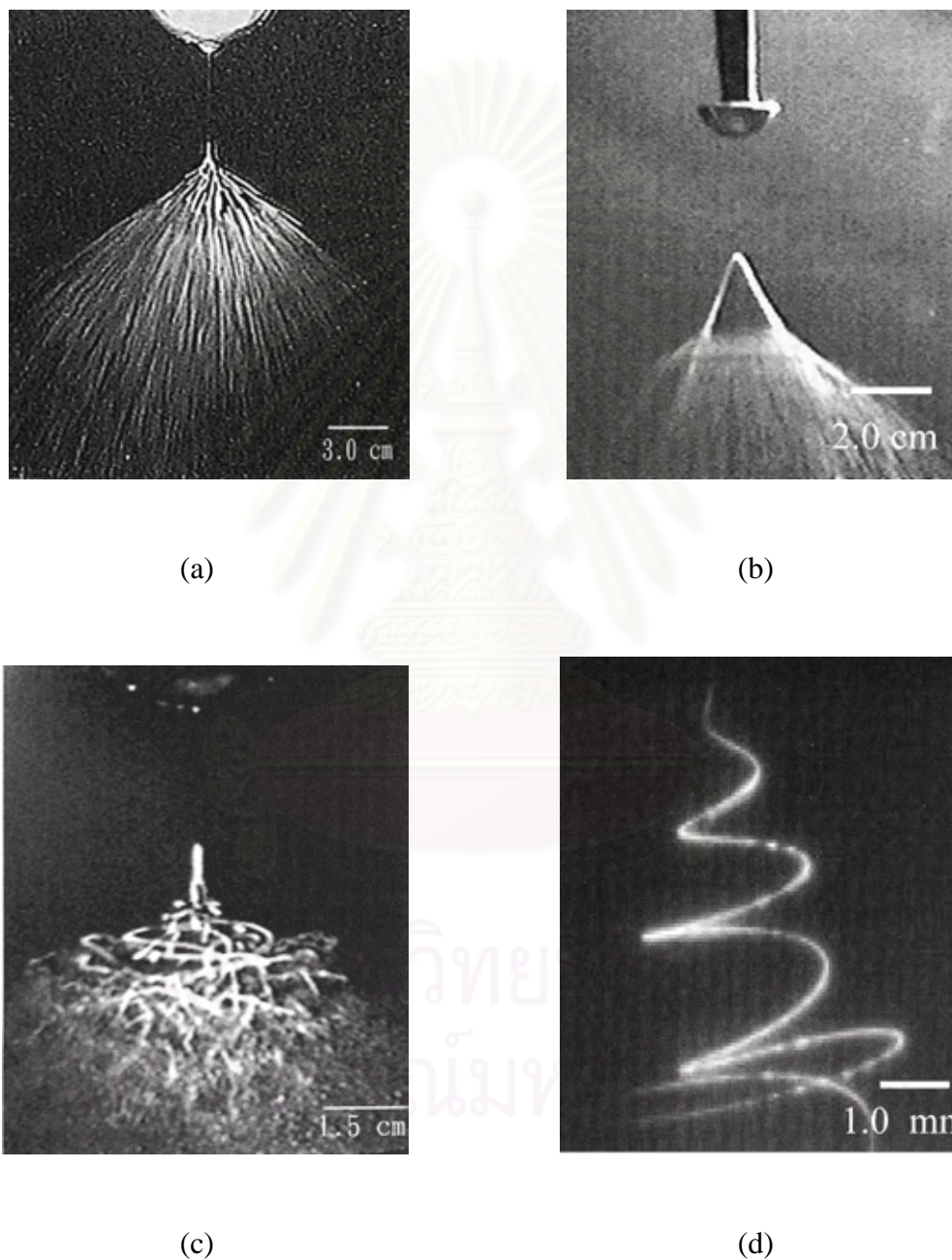


Figure 2.5 Images of electrospinning jet with different exposure times. (a), (b), and (c), shutter speed was 1.0 ms. The spots in (d) are artifacts produced by a faceted reflector used in the illuminating system.

### 2.3.3 Applications of Electrospinning

Nanofibers made from many new synthetic polymers, and biologically derived polymers are being considered for use in tissue engineering, artificial organ applications, drug delivery, and for wound dressings. Nanofibers of DNA were made by Fang and Reneker (Fang and Reneker 1997). The growth of cells on nanofibers was reported by Ko and Reneker (Ko et al. 1998).

Many kinds of bio-generated and bio-compatible materials are of interest. Conventional methods for making fibers require so much material that they are often impractical. Electrospinning provides a convenient way to fabricate nanofibers using as little as a few hundred milligrams of the starting materials.

Nanofibers have found use in filters to remove particles and droplets smaller than 100 nm from liquids or gases. They are also being considered for the absorption of noxious molecules, since their specific surface area is so large, and their surface chemistry can be tailored to be selective to many kinds of substances.

The application of pesticides to plants is another area where nanofibers may find large-scale applications. Nanofibers, spun in the field, and directed onto plants by a combination of electrical forces and air stream, will attach to plants with nearly 100% efficiency. This contrasts with the 3 to 5% sticking efficiency of conventional application methods for applying pesticides in form of dusts or sprays. The use of nanofibers to carry and attach pesticides could make the use of sophisticated but expensive pesticides cost effective. The burden placed on the environment by wasted pesticides would also be reduced.

Electrospinning of nanofibers from a polymer melt works better in a vacuum than in air because the dielectric breakdown strength of air is much less than the electric fields that can be applied to a polymer in a high vacuum. It is feasible to electrospin polymer nanofibers in space to create thin sheets with large areas, and as tensile member of other large scale structures. Solar sails to transport cargo between the Earth and Mars need to be less than one micron thick, with an area of about five square kilometers. Electrospun polymer nanofibers could create such structure, along

with the shroud lines needed to attach the cargo. Proposals to explore interstellar space utilize light sails, similar to solar sails, driven by high power lasers, to carry instruments outside the solar system. The use of large mirrors to direct and focus sunlight, or microwaves generated by solar collectors in space, onto the earth, has been proposed (Salem 2001).

Nanofibers, perhaps at the scale of single polymer molecules, can be expected to play a role in micro-electro-mechanical devices (MEMS). The possibility of making ceramic material by chemical routes that use linear polymers as intermediates provides suggestions for ways to make ceramic nanofibers.

Commercialization of synthetic fibers with diameters in the range of nanometers has not been significantly developed, even though micron-scale fibers are the basis of large industries. However, the future for nanofibers now looks brighter.

#### **2.4. Photocatalytic Process**

Atoms have discrete energy levels for their electrons. Molecules often contain like atoms but the Pauli exclusion principle forbids identical quantum numbers in all respects, resulting in the "splitting" of a given atomic energy level into a set of closely spaced levels typically in order of the numbers of atoms, which involves energy level splitting so finely that a so-called "band" structure of allowed energies (quantum states) emerges, with infinitesimal or virtually continual distribution of energy level within a given "orbital". For a semiconductor such as titania, the highest filled band is termed the valence band, and the lowest unoccupied level is the conduction band. The separation of the valence band top from the conduction band bottom is called the band gap.

The photocatalytic reaction starts with the exposure of photocatalyst to light. After light is absorbed by photocatalyst, two types of carriers, i.e. electron ( $e^-$ ) and holes ( $h^+$ ), are generated. Unlike metal oxide, a semiconductor oxide is good photocatalyst because of the long life for both of these carriers. For this reason

semiconductor oxides such as  $\text{TiO}_2$ ,  $\text{ZnO}$ ,  $\text{SrTiO}_3$ ,  $\text{K}_4\text{NbO}_2$ ,  $\text{Fe}_2\text{O}_3$  and  $\text{SnO}_2$  are used in photocatalytic process.

One of the reasons for the anatase titania to be more photoactive than the rutile may lie in the difference in their so-called energy band structures. The band gap of a semiconductor is the minimum energy of light required to make the material electrically conductive or in the other words, to get the electrons excited enough to get moving. For anatase titania, this energy is 3.2 electron volts (eV), which corresponds to UV light (wavelength of 388 nanometers), while the band gap for the rutile is 3.0 eV, corresponding to violet light (wavelength of 413 nanometers). In more technical terminology, the band gap for a semiconductor indicates the minimum energy of light necessary to produce conduction band (CB) electrons, which can give rise to electrical conductivity (photoconductivity) and valence band (VB) "holes," which are actually the absence of electrons. These holes can react with water to produce the highly reactivity hydroxyl radical ( $\text{OH}^\cdot$ ). Both the holes and the hydroxyl radicals are very powerful oxidants, which can be used to oxidize most organic materials. The energy level of the CB for anatase turns out to be 0.2 eV higher than that of rutile.

The VB energies for anatase and rutile are both similar, which is very low in the energy diagram. It means that, for both materials, the VB holes (and the hydroxyl radicals) have great oxidizing power. The CB energy for rutile is close to the potential required to electrolytically reduce water to hydrogen gas, but that for anatase is higher in the energy diagram, which means that it has higher reducing power. Therefore, it can drive the very important reaction involving the electrolytic reduction of molecular oxygen ( $\text{O}_2$ ) to superoxide ( $\text{O}_2^-$ ). Superoxide is found to be almost as important as the holes and hydroxyl radicals in breaking down organic compounds (Fujishima et al. 1999b).

The primary photocatalytic process occurs upon irradiation of a semiconductor catalyst. A semiconductor (SC) is characterized by an electronic band structure in which the highest occupied energy band, called valence band (VB), and the lower empty band called conduction band (CB), are separated by a band gap. The magnitude of the fixed energy gap between the electronically populated valence band and the

largely vacant conduction band governs the extent of thermal population of the conduction band in its intrinsic state. The band gap also defines the wavelength sensitivity of the semiconductor to irradiation. When a photon of energy higher or equal to the band gap energy is absorbed by a semiconductor particle, an electron from the valence band is promoted to the conduction band with simultaneous generation of an electronic vacancy or "hole" ( $h^+$ ) in the valence band. Figure 2.6 shows the primary steps in the photoelectrochemical mechanism (Hoffmann et al. 1995):

- (1) formation of charge carriers by a photon.
- (2) charge carrier recombination to liberate heat.
- (3) initiation of an oxidative pathway by a valence-band hole.
- (4) initiation of a reductive pathway by a conduction-band electron.
- (5) further thermal (e.g., hydrolysis or reaction with active oxygen species) and photocatalytic reactions to yield mineralization products.
- (6) trapping of a conduction- band electron in a dangling surficial bond to yield Ti(III).
- (7) trapping of a valence-band hole at a surficial titanol group.

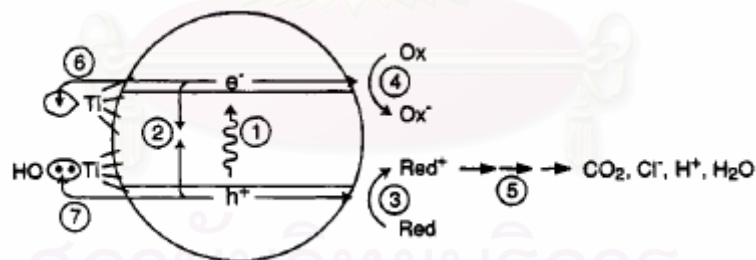


Figure 2.6 Primary steps in the photoelectrochemical mechanism(Hoffmann et al. 1995).

Among the new oxidation methods or advanced oxidation processes (AOP), heterogeneous photocatalysis on titania appears as an emerging destructive technology leading to the total mineralization of most of the organic pollutants, following the usually proposed mechanism (Ammar et al. 2001).

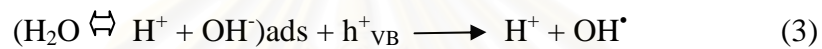
1. Absorption of efficient photons ( $h\nu \geq E_G = 3.2 \text{ eV}$ ) by titania



2. Oxygen ionosorption (first step of oxygen reduction; oxygen's oxidation degree passes from 0 to .1/2)



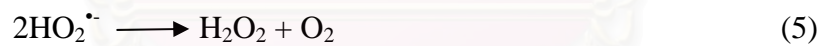
3. Neutralization of  $\text{OH}^-$  groups by photoholes which produces  $\text{OH}^\bullet$  radicals



4. Neutralization of  $\text{O}_2^{\cdot-}$  by protons



5. Transient hydrogen peroxide formation and dismutation of oxygen



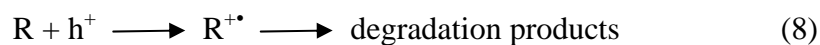
6. Decomposition of  $\text{H}_2\text{O}_2$  and second reduction of oxygen



7. Oxidation of the organic reactant via successive attacks by  $\text{OH}^\bullet$  radicals



8. Direct oxidation by reaction with holes



As an example of the last process, holes can react directly with carboxylic acids generating  $\text{CO}_2$



In 2000, Jung and Park (2000) were prepared silica-embedded titania particles by sol-gel technique. They found that the increase of photoactivity with increasing the silica content is due to the increase in both surface area and surface hydroxyl group. Furthermore, they observed that higher crystallinity obtained by higher calcinations temperature had higher photoactivity if rutile phase is not formed (Jung and Park. 1999; Jung and Park 2000). In 2003,  $\text{TiO}_2/\text{SiO}_2$  particles prepared by microemulsion technique showed higher photocatalytic activity than pure  $\text{TiO}_2$ . Furthermore, they observed that the increase in surface area by the formation of small pores is not always effective for high photocatalytic activity because large pore volume and pore size facilitate the mass transfer of reactants (Hong et al. 2003).

In 2004, Hirano and Ota (2004) synthesized anatase-type  $\text{TiO}_2/\text{SiO}_2$  composite nanoparticles directly from the metal alkoxides, i.e., tetraisopropoxide (TTIP) and TEOS by sol-gel method. Their photocatalytic activities were evaluated by measurements of the relative concentration of methylene blue after UV irradiation. They found that anatase-type  $\text{TiO}_2/\text{SiO}_2$  composite nanoparticles possessed a much higher photocatalytic activity than the anatase-type pure  $\text{TiO}_2$  due to the difference in crystallinity of the anatase (Hirano and Ota 2004).

## CHAPTER III

### EXPERIMENTAL

#### 3.1 Materials

The starting materials are Titanium Tetraisopropoxide (TTIP), Tetra Ethyl Ortho Silicate (TEOS), Poly Vinylpyrrolidone (PVP), Ethyl Alcohol, and Acetic Acid.

Titanium tetraisopropoxide (TTIP) 97% was purchased from Sigma-Aldrich Chemical Company and used as received. It was kept in a dry environment prior to use to prevent moisture adsorption.

Tetraethyl orthosilicate (TEOS) 98% was purchased from Sigma-Aldrich Chemical Company and used as received.

Poly Vinylpyrrolidone (PVP),  $M_w \approx 1,300,000$ , was purchased from Sigma-Aldrich Chemical Company and used as received.

Ethyl Alcohol 98 % and Acetic Acid were purchased from Sigma-Aldrich Chemical Company and used as received.

Methylene Blue ( $C_{16}H_{18}N_3S$ ) 96.0-101.0% were purchased from Asia Pacific Specialty Chemicals Limited and used as received.

#### 3.2 Electrospinning Apparatus

The schematic of the electrospinning apparatus used in this work is shown in Figure 3.1. The components of the apparatus and their functions are described as follows.

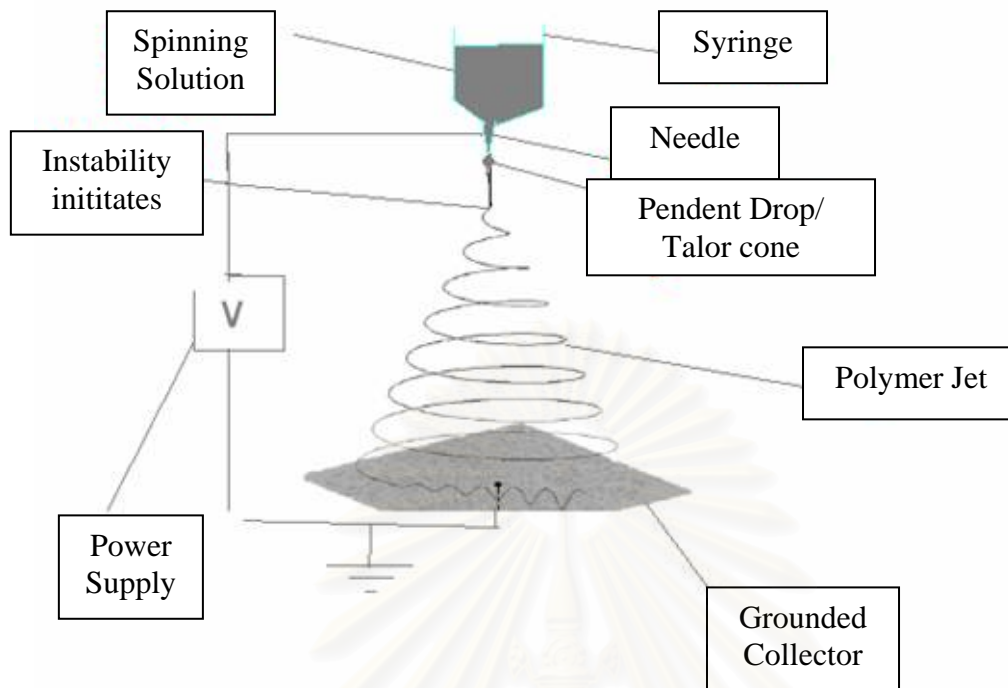


Figure 3.1 Experimental set up for electrospinning process.

- A high voltage power supply (ES30PN, Gamma High Voltage Research Inc., Ormond Beach, Florida) is used to generate either positive or negative DC voltage upto 30 kV, with very low electrical current of 166 microamperes.
- A 5 ml syringe is used as a container for electrospinning solutions. The syringe is built by a plastic structure and is set in vertical orientation.
- A stainless steel needle (guage number 20 and the outside diameter of 0.90 mm) is used as a nozzle and as an electrode to conduct the electrical energy from the power supply to the solutions. The tip of the needle is cut into a flat shape and the length of the needle is 2 cm.
- Aluminum foil and stainless steel 40 mesh (3cm x 3cm) are used as a ground collector which is covered on the plastic stand.

### 3.3 Procedures

#### 3.3.1 Spinning Solution Preparation

In a typical procedure, 1.5 g of titanium tetraisopropoxide (TTIP) was mixed with 3 ml of acetic acid and 3 ml of ethanol. The solution was rest for 10 min before being added into 7.5 ml of polyvinylpyrrolidone (PVP,  $M_w \approx 1,300,000$ ) solution in ethanol. The concentration of the PVP solution was varied between 7 and 13 wt.% and the resulting mixture was constantly stirred for 10 min. Tetraethyl orthosilicate (TEOS) was finally added to the as-prepared mixture. The amount of TEOS was typically 2 wt.% (unless stated otherwise) based on the total amount of the final mixture and the mixture was constantly stirred for another hour. The as-prepared solution was referred to as the spinning solution.

#### 3.3.2 Spinning of the $TiO_2$ /PVP Composite Fibers

The spinning solution was immediately loaded into a plastic syringe. A blunt-ended 20-gauge stainless steel needle was used as the nozzle. The emitting electrode from a Gamma High Voltage Research ES30PN power supply capable of generating DC voltages up to 30 kV was attached to the needle. The grounding electrode from the same power supply was attached to a piece of aluminum foil or stainless steel 40 mesh (3cm x 3cm) which was used as the collector plate and was placed approximately 7 cm below the tip of the needle. Upon the application of a high voltage ranging between 9 and 22.5 kV across the needle and the collective plate, a fluid jet was ejected from the nozzle. As the jet accelerated towards the collector, the solvent evaporated, leaving only ultrathin fibers on the collector. The obtained fibers were left exposed to moisture for approximately 5 hours to allow complete hydrolysis of TTIP.

### 3.3.3 Calcination of the TiO<sub>2</sub>/PVP Composite Fibers

The electrospun TiO<sub>2</sub>/PVP composite fibers are subjected to heat treatment at a high temperature ranging between 500 and 800°C for 3 hours and heating rate of 10°C/min by using box furnace to remove residual PVP.

### 3.3.4 Photocatalytic Activity Evaluation

Photocatalytic activity was evaluated from the decomposition of methylene blue (MB), C<sub>16</sub>H<sub>18</sub>N<sub>3</sub>S, aqueous solution at the concentration of 10 ppm. The titania fibers calcined at different temperatures with different amount of doping silicon were used as photocatalysts. A total of 0.012 g titania fibers were added into 50 ml of the above methylene blue solution under vigorous agitation. The photoreactor was employed 50-ml beaker surrounded by 6 low-pressure mercury lamps. The distance between the lamps and the beaker was 10 cm. Two electric fans were used to cool the reaction solution. Complete mixing was achieved by magnetic stirring. The average power of the mercury lamp, with wavelengths ranging from 300 to 400 nm, is 1.4 mW/cm<sup>2</sup>. The Ultraviolet-Visible spectrometer (UV-Vis Lambda 650, Perkin Elmer) was used to monitor the change of concentration of the methylene blue solution. In order to study the effect of intensity of UV rays, solar radiation was used instead of UV irradiation. All titania fibers was kept in methylene blue solution in darkness for 1 h before UV light illumination, in order to eliminate the effect of methylene blue absorption onto the catalyst. For comparison, a photocatalytic reaction was also carried out using the standard anatase phase pure TiO<sub>2</sub> (JRC-TIO1), obtained from the Catalysis Society of Japan, as the reference catalyst.

## 3.4 Sample Characterizations

### 3.4.1 Scanning Electron Microscopy (SEM)

The surface morphology and size of the resulting electrospun TiO<sub>2</sub>/PVP composite fibers, pure TiO<sub>2</sub> fibers and Si-doping TiO<sub>2</sub> fibers were observed by a JSM 5800 Scanning Electron Microscopy (SEM), which operated at 20 kV, at the

Scientific and Technological Research Equipment Center (STREC), Chulalongkorn University. Samples were coated by thin film of gold prior to analysis.

#### *3.4.2 X-ray Diffractometry (XRD)*

The crystalline phase of pure TiO<sub>2</sub> fibers and Si-doping TiO<sub>2</sub> fibers were identified by a Siemens D5000 X-ray diffractometer. The experiments were carried out by using Ni-filtered CuK $\alpha$  radiation and operated in the 2 $\theta$  range of 20-80 degree at the scan step of 0.04 degree.

#### *3.4.3 Fourier Transform Infrared Spectroscopy (FTIR)*

The functional groups of the as-prepared fibers and calcined fibers were identified by a Nicolet Impact 400 Fourier transform infrared spectrophotometre (FT-IR). Each sample was mixed with KBr by ratio of sample : KBr of 1: 100 and then pressed into a thin pellet. Infrared spectra were recorded between 400 and 4000 cm<sup>-1</sup>

#### *3.4.4 Thermogravimetric and Differential Thermal Analysis (TG-DTA)*

The as-spun titania fibers were subjected to thermogravimetric and differential thermal analysis (Diamond Thermogravimetric and Differential Thermal Analyzer, TG-DTA, Perkin-Elmer) to determine the temperature of possible decomposition and phase change.

#### *3.4.5 Surface Area Measurement*

The single point BET surface area of titania fibers were measured by using nitrogen as the adsorbate. The operating conditions are as follows:

|                   |                                 |
|-------------------|---------------------------------|
| Sample weight     | ~ 0.3 g                         |
| Degas temperature | 200°C for as-synthesized sample |

### 3.4.6 UV-Vis Spectrophotometry

In this work, the change of concentration of the methylene blue solution in photodegradation was monitored by the absorbance at wavelength  $650\text{ nm}$  using The Ultraviolet-Visible spectrometer (UV-Vis Lambda 650, Perkin Elmer)



สถาบันวิทยบริการ  
จุฬาลงกรณ์มหาวิทยาลัย

## CHAPTER IV

### RESULTS AND DISCUSSION

Titania/PVP composite was successfully prepared by combination of electrospinning technique and sol-gel method using solutions containing titanium tetraisopropoxide (TTIP) and polyvinylpyrrolidone (PVP). By applying high electrical potential across the syringe needle and the collector plate, ultrafine fibers with smooth surface were spun and deposited as a non-woven mat on the collector plate.

#### 4.1 Effects of Electrospinning Conditions on As-spun Fibers

##### 4.1.1 Effect of PVP Concentration

Titania/PVP composite nanofibers were prepared from different PVP concentration. The effects of PVP concentration on morphology of the as-spun fibers are shown in Figure 4.1. It should be noted that the applied electric field strength was fixed at 9 kV/7 cm. All fibers are smooth fibers with diameter in nanometer scale. It can be clearly seen that ultrathin fiber with average diameter as low as about 200 nm are produced from the spinning solution with PVP concentration of 7 wt.% as shown in Figure 4.1(a). From Figure 4.1(b)-(d), where the PVP concentration is increased from 10 wt.% to 15 wt.%, it is indicated that increasing PVP concentration leads to an increase in the average fiber diameter as well as a broader size distribution.

The frequency distribution of the electrospun fiber diameter is presented in Figure 4.2. Fiber diameters are measured by program SemAfore 4.0, which random 100 fibers in selected area from SEM images. The fiber size distribution becomes gradually broader with increasing concentration of PVP in the spinning solution. The average diameters of the TiO<sub>2</sub>/PVP composite fibers with PVP concentration of 7, 10, 13 and 15 wt.% are 192, 355, 345 and 330 nm, respectively. It is more clearly represented by a graph in Figure 4.3, which shows the relationship of the diameter of as-spun fibers with respect to PVP concentration of the spinning solutions. Noted that the error bars in the figure represent standard deviation of the fiber diameter data.

Based on the above results, the PVP concentration has a significant effect on the final diameter of TiO<sub>2</sub>/PVP composite nanofibers. The increase in the average fiber diameter with increasing PVP concentration should be a result of the increase in the viscosity of the spinning solutions (Mit-uppatham et al. 2004). However, the increase in the viscosity of the spinning solution could lead to non-uniform ejection of the jet, when the viscosity becomes too high. It is responsible for broad size distribution of fibers having high PVP concentration (Frenot and Chronakis 2003; Huang et al. 2003).

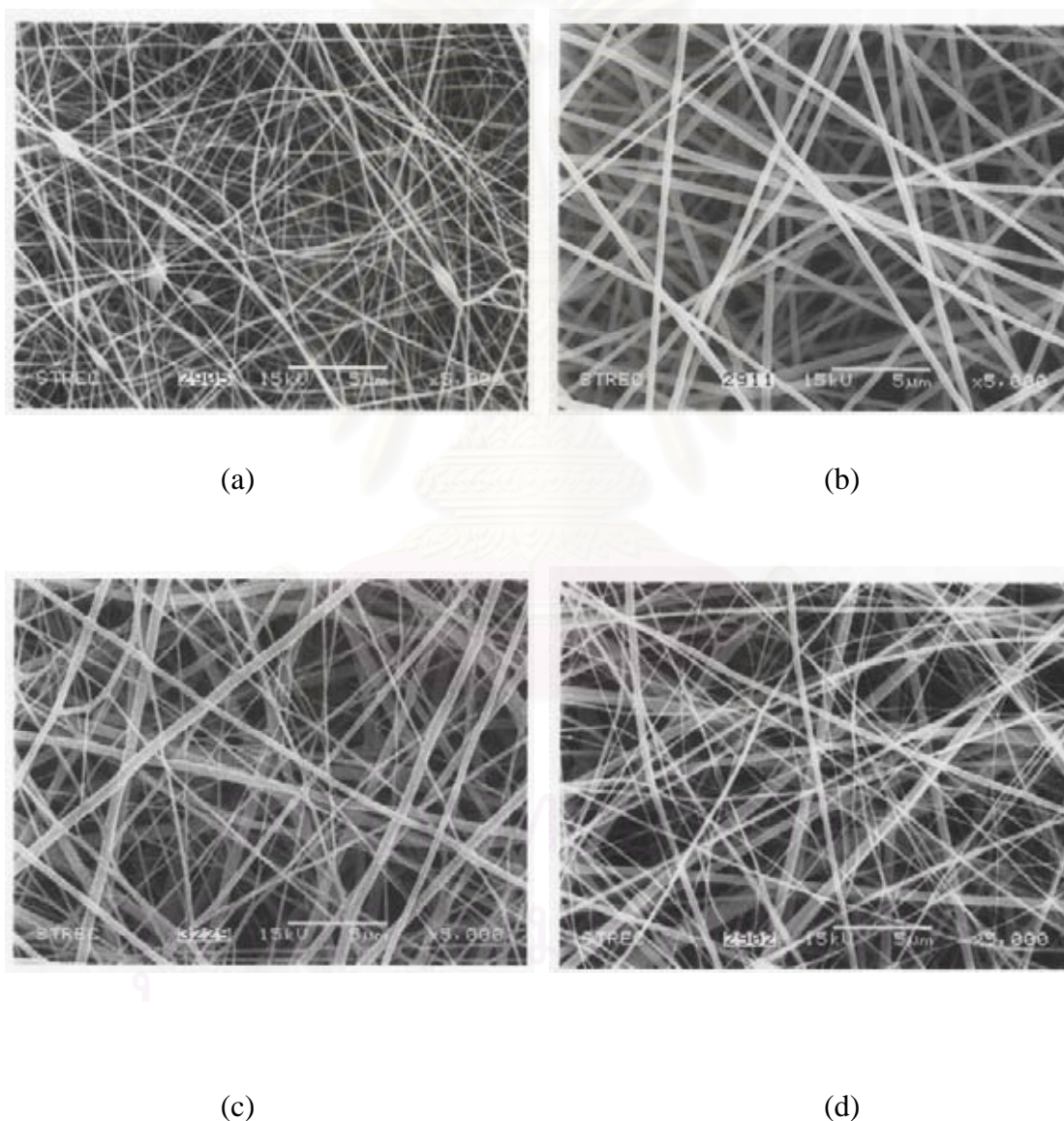


Figure 4.1 SEM images of pre-calcined as-spun fibers from spinning solutions containing (a) 7, (b) 9, (c) 13, and (d) 15 wt.% PVP solution. The applied electric field strength was 9 kV/7cm.

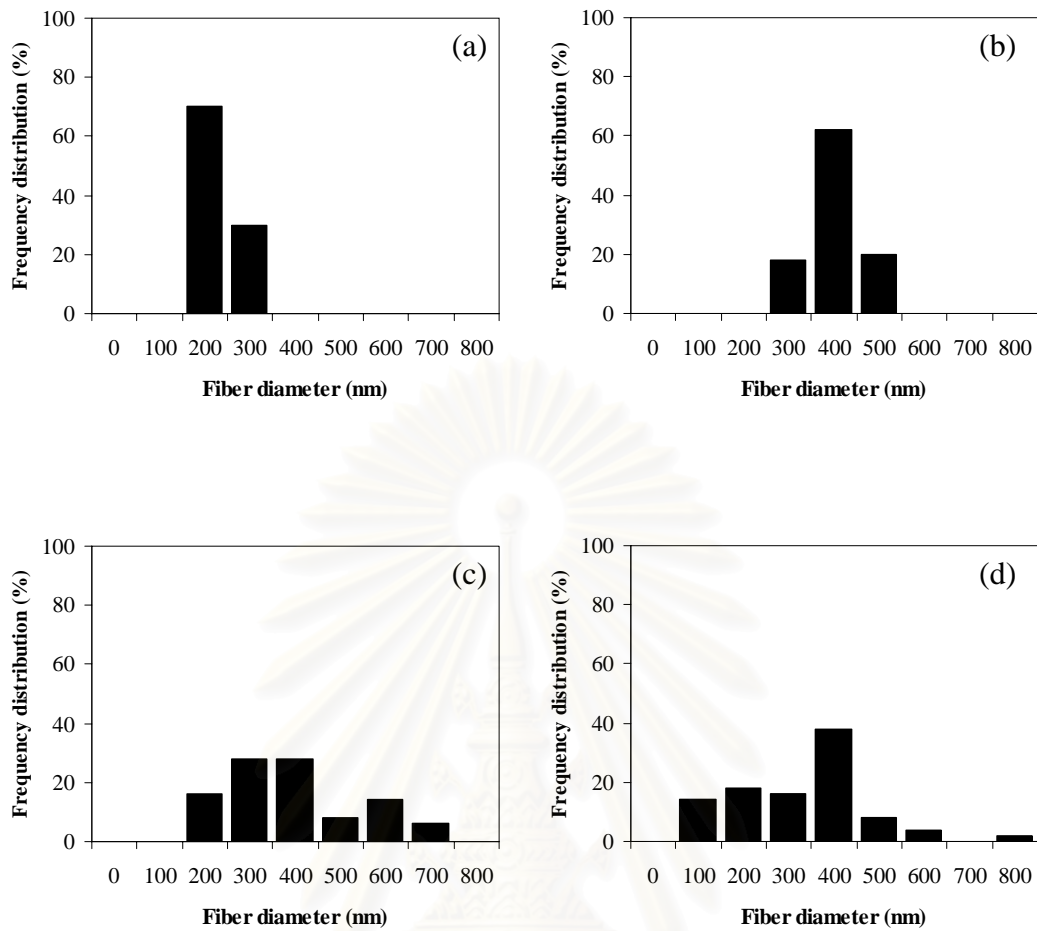


Figure 4.2 Frequency distribution of fiber diameters of pre-calcined as-spun fibers from spinning solution containing (a) 7, (b) 10, (c) 13, and (d) 15 wt.% PVP.

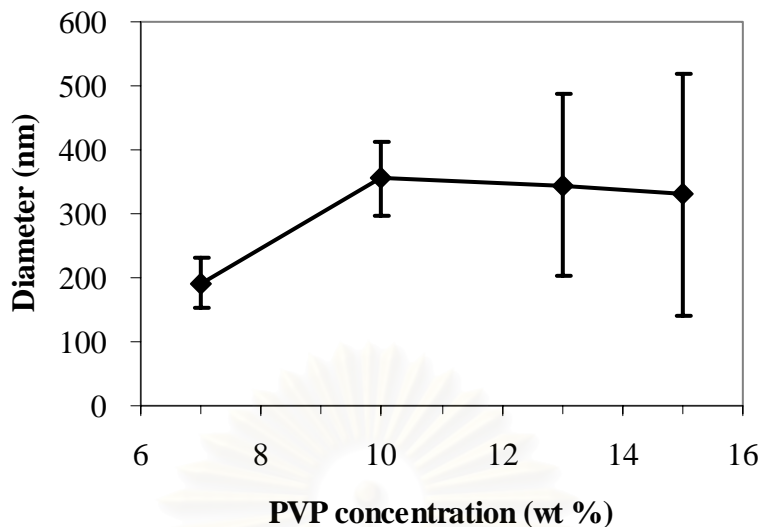


Figure 4.3 Diameters of pre-calcined as-spun fibers as a function of PVP concentration

#### 4.1.2 Effect of Applied Electric Field Strength

The strength of the electric field is another key factor determining the morphology and diameter of the electrospun fibers. In this work, TiO<sub>2</sub>/PVP composite nanofibers were produced by using applied electric field strength of 9, 11.25, 15, 18.75, and 22.5 kV, respectively. It should be noted that the PVP concentration in the spinning solution was fixed at 13 wt.% and the distance between the injection orifice and the collector was kept at 7 cm for all experiments in this part. SEM micrographs of TiO<sub>2</sub>/PVP composite nanofibers spun by using different electric field strength are shown in Figure 4.4. It can be seen that the surfaces of the as-spun fibers are smooth due to the amorphous nature of the TiO<sub>2</sub> and PVP composite. If electric field is too low, no stable liquid jets is formed. When electric field strength is increased, the fibers obtained appears to be not only smaller in diameter but narrower size distribution as well. Increasing electric field strength results in an increase in both the electrostatic force, which is responsible for the transport of the charged jet from injection orifice to the collective target, and the Coulombic repulsion force, which is responsible for the stretching of an ejected jet segment (Frenot and Chronakis 2003; Huang et al. 2003).

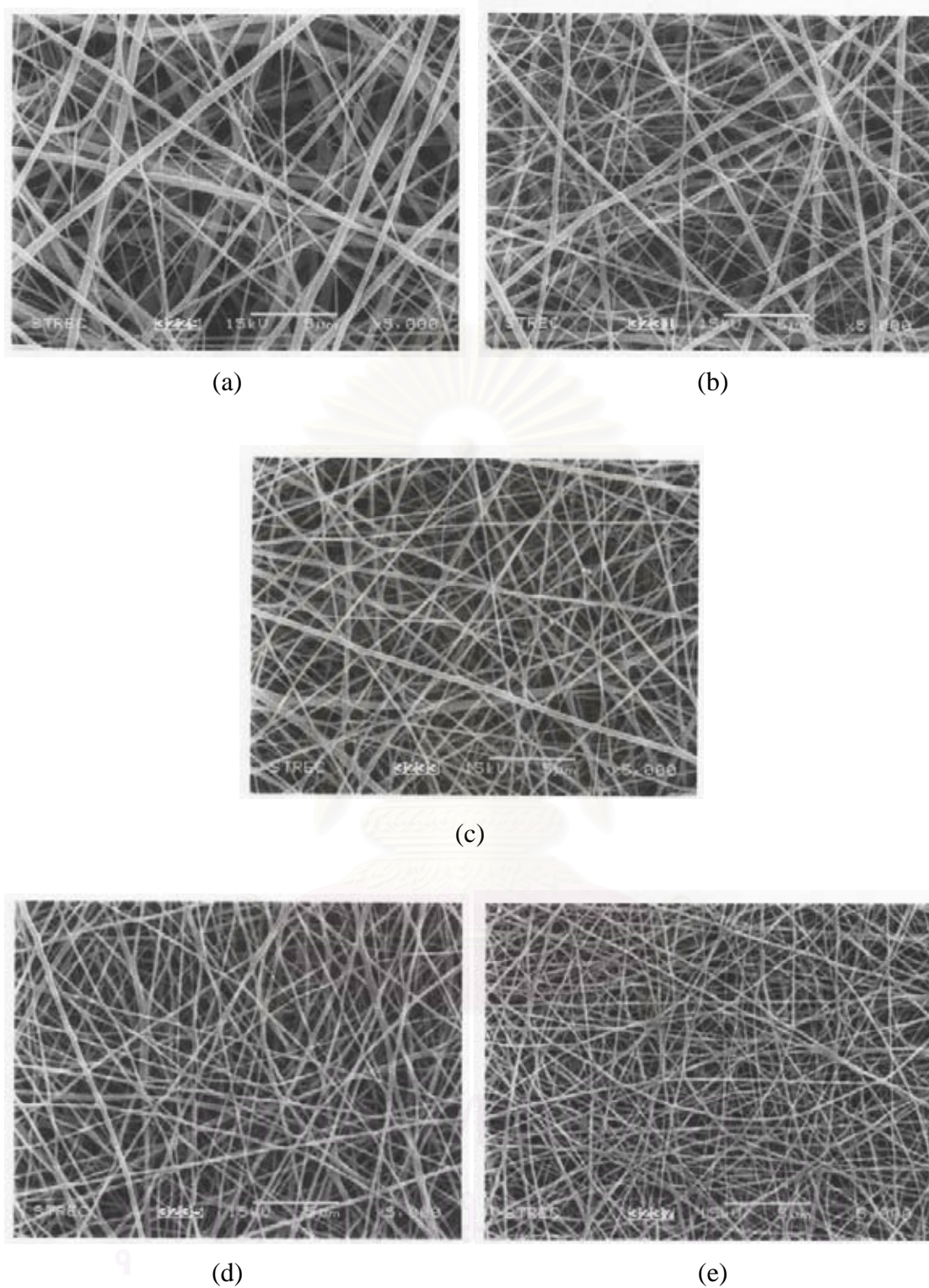


Figure 4.4 SEM images of pre-calcined as-spun fibers from spinning solution containing 13 wt.% PVP solution under different applied electric field strengths: (a) 9, (b) 11.25, (c) 15, (d) 18.75, and (e) 22.5 kV. The distance between the injection orifice and the collector was kept at 7 cm.

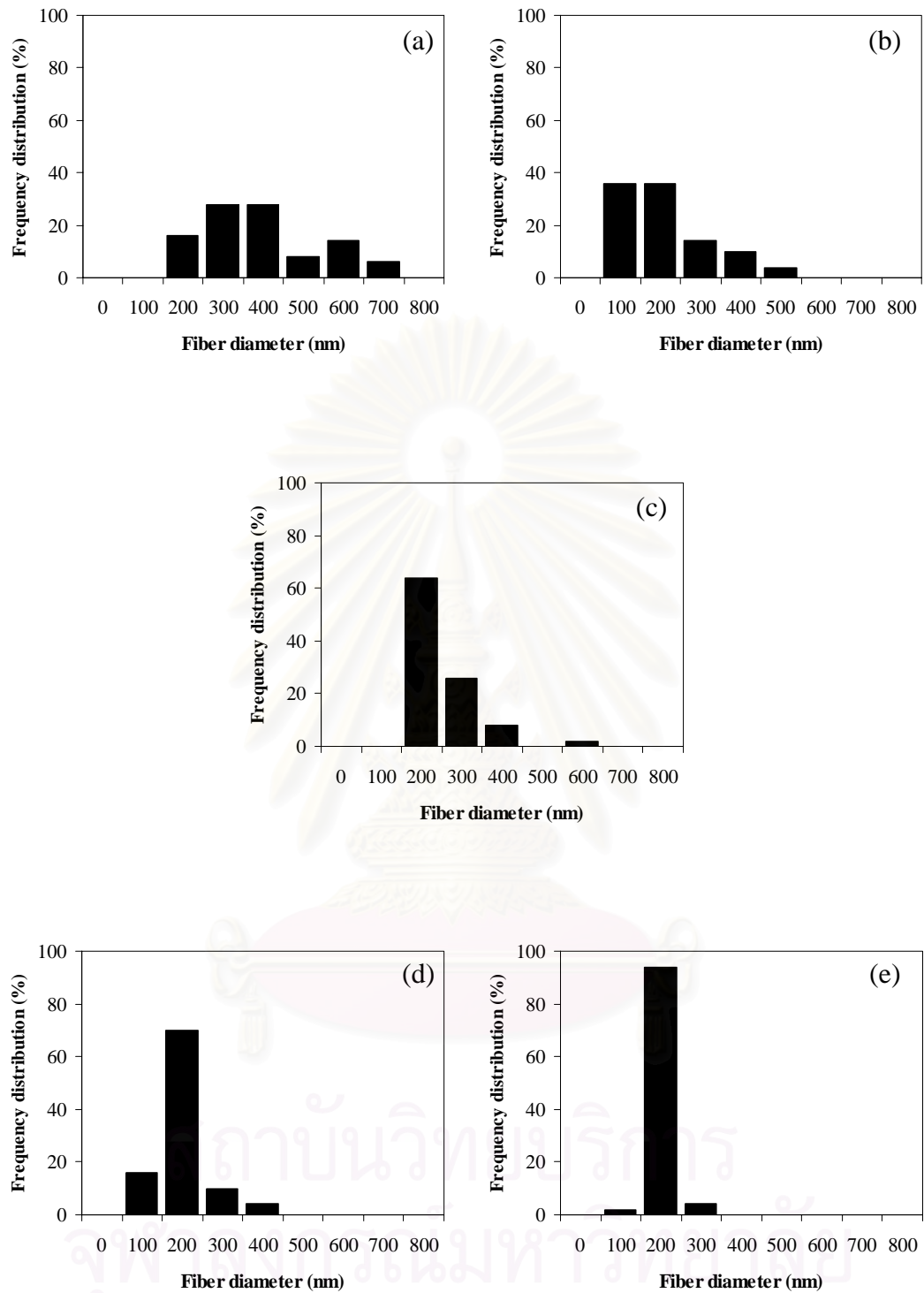


Figure 4.5 Frequency distribution of fiber diameters of pre-calcined as-spun fibers using applied electric potential of: (a) 9, (b) 11.25, (c) 15, (d) 18.75, and (e) 22.5 kV/7 cm.

The increased electrostatic force could lead to an increase in the mass throughput of the liquid jet from the nozzle, while the increased Coulombic repulsion force could lead to a decrease in the fiber diameters. However, when electric field strength becomes too great, the spinning jet becomes unstable, and the average diameter of fibers is was found to increase slightly with increasing electric field strength.

Figure 4.5 indicates the frequency distribution of electrospun fiber diameters. The fiber distribution becomes more narrow with increasing electric field strength. The average fiber diameter decreases from 345 to 145 nm when the applied electric field strength is increased from 9 to 22.5 kV (Figure 4.5(a)-(e), respectively). This observation is contrast with the effect of PVP concentration.

The diameter of  $\text{TiO}_2/\text{PVP}$  composite nanofibers could also be controlled from the distance between the injection orifice and the collector, instead of the applied electric potential. As shown in Figure 4.6, the diameter of nanofibers increases as the distance is increased. In this section, the PVP concentration is fixed at 13 wt.% and a applied voltage is fixed at 15 kV. Figure 4.7 shows the frequency distribution of the pre-calcined as-spun fiber diameter using different values of the collector distance. It can be seen that the fiber diameter is significantly increased with the increasing distance. The average fiber diameter increases from 163 to 350 nm for an increase in the collector distance from 7 to 13 cm (Figure 4.7 (a)-(c), respectively). The relationships of the as-spun fiber diameter with respect to applied electric field strength and the collector distance between the injection orifice and the collector are shown in Figure 4.8.

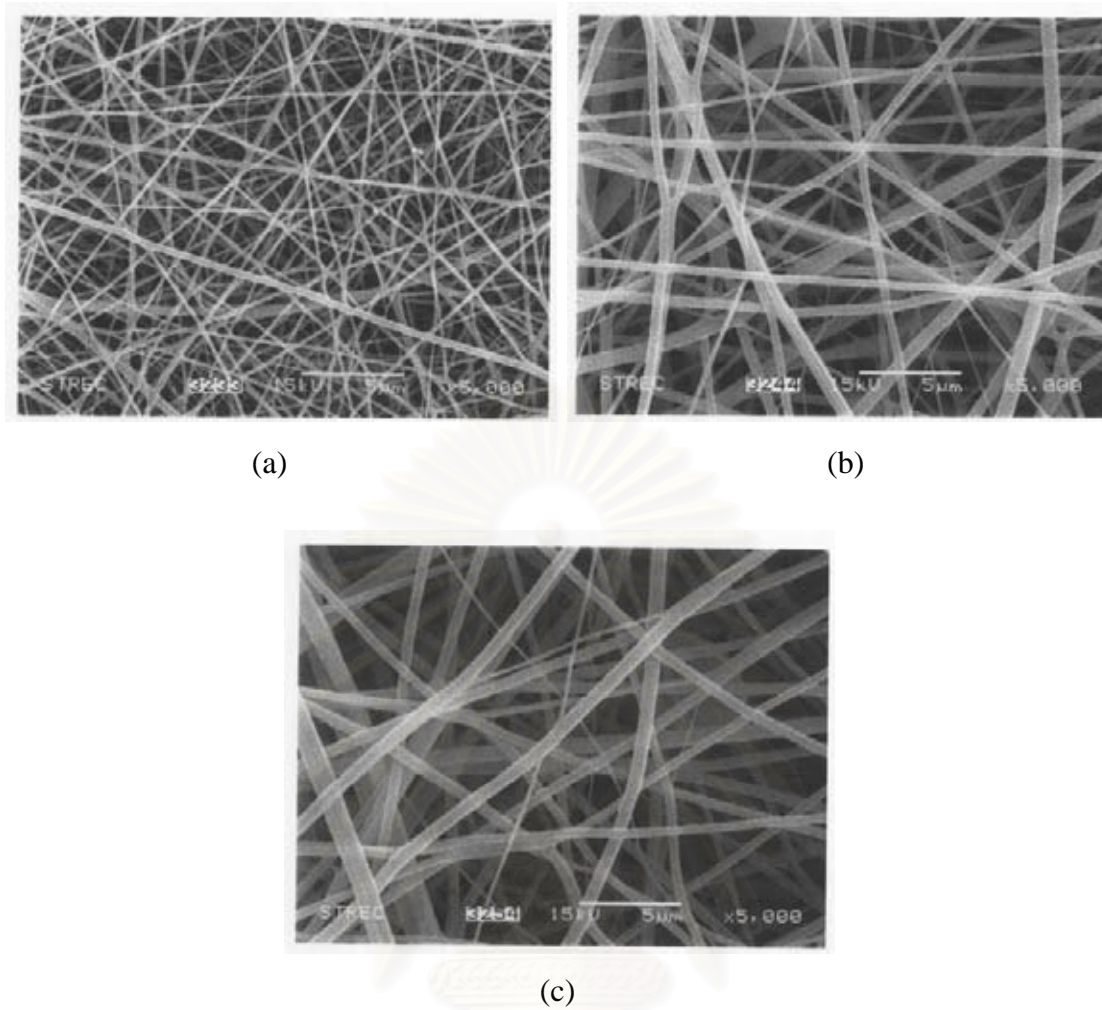


Figure 4.6 SEM images of pre-calcined as-spun fibers across the collection distance of (a) 7, (b) 10, and (c) 13 cm. The PVP concentration of the spinning solution was 13wt.% and the applied electric potential was 15 kV.

สถาบันวิทยบริการ  
จุฬาลงกรณ์มหาวิทยาลัย

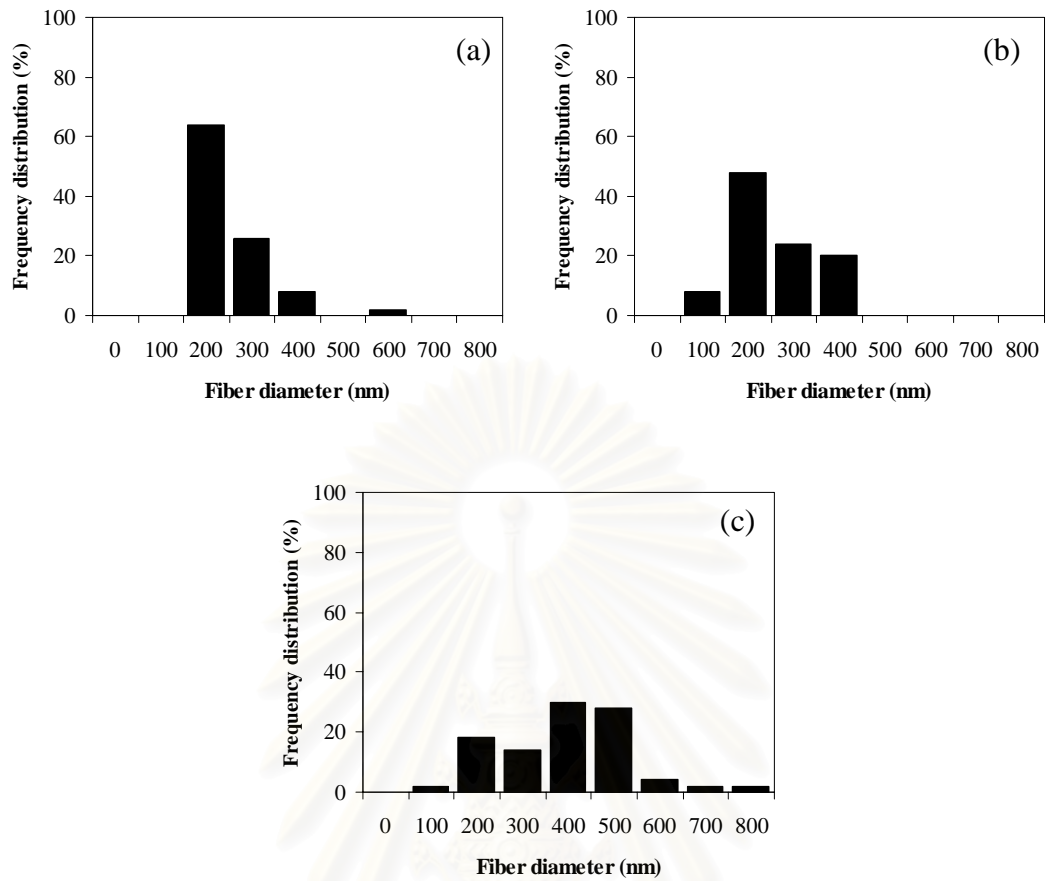


Figure 4.7 Frequency distribution of fiber diameters of pre-calcined as-spun fibers using the collection distance of: (a) 7, (b) 10, and (c) 13 cm.

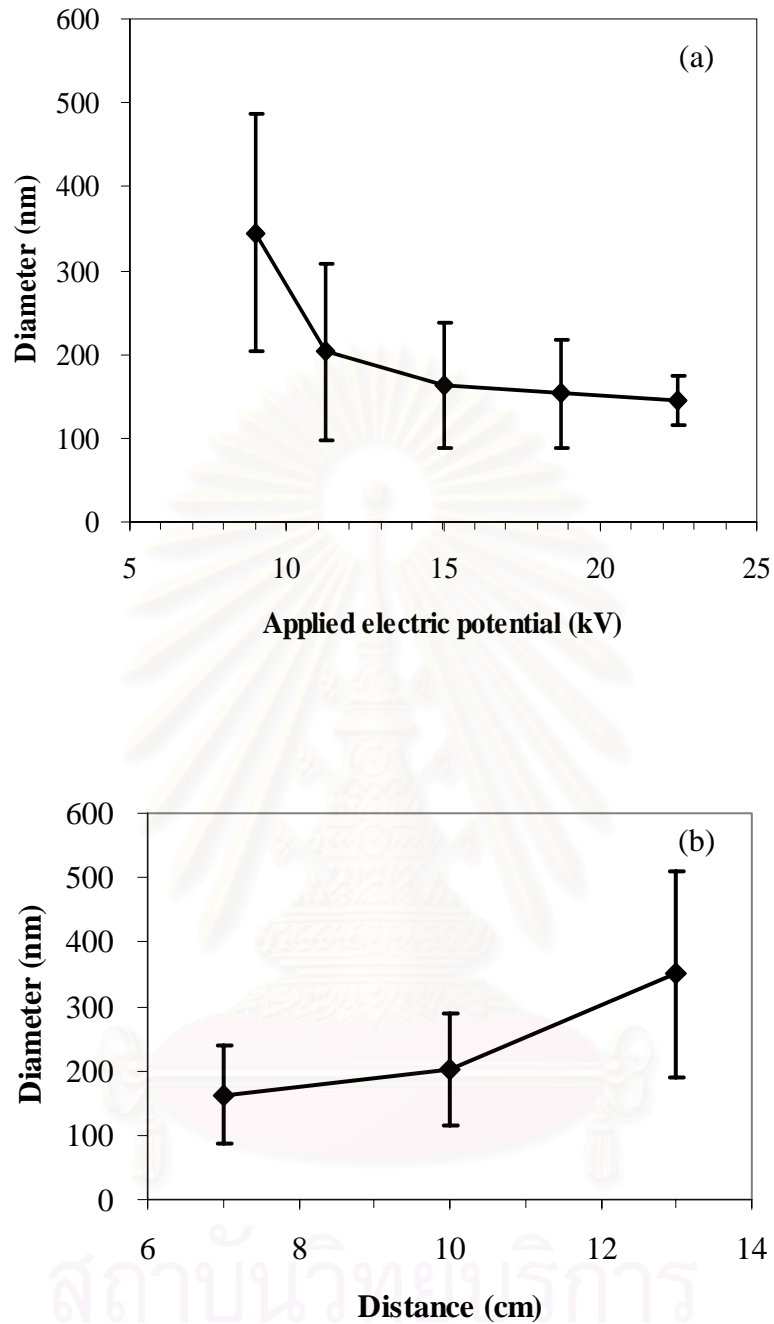


Figure 4.8 Diameters of pre-calcined as-spun fibers as a function of (a) applied electric potential (across a fixed collection distance of 7 cm) and (b) collection distance.

## 4.2 Properties of Titania Nanofibers

After the  $\text{TiO}_2/\text{PVP}$  composite nanofibers were prepared, these fibers were left in air overnight to allow complete hydrolysis of TTIP (fibers prepared from spinning solution containing 13 wt.% PVP solution under applied electric field strengths 15 kV, the distance between the injection orifice and the collector was kept at 7 cm). Then, these nanofibers were subjected to calcination in air at 500, 600, and 800 °C for 3h for the conversion into anatase titania fibers.

### 4.2.1 Thermal Analysis

Figure 4.9 shows the DTA and TGA thermodiagrams for the obtained  $\text{TiO}_2$  nanofibers. According to the TGA analysis, mass of fibers are sharply decreased at temperature up to 500°C and slowly decreases from 500 to 1000°C.

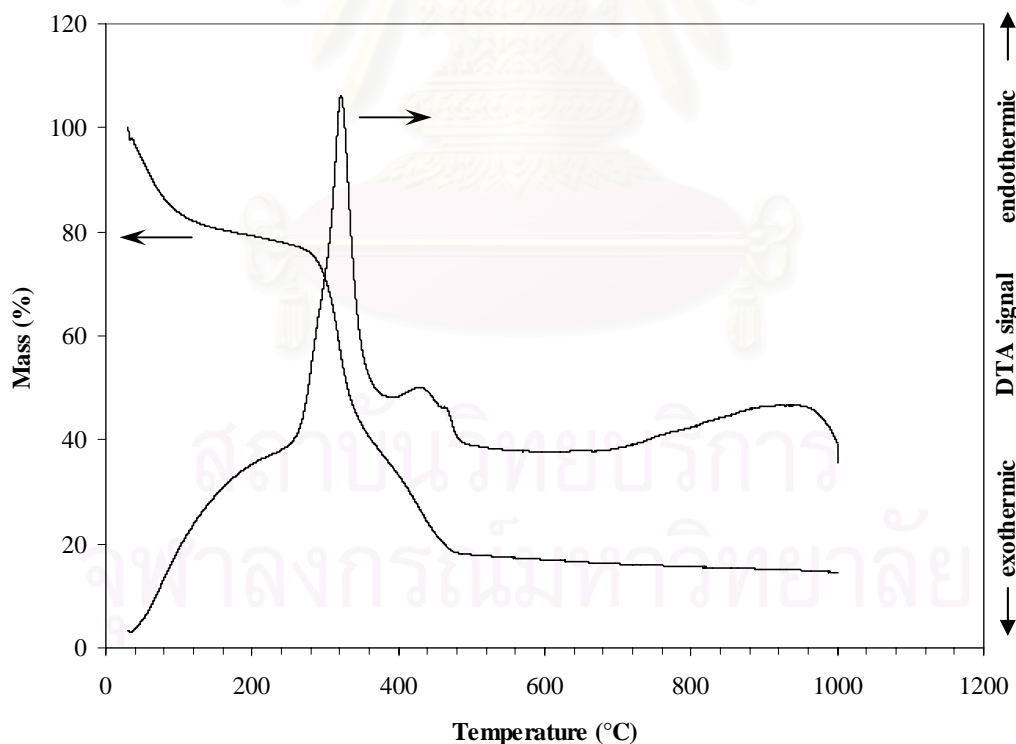


Figure 4.9 TGA-DTA thermodiagram for the undoped  $\text{TiO}_2$  nanofibers.

DTA analysis of the undoped TiO<sub>2</sub> fibers also shows the endothermic peak at 330 and 440 °C. The peak at 330°C is corresponding to the decomposition of PVP and the residual hydroxy group (Hong et al. 2003). On the other hand, the peak at 440°C corresponds to the crystallization of amorphous phase into the anatase phase (Hong et al. 2003). Above 500°C, it can be assumed that the product completely transforms into the anatase phase because there is no further change in fiber weight. It is clear from the TG curve that all the PVP and organic content are completely removed at 500°C, resulting in pure TiO<sub>2</sub> nanofibers.

#### *4.2.2 Morphology of Titania Fibers*

The SEM micrographs of fibers are calcined at different temperatures are shown in Figure 4.10. It can be seen that the surface of the pre-calcined as-spun fibers is smooth according to amorphous nature of TiO<sub>2</sub>/PVP composite fibers (Figure 4.10(a)). Crystallization, however, takes place during the calcination. The titania fibers obtained after calcination at 500°C (Figure 4.10(b)) exhibit significant shrinkage as well as a reduction in fiber diameter due to the decomposition of PVP and the removal of organic content, which is already proved by TGA analysis. After calcination at 600 and 800°C (Figure 4.10(c)-(d)), the average diameter of the titania fibers is only slightly smaller than that of fibers calcined at 500°C. It is thought to be due to the complete removal of organic molecules and the development of titania crystalline after 500°C. Nevertheless, the calcined fibers appear to be more distorted and the surface appeared to be rough. In addition, the fibers structure is retained with polymorphic structures even at high calcination temperature. However, it can be also seen that the fiber surface is much smoother and the particle morphology has changed to one where the fibers appear to consist of linked particles or crystallites.

The frequency distribution for diameters of calcined fibers are shown in Figure 4.11. Before the calcination, the average diameter of the TiO<sub>2</sub>/PVP composite fibers is 240 nm (Figure 4.11(a)). After calcination at 500, 600 and 800°C, the average diameter decreases to 145, 122 and 109 nm, respectively. Figure 4.12 shows the relationship between average diameter of the calcined titania fibers and the calcination temperature, comparing with the diameter of the pre-calcined ones (shown at

temperature of 25°C). Apparently, higher calcination temperature results in greater shrinkage.

The elemental analysis by the Energy Dispersive X-ray Spectroscopy (EDX) equipped on SEM instrument, shown in Figure 4.13, reveals only the presence of Ti and O on the surface. No other metallic element is detected in the final product. It should be noted that gold (Au) was coated on the sample to enhance the contrast of the SEM image.

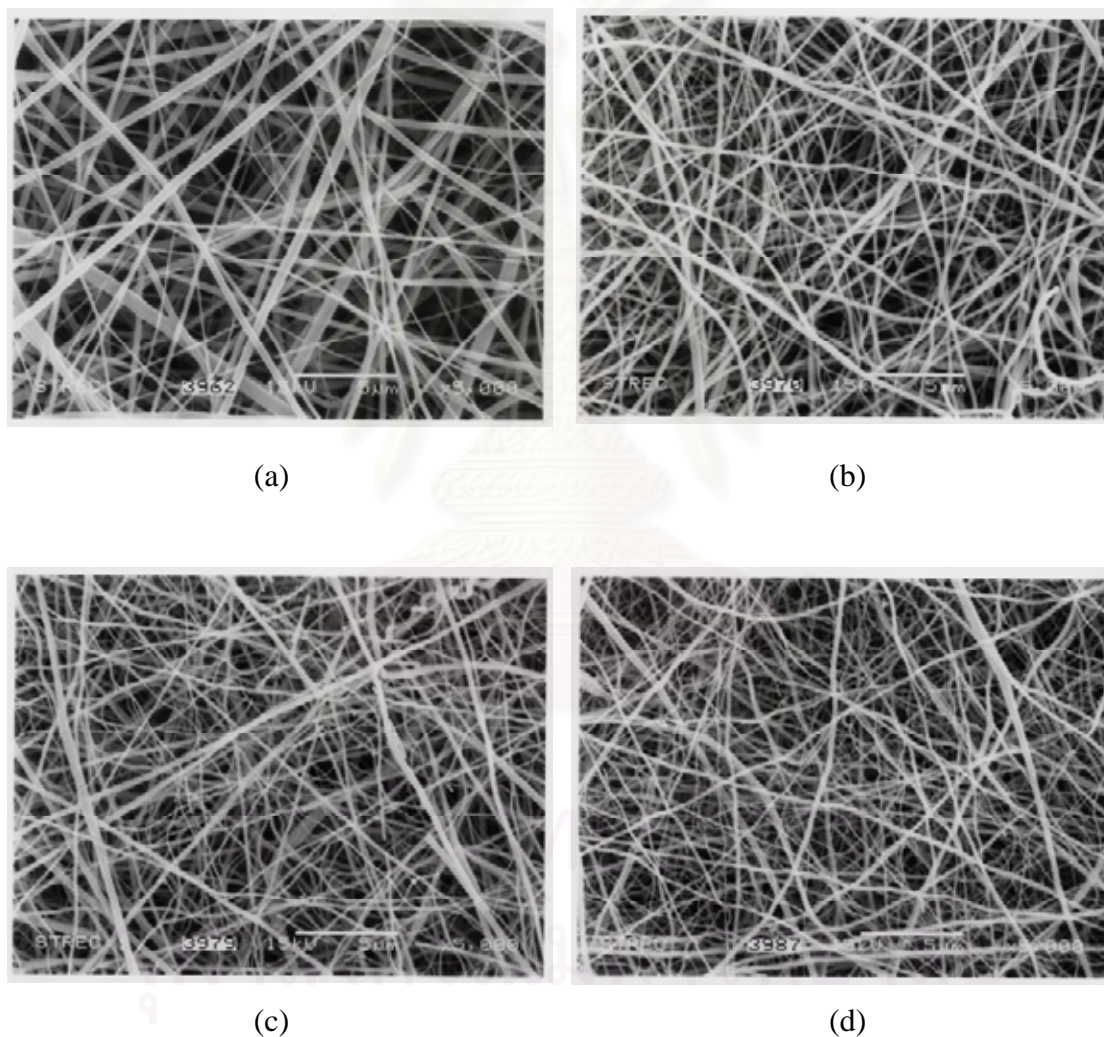


Figure 4.10 SEM images of fibers calcined at different temperature: (a) as-spun fibers, (b) calcined at 500°C, (c) calcined at 600°C, and (d) calcined at 800°C. The PVP concentration of the spinning solution was 13 wt.% and the applied electric field strength was 15 kV/7 cm.

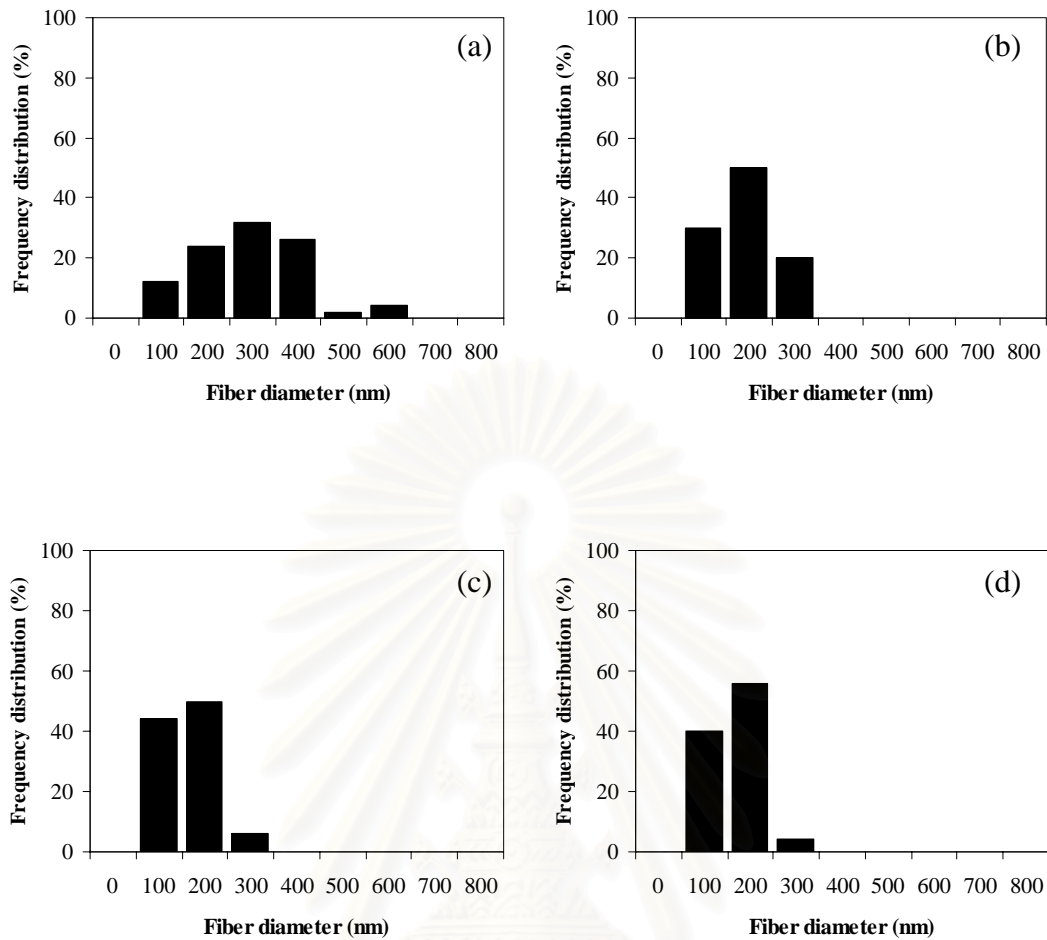


Figure 4.11 Frequency distribution of fiber diameters of titania fibers calcined at different temperatures : (a) pre-calcined as-spun fibers, (b) 500°C, (c) 600°C, and (d) 800°C.

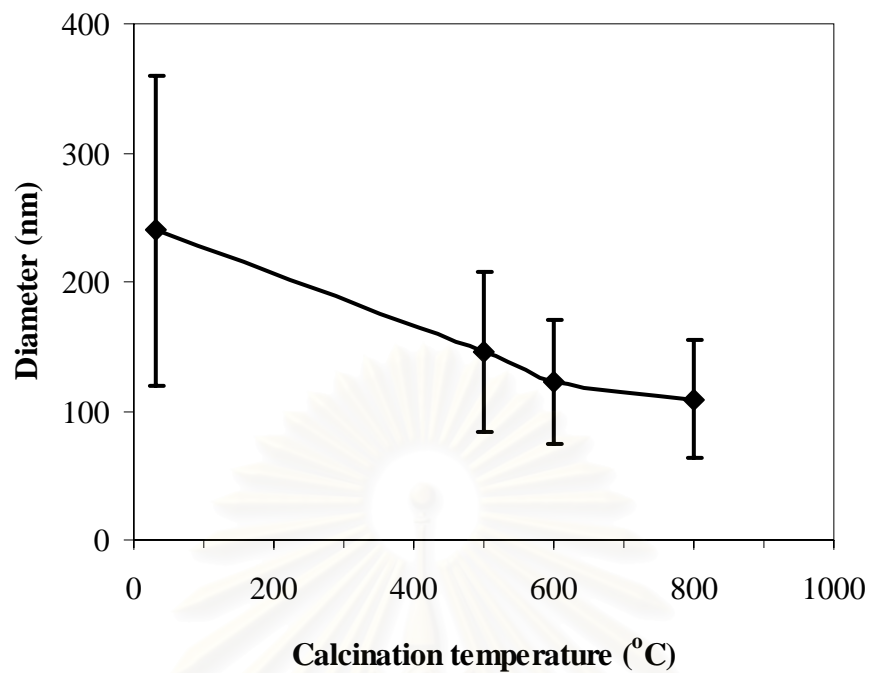


Figure 4.12 Diameters of calcined titania fibers as a function of calcination temperature.

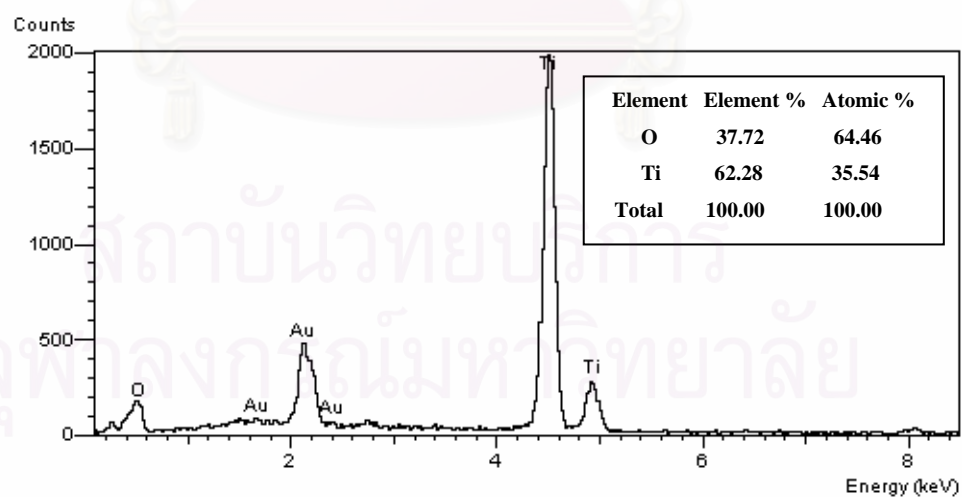


Figure 4.13 EDX spectrum and elemental analysis result of titania fiber.

### 4.2.3 X-ray Diffraction Analysis

The XRD patterns of pre-calcined as-spun TiO<sub>2</sub>/PVP composite fibers and titania fibers after calcination at different temperatures are shown in Figure 4.14. The XRD pattern of the reference anatase titania, JRC-TIO1, from the Catalysis Society of Japan is also shown for comparison. XRD analysis reveals that all of the as-spun fibers prior to calcination are amorphous (Figure 4.14(a)). After calcination at 500°C for 3 h (Figure 4.14 (b)), the major phase of the fiber is an anatase titania with a trace of rutile. No significant amount of rutile phase is observed even at the calcination temperature of 600°C (Figure 4.14(c)), although the content of rutile phase was slightly increased from the calcination at 500°C due to the increasing calcination temperature. At 800°C, only rutile phase is observed (Figure 4.14 (d)). The heat-induced growth of titania crystals contributes to the increase of crystallinity observed from the fact that the X-ray peak becomes sharper and more narrow. The crystallinity of all the titania fibers is increased with an increase in the calcination temperature.

### 4.2.4 FT-IR Analysis

The formation of pure titania fiber is further supported by FT-IR spectra as shown in Figure 4.15. These spectra were recorded in the wave number range of 400 - 4000 cm<sup>-1</sup>. For the pre-calcined as-spun fiber (Figure 4.15(a)), strong bands are observed at wave number between 1000 and 2000 cm<sup>-1</sup>, which can be assigned to the bending and stretching frequencies of PVP (Viswanathamurthi et al. 2004). After calcination at 500°C, all of these strong features are removed. Instead, the band associated with the vibrational mode of the skeletal Ti-O-Ti bonding in anatase titania appears at 470 cm<sup>-1</sup> (Viswanathamurthi et al. 2004) (Figure 4.15 (b)). No sign of adsorbed water, hydroxyl, or hydrocarbon impurities is observed. This result is complimentary with the results from thermal analysis that the organic molecules is completely removed from TiO<sub>2</sub>/PVP composite fibers after calcination at 500°C. It should be noted that there is a shift of the main Ti-O-Ti band from 470 to 700 cm<sup>-1</sup> when the calcination temperature takes place at 600 and 800 °C, (Figure 4.15 (c)-(d), respectively). This is due to the formation of rutile phase in titania fibers structure (Viswanathamurthi et al. 2004). In addition, the broad absorption peak appears near at the wave number 3400 cm<sup>-1</sup> which relates to a stretching vibration of Ti-OH group. At

1620  $\text{cm}^{-1}$ , a band assigned to water also appears. The intensity of absorption peaks due to OH group near 1620 and 3400  $\text{cm}^{-1}$  decrease and finally disappear with an increase of the calcination temperature (Hong et al. 2003).

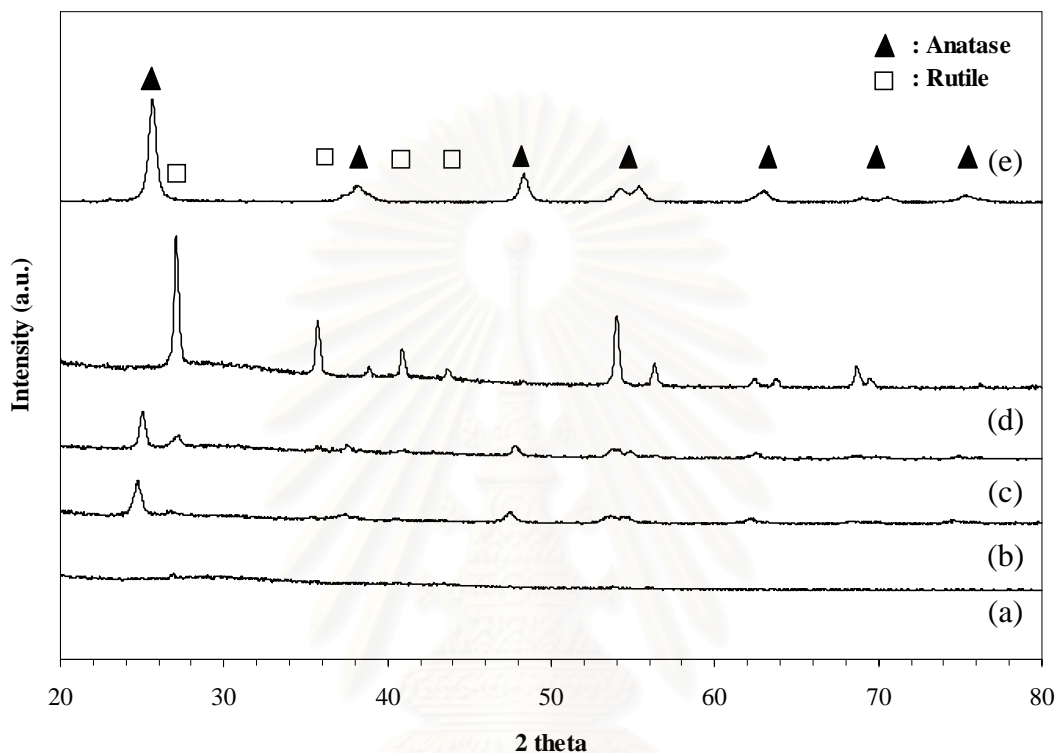


Figure 4.14 XRD patterns of pre-calcined as-spun fibers (a) and titania fibers calcined at temperature of: (b) 500, (c) 600, and (d) 800 °C, comparing with the reference titania (e). The PVP concentration of the spinning solution was 13 wt.% and the applied electric field strength was 15 kV/7 cm.

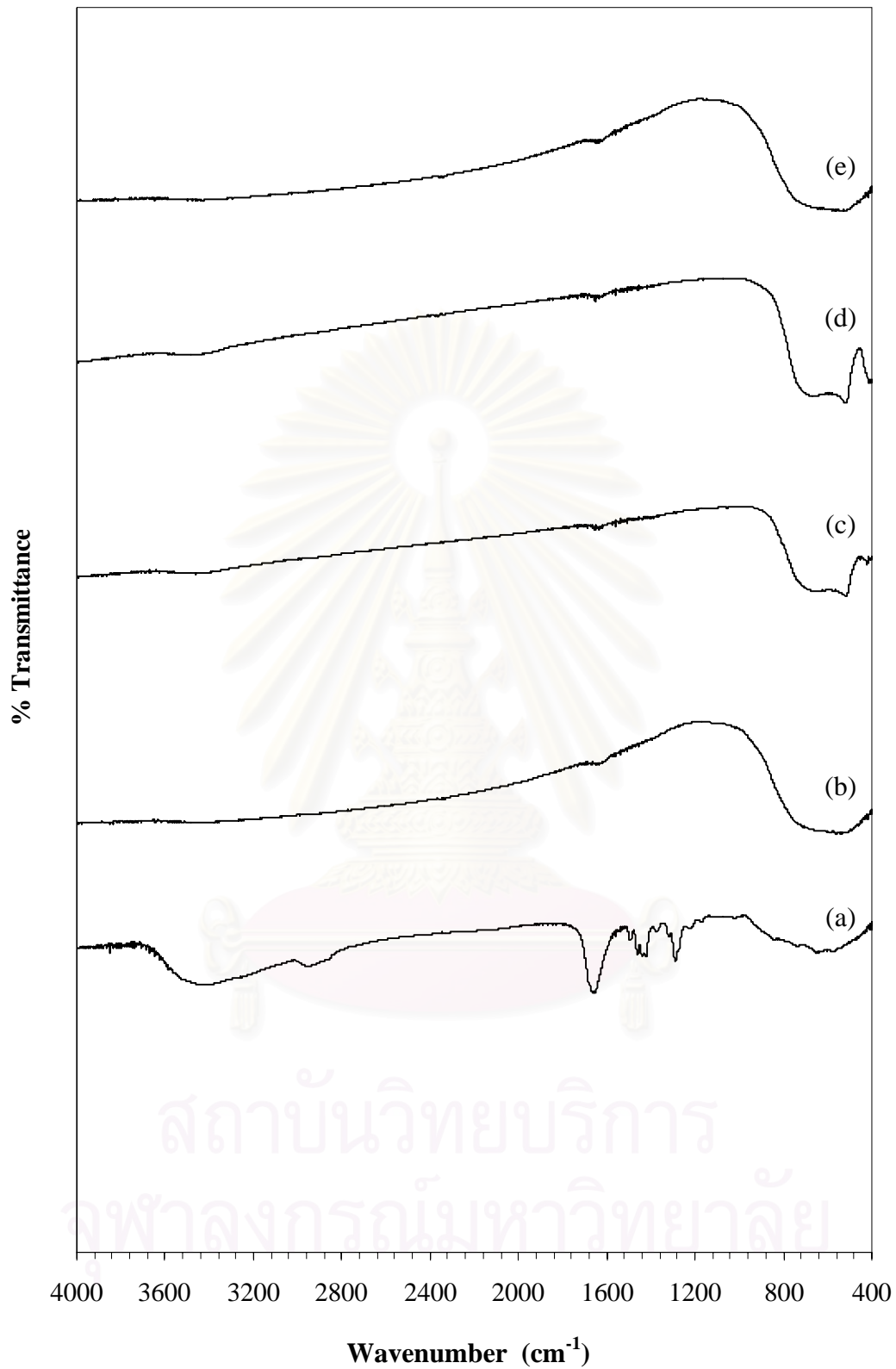


Figure 4.15 FT-IR spectra of pre-calcined as-spun fibers (a) and titania fibers calcined at temperature of: (b) 500, (c) 600, and (d) 800°C, comparing with the reference titania (e).

### 4.3 Effect of Silicon as Secondary Metal Dopant

To improve the photocatalytic activity of titania nanofibers, the major idea of this work is to increase both crystallinity and surface area simultaneously while keeping the major phase of titania as anatase by doping silicon into anatase titania matrix. Silicon is added into titania fibers by doping the spinning solution with TEOS, as previously described in Chapter III. Effects of the content of silicon on size distribution, thermal stability and surface area of fibers are investigated. Finally, photocatalytic activity of the silicon-doped titania fibers is examined from the decomposition of methylene blue (MB).

#### 4.3.1 Properties of Silicon-Doped Titania Fibers

The results from DTA analysis of titania fibers prepared with different amount of silicon (0, 1 and 2 wt.% TEOS, respectively) are shown in Figure 4.16. For the undoped titania (Figure 4.16(a)), the exothermic peak at 440°C corresponding to crystallization of amorphous phase into anatase phase is observed. It is suggested that the exothermic peak at 470°C corresponding to phase transformation from anatase to rutile. According to DTA curves shown in Figure 4.16(a)-(c), however the obtained titania fibers doped with 1 and 2 wt.% of TEOS show the shift of exothermic peak from 470°C to 500 and 520°C, respectively. This result confirms that the addition of silicon into titania fibers, results in suppressing the phase transformation from anatase to rutile.

Figure 4.17-4.19 present the FT-IR spectra of the undoped and silicon doped titania fibers at different calcination temperature with varying the silicon content in the wave number range from 4000 to 400  $\text{cm}^{-1}$ . The peak at the wave number of 800 or 810  $\text{cm}^{-1}$  corresponds to the symmetric vibration of Si-O-Si, 1080-1105  $\text{cm}^{-1}$  for asymmetric  $\nu(\text{Si-O-Si})$  stretching vibration, and 940-960  $\text{cm}^{-1}$  for Ti-O-Si vibration. When silicon was added into titania fibers, the distinct band for Ti-O-Si vibration (960 $\text{cm}^{-1}$ ) was observed. The band for the asymmetric  $\nu(\text{Si-O-Si})$  stretching vibration was observed for all obtained fibers. From the results, it is clear that the silicon exists in the anatase titania fibers and some fraction of metal-O-metal bonding are Ti-O-Si.

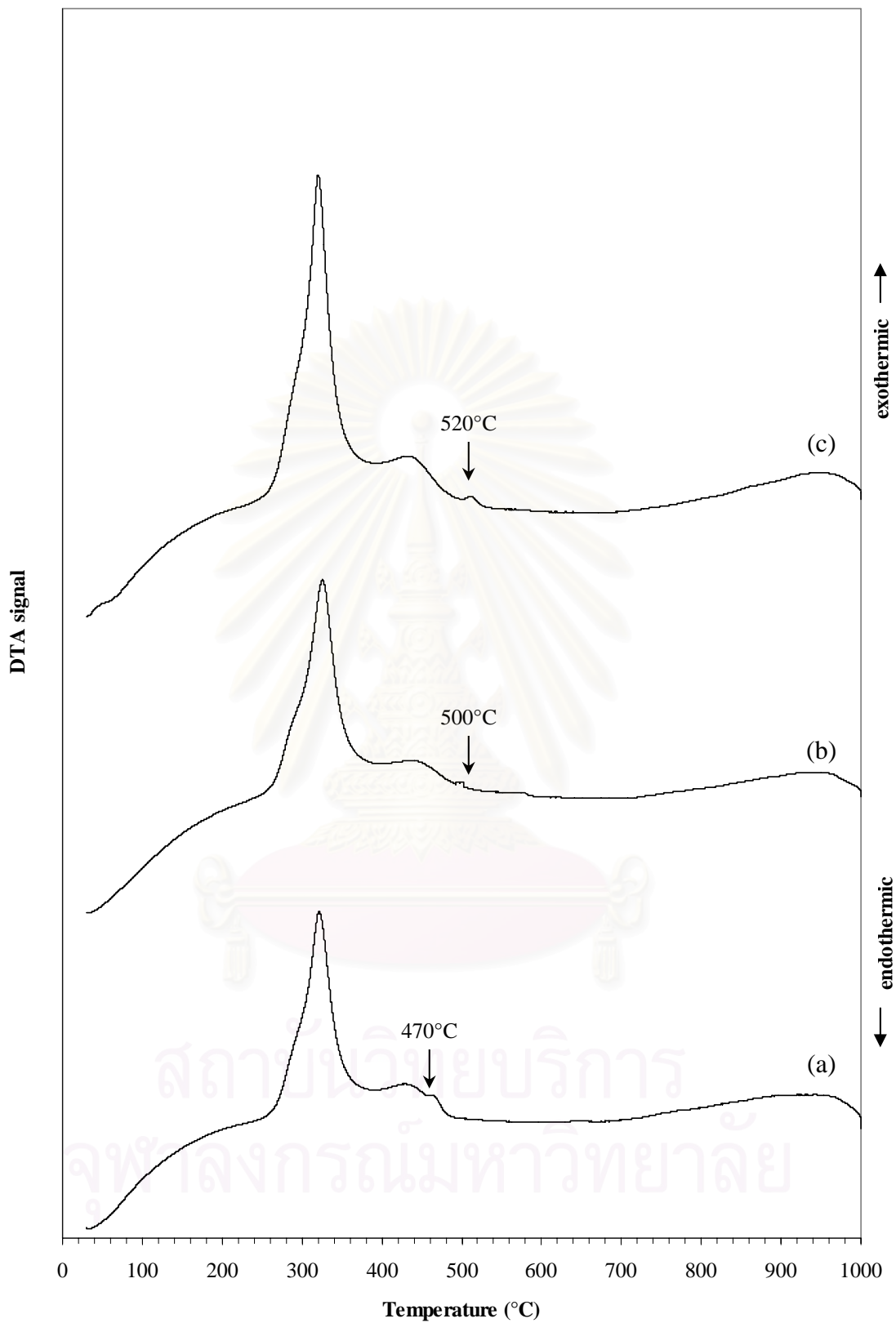


Figure 4.16 DTA thermodiagram for TiO<sub>2</sub> nanofibers: (a) undoped, (b) doped with 1 wt.% TEOS, and (c) doped with 2 wt.% TEOS.

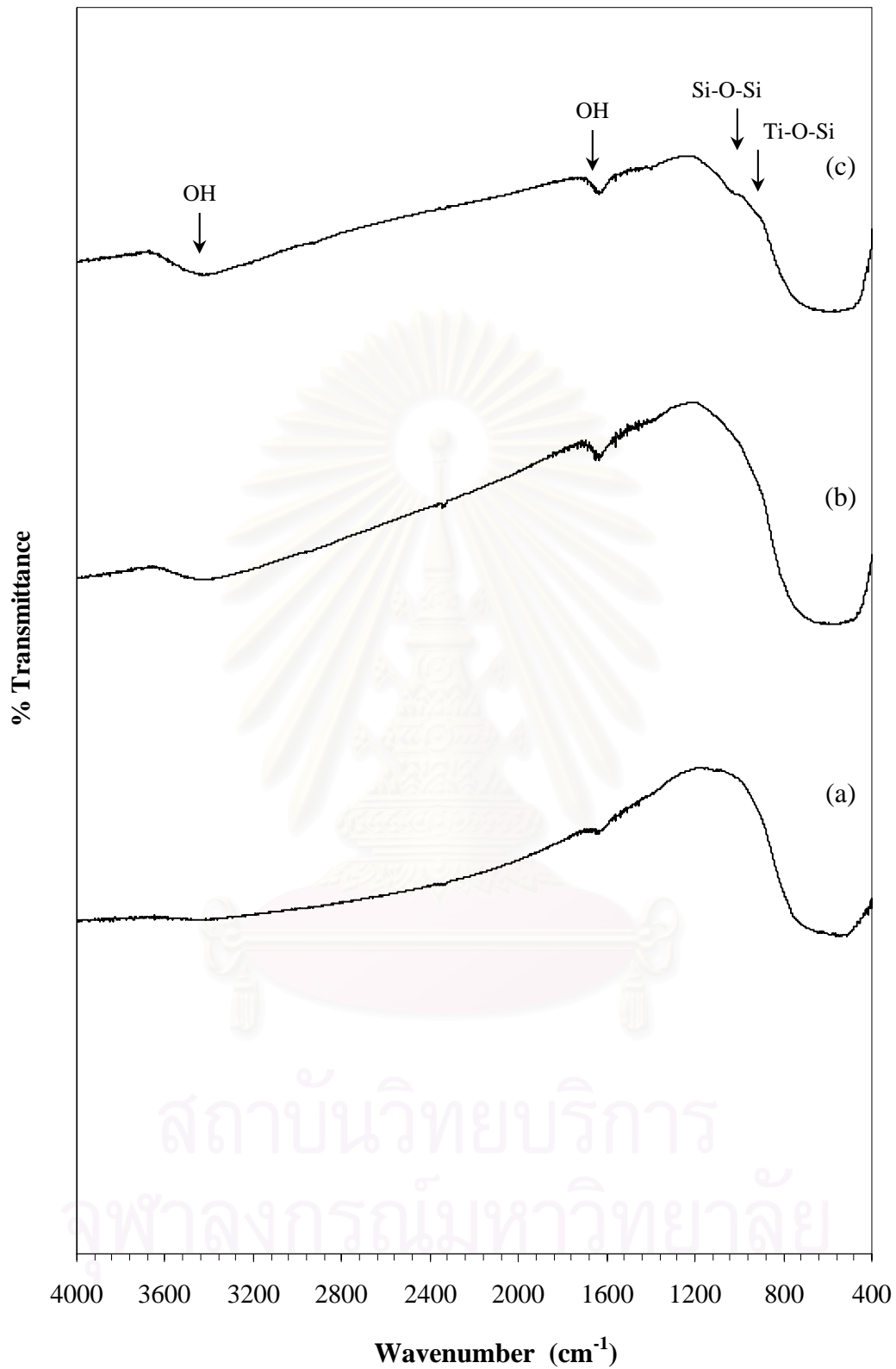


Figure 4.17 FT-IR spectra of titania fibers calcined at 500°C with different silicon content: (a) undoped, (b) 1 wt.% TEOS, and (c) 2 wt.% TEOS.

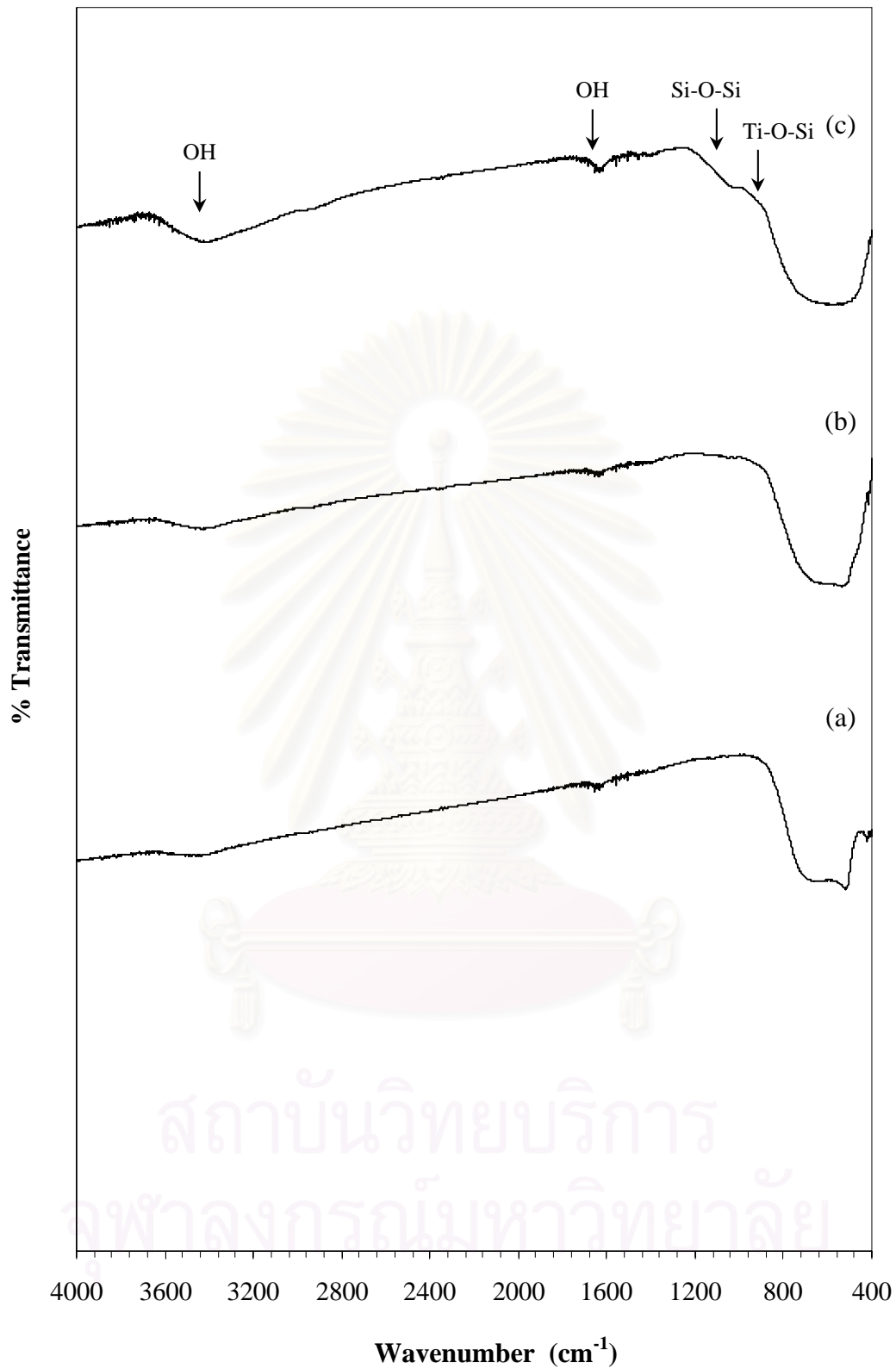


Figure 4.18 FT-IR spectra of titania fibers calcined at 600°C with different silicon content: (a) undoped, (b) 1 wt.% TEOS, and (c) 2 wt.% TEOS.

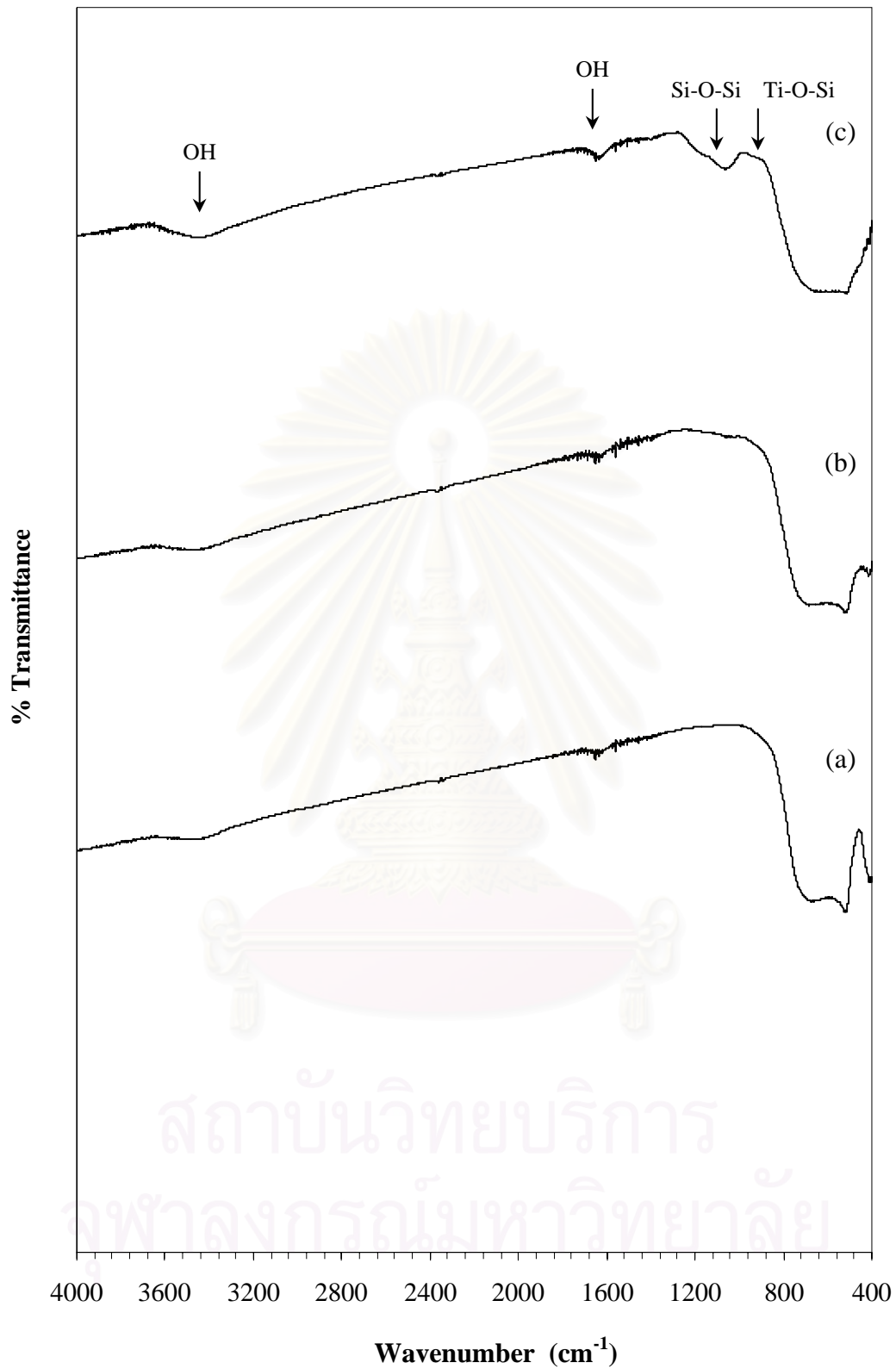
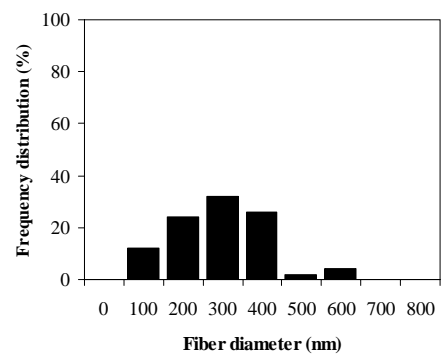
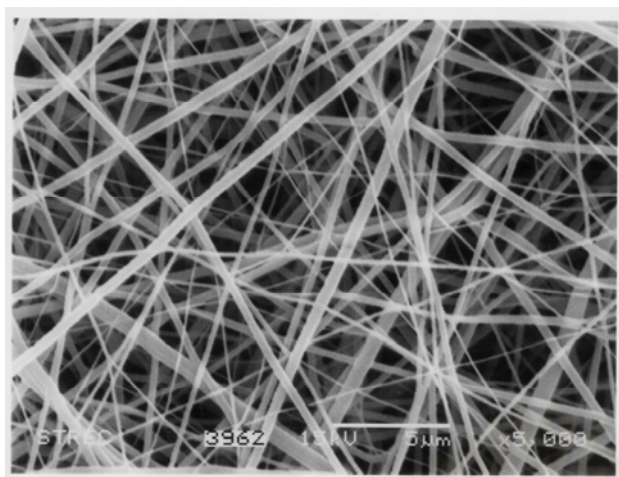


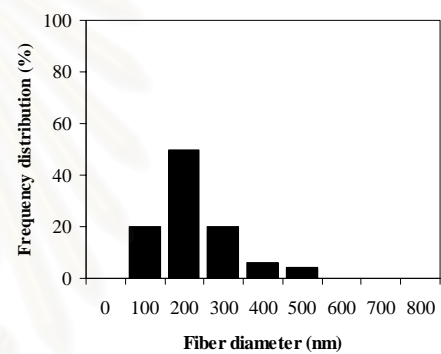
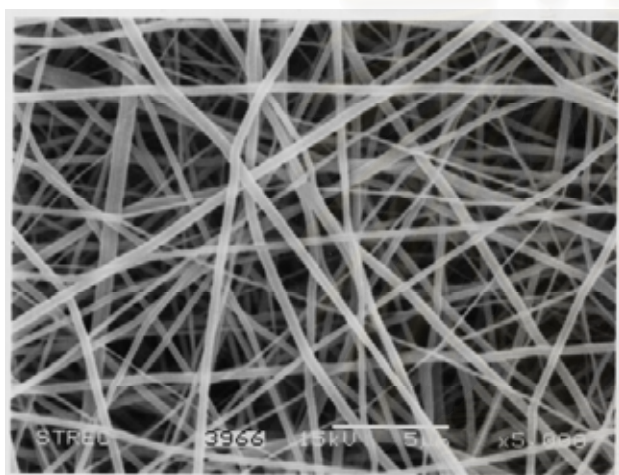
Figure 4.19 FT-IR spectra of titania fibers calcined at 800°C with different silicon content: (a) undoped, (b) 1 wt.% TEOS, and (c) 2 wt.% TEOS.

### 4.3.2 Morphology of Silicon-Doped Titania Fibers

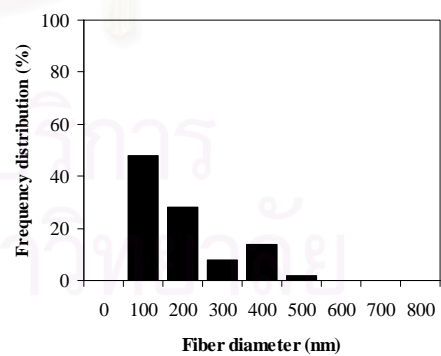
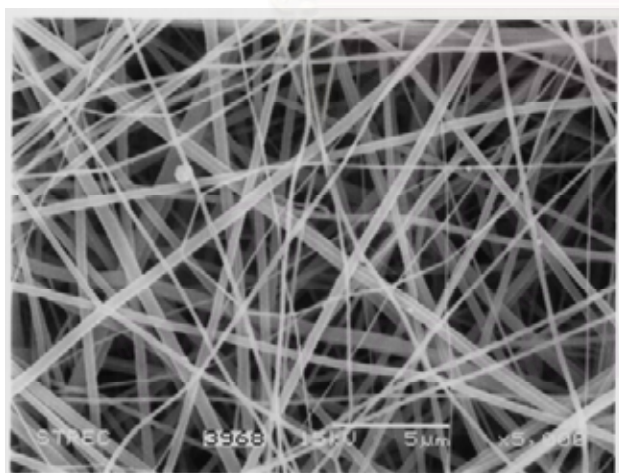
The effect of silicon doping on surface morphology of titania fibers is studied by scanning electron microscopy (SEM). Figure 4.20 shows the morphology of as-spun fibers for both undoped and silicon doped titania fibers. It can be seen that the diameter of the fibers is significantly decreased by small addition of silicon. However, the fiber diameter is slightly increased with an increase in silicon content. It can also be seen that the surface of all fibers is smooth, regardless of silicon doping, because of their amorphous nature. Figure 4.21 shows the morphology of titania fibers with various silicon contents calcined at 500°C. The fiber diameter is markedly decreased, comparing to pre-calcined as-spun fibers. Moreover, the fibers still show shrinkage after the addition of silicon. The fibers are no longer straight and some of the fibers are broken if the silicon content is increased. Similar behavior is also observed from fibers calcined at higher temperatures. Surface morphology of the fibers obtained after calcination at 600 and 800°C are shown in Figure 4.22 and 4.23, respectively. The fibers also show more shrinkage and roughness with addition of silicon.



(a)



(b)



(c)

Figure 4.20 SEM images and frequency distribution of fiber diameters of pre-calcined as-spun fibers: (a) undoped, (b) doped with 1 wt.% TEOS, and (c) doped with 2 wt.% TEOS.

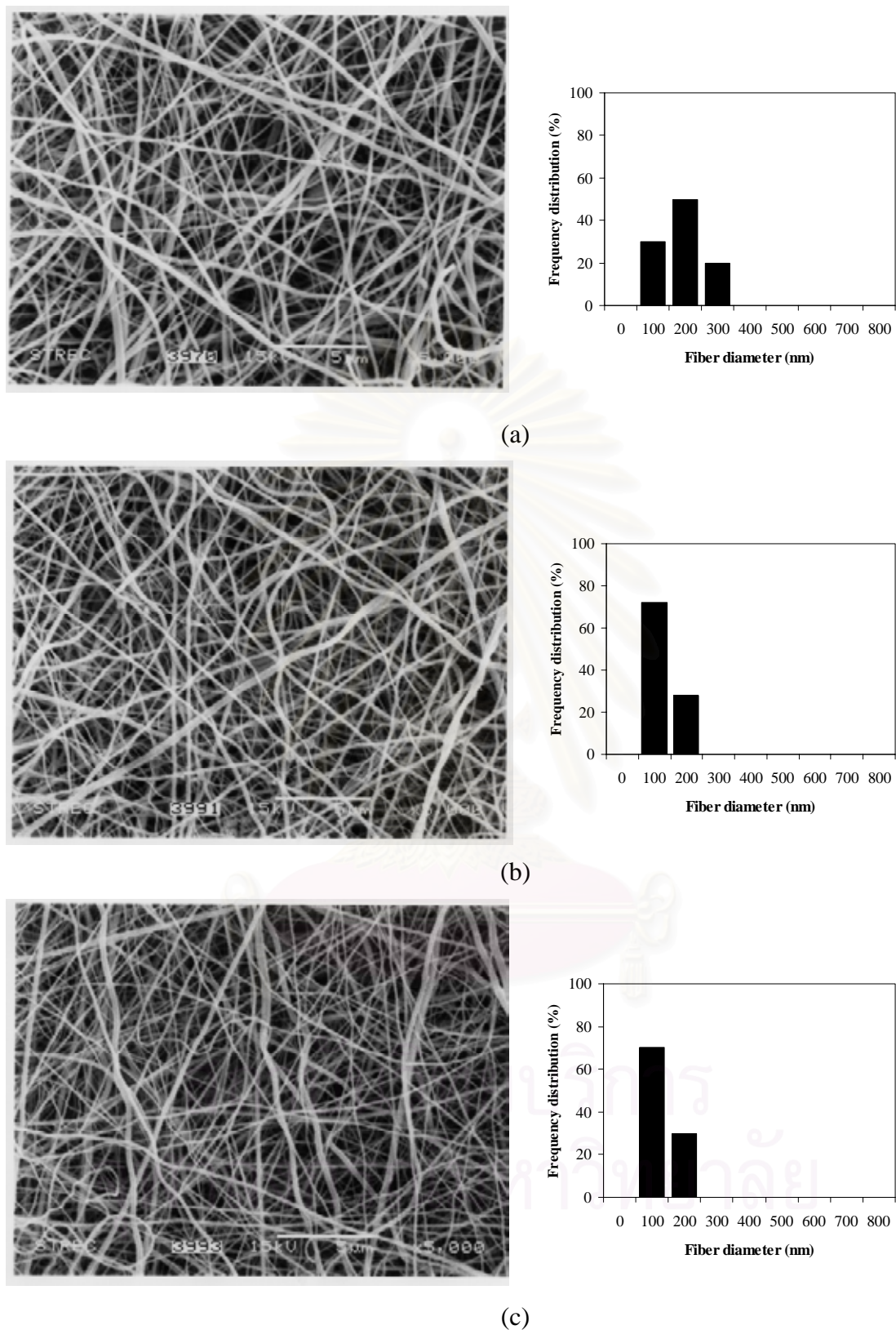


Figure 4.21 SEM images and frequency distribution of fiber diameters of titania fibers calcined at 500°C: (a) undoped, (b) doped with 1 wt.% TEOS, and (c) doped with 2 wt.% TEOS.

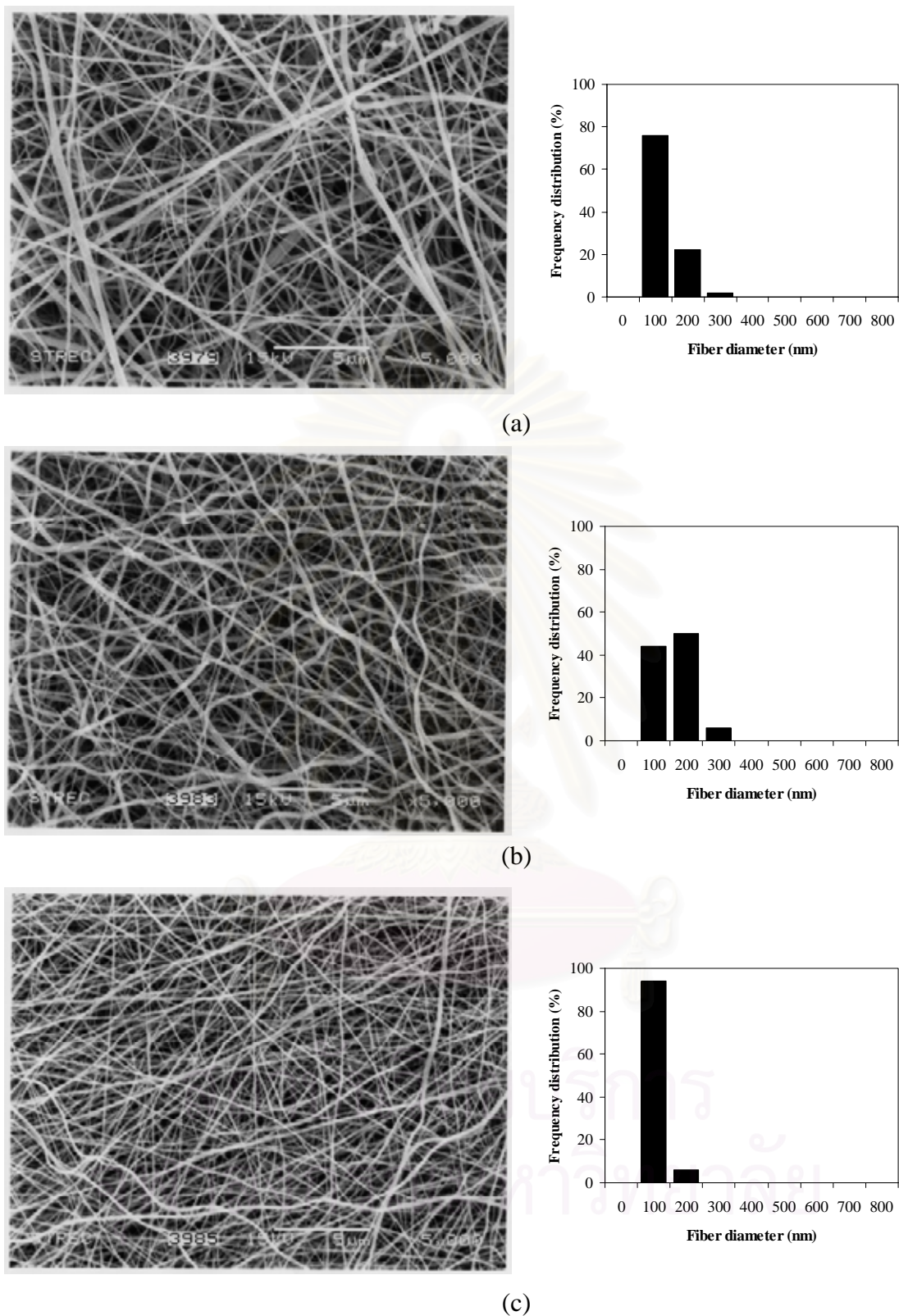


Figure 4.22 SEM images and frequency distribution of fiber diameters of titania fibers calcined at 600°C: (a) undoped, (b) doped with 1 wt.% TEOS, and (c) doped with 2 wt.% TEOS.

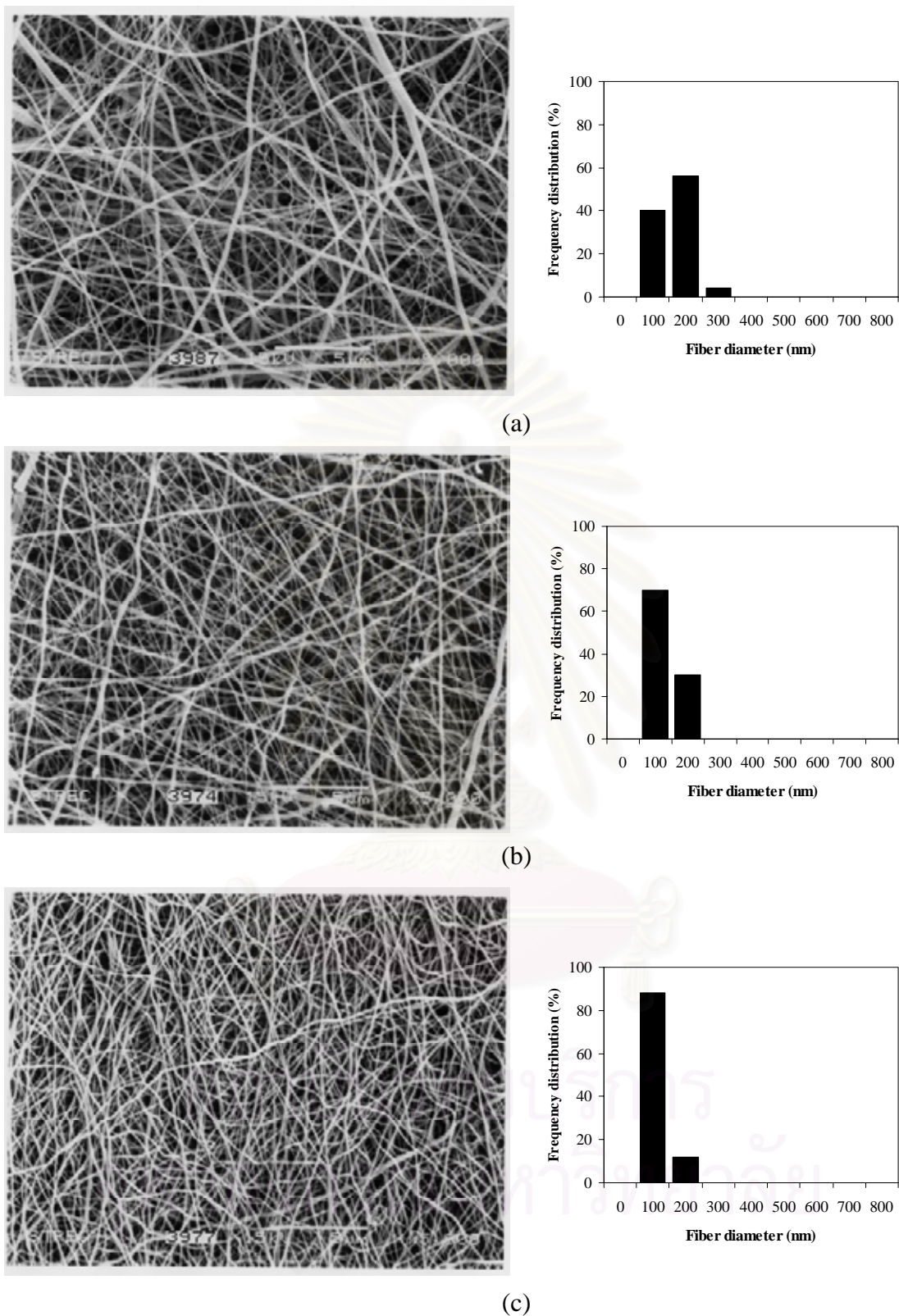


Figure 4.23 SEM images and frequency distribution of fiber diameters of titania fibers calcined at 800°C: (a) undoped, (b) doped with 1 wt.% TEOS, and (c) doped with 2 wt.% TEOS.

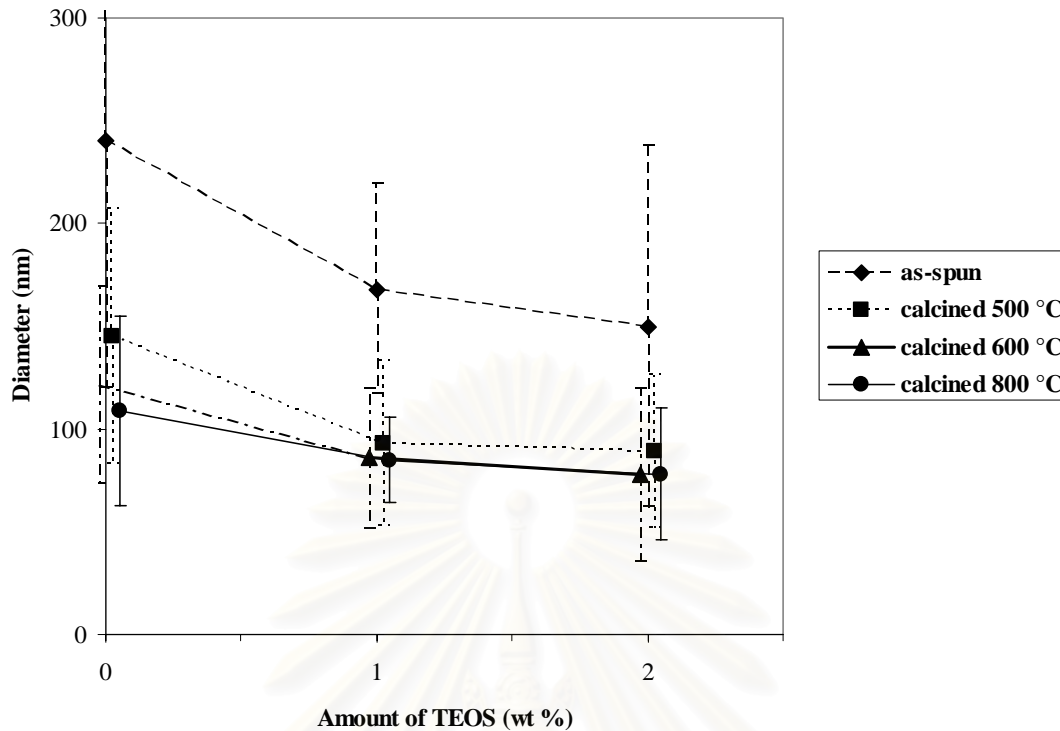
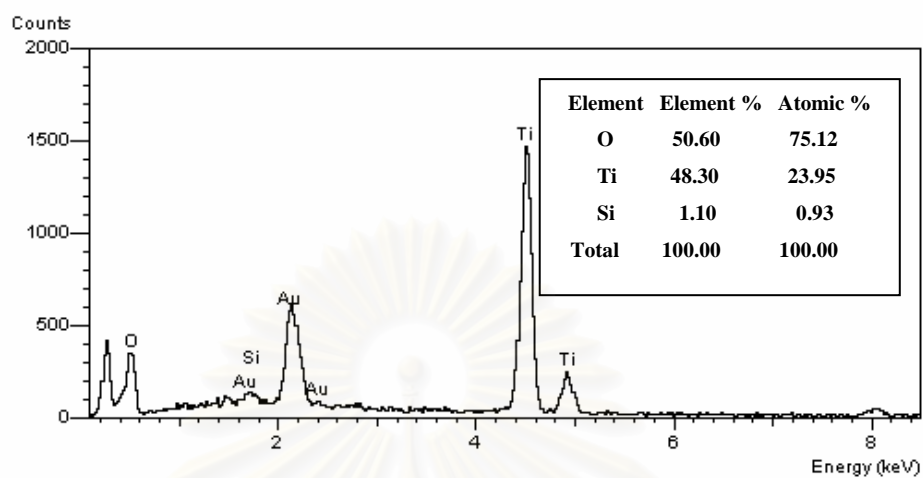


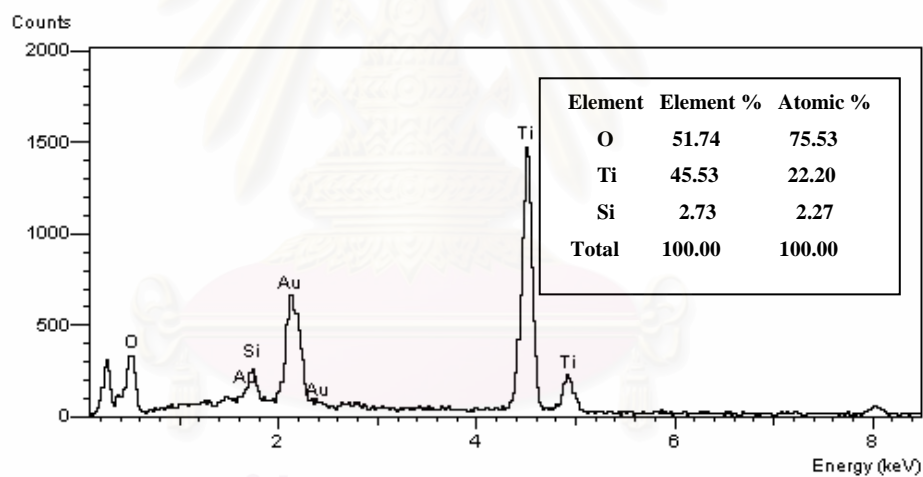
Figure 4.24 Average diameters of as-spun and calcined titania fibers doping with various amount of silicon.

The frequency distribution for diameters of titania fibers are determined from SEM images shown in Figure 4.20-4.23. Before the calcination, average diameter of the fibers decreases from 240 to 150 nm with an increase in silicon content from 0 to 2 wt.% due to the decrease of viscosity of spinning solution. After the calcination at 500, 600 and 800°C, the changes in average diameter of the fibers from silicon doping are found to be decreasing from 145 to 89 nm, from 122 to 78 nm and from 109 to 78 nm, respectively. The average diameters of fibers from various preparation conditions are summarized in Figure 4.24. It should be noted that the points in the plot are intentionally shifted for clarity. The error bar represents standard deviation of the fiber diameters.

The elemental analysis by EDX equipped on SEM instrument reveals the presence of Ti, O and Si on the surface as shown in Figure 4.25. No other metallic element, except Au which is used for sample coating, is observed in the product. The measured Si content (1.10 and 2.73 wt.%) is a slightly higher than that of original calculation (1.00 and 2.00 wt.%).



(a)



(b)

Figure 4.25 EDX spectrum and elemental analysis results of titania fibers doped with: (a) 1 wt.% TEOS and (b) 2 wt.% TEOS.

Surface morphology of undoped and 2 wt.% silicon doped titania fibers are observed by transmission electron microscopy (TEM) as shown in Figure 4.26. It is confirmed that the surface roughness is increased, while fiber diameter is decreased when silicon content in titania is increased. Similar observation has been reported for silicon-doped titania nanoparticles (Viswanath and Ramasamy 1998; Jung and Park. 1999; Jung and Park 2000). The crystallite size of titania decreases when silicon is incorporated into titania crystal (Viswanath and Ramasamy 1998; Jung and Park. 1999; Jung and Park 2000). The higher the silicon content, the smaller the crystal. Consequently, in case of titania fiber which is consisted of numbers of titania nanosized grains as clearly witnessed in Figure 4.26, aggregation of small crystals results in fiber with small diameter. Selected Area electron diffraction (SAED) of the obtained fibers are shown in Figure 4.27. This result indicated that the obtained fibers have polycrystal structure with very high crystallinity. It is further suggested that each grain in the fiber is in fact nanosized titania single crystal. The crystallinity increases with the increase in silicon content. Table 4.1 shows BET surface area of undoped and silicon-doped titania nanofibers at different calcination temperature. It is believed that the addition of silicon into titania fibers resulted in an increase of specific surface area.

#### *4.3.3 Thermal Stability of Silicon-Doped Titania Fibers*

The thermal stability of both undoped and silicon-doped titania fibers was studied by monitoring of crystalline phase of the fibers as a function of calcination temperature. Figure 4.28-4.30 show XRD patterns of the undoped and silicon-doped titania fibers calcined at several temperatures by varying the silicon content. The fibers calcined at 500°C (Figure 4.28) show strong crystalline peaks corresponding to anatase phase of titania fiber with small peaks of rutile phase. The content of rutile phase is slightly decreased by increasing amount of silicon doping. At calcination temperature of 600°C (Figure 4.29), peaks of anatase phase become sharper, which indicates the growth of crystallite grains of anatase. Trace of rutile phase is more distinct after calcination at higher temperature. Nevertheless, fraction of rutile in sample doped with high content of silicon is still significantly smaller than that of undoped titania fibers. After calcination at 800°C (Figure 4.30), only rutile phase is found in the undoped titania fibers, while the silicon-doped titania fibers still contain

appreciable amount of the anatase phase. According to the results, it is confirmed that the silicon-doped titania fibers has high thermal stability. The presence of silicon in titania structure results in the suppression of phase transformation from anatase to rutile as shown in Table 4.2. This observation is in agreement with the findings reported in the literature for titania nanoparticles (Viswanath and Ramasamy 1998; Jung and Park. 1999; Jung and Park 2000).

Table 4.1 BET surface area of undoped and silicon-doped titania nanofibers at different calcination temperature.

| Calcination<br>Temperature (°C) | BET surface area (m <sup>2</sup> /g) |             |             |
|---------------------------------|--------------------------------------|-------------|-------------|
|                                 | 0 wt.% TEOS                          | 1 wt.% TEOS | 2 wt.% TEOS |
| 500                             | 64.48                                | 82.59       | 98.28       |
| 600                             | 51.26                                | 63.04       | 70.57       |
| 800                             | 37.47                                | 50.34       | 60.21       |

\* Surface area of JRC-TIO1 is 53 m<sup>2</sup>/g.

Table 4.2 Percent of rutile phase of undoped and silicon-doped titania nanofibers at different calcination temperature.

| Calcination<br>Temperature (°C) | % of rutile** |             |             |
|---------------------------------|---------------|-------------|-------------|
|                                 | 0 wt.% TEOS   | 1 wt.% TEOS | 2 wt.% TEOS |
| 500                             | 9.97          | 4.00        | 2.48        |
| 600                             | 30.38         | 22.96       | 12.39       |
| 800                             | 100.00        | 80.60       | 24.65       |

\* JRC-TIO1 is pure-anatase titania.

\*\* Calculation according to literature (Jung and Park. 1999).

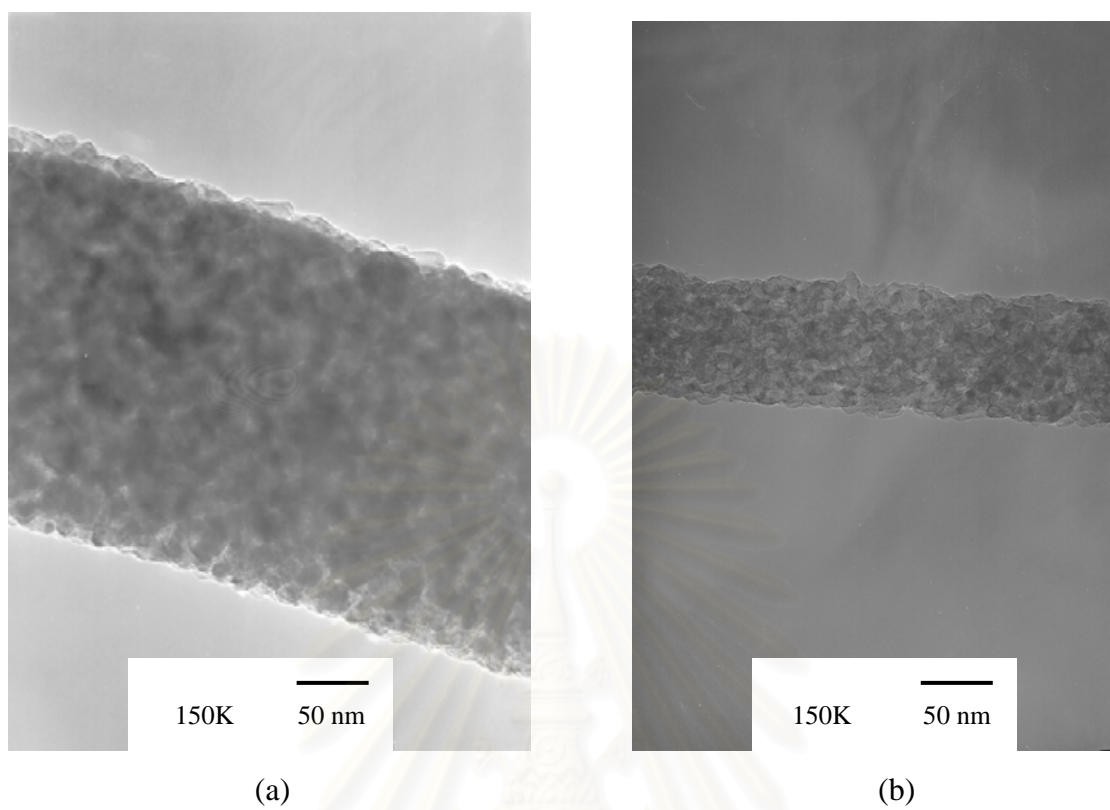


Figure 4.26 TEM images of titania fibers calcined at 500°C: (a) undoped and (b) doped with 2 wt.% TEOS.

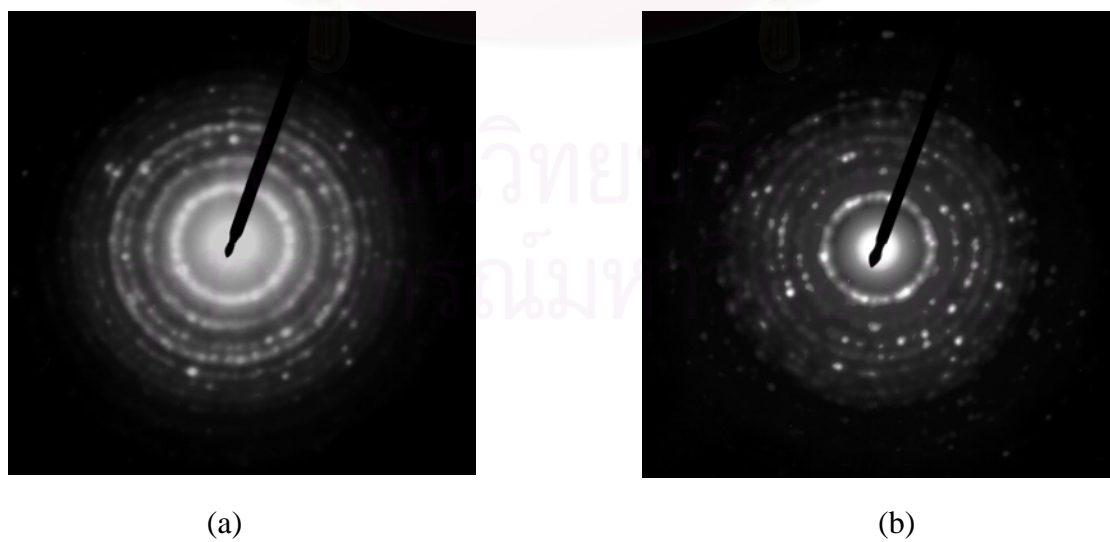


Figure 4.27 SAED images of titania fibers calcined at 500°C: (a) undoped and (b) doped with 2 wt.% TEOS.

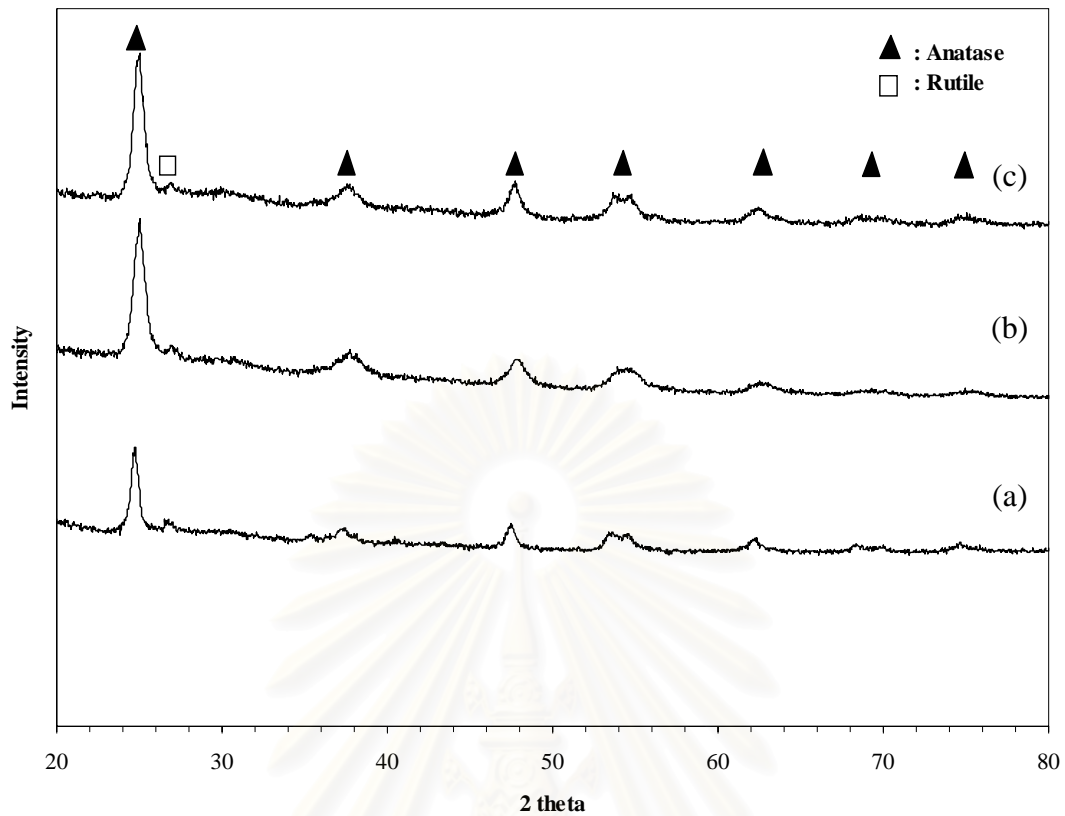


Figure 4.28 XRD patterns of titania fibers calcined at 500°C with different silicon content: (a) undoped, (b) 1 wt.% TEOS, and (c) 2 wt.% TEOS.

สถาบันวิทยบริการ  
จุฬาลงกรณ์มหาวิทยาลัย

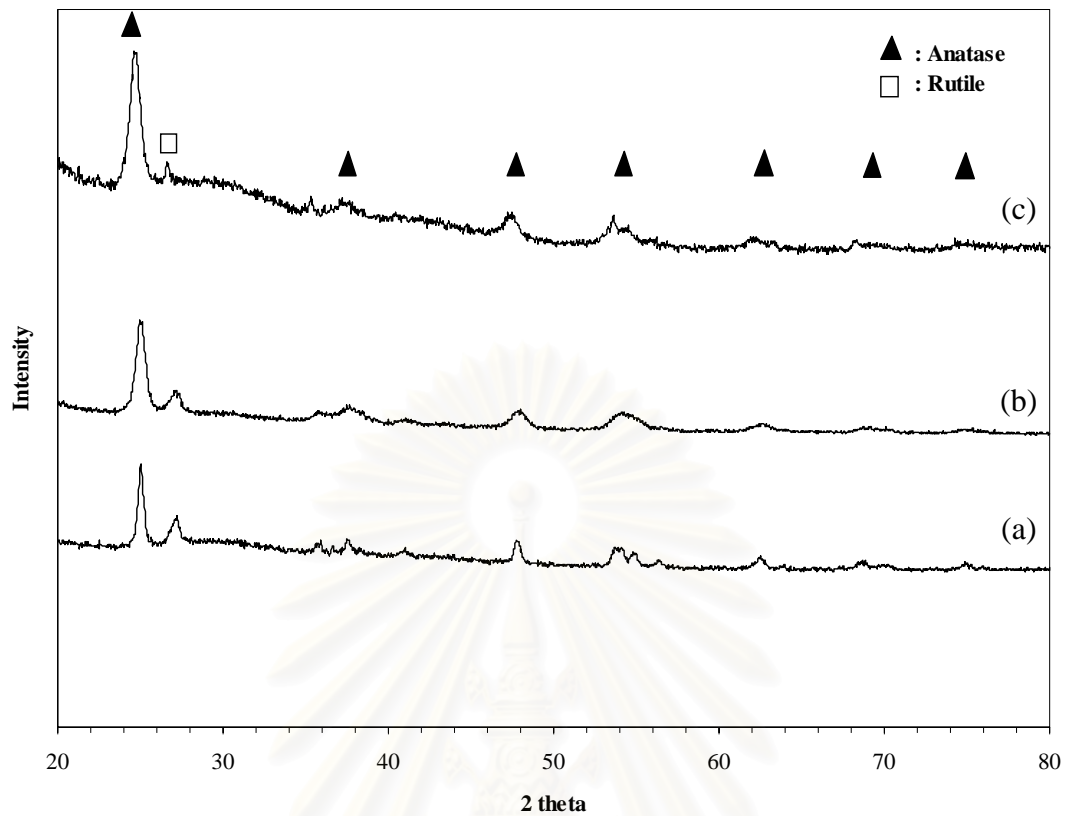


Figure 4.29 XRD patterns of titania fibers calcined at 600°C with different silicon content: (a) undoped, (b) 1 wt.% TEOS, and (c) 2 wt.% TEOS.

สถาบันวิทยบริการ  
จุฬาลงกรณ์มหาวิทยาลัย

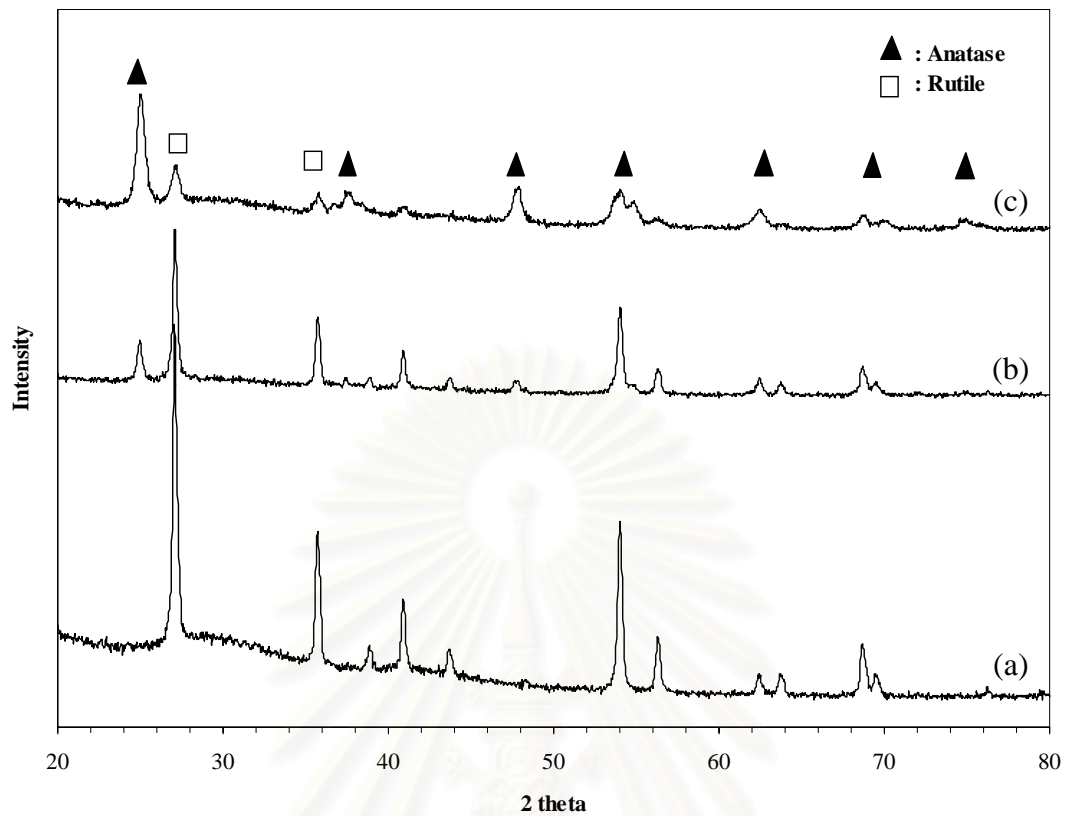


Figure 4.30 XRD patterns of titania fibers calcined at 800°C with different silicon content: (a) undoped, (b) 1 wt.% TEOS, and (c) 2 wt.% TEOS.

สถาบันวิทยบริการ  
จุฬาลงกรณ์มหาวิทยาลัย

#### 4.3.4 Photocatalytic Activity

Photocatalytic activity of the synthesized titania fibers is evaluated from the degradation of methylene blue (MB), under UV light irradiation. Preliminary evaluations indicate that insignificant amount of MB is degraded in absence of UV light (dark condition). Moreover, self degradation of MB, i.e. degradation of MB without using titania as catalyst, is much slower than photocatalytic degradation of MB on titania (Cheng et al. 2003; Hirano and Ota 2004). In this work, standard anatase pure  $\text{TiO}_2$  (JRC-TIO1) is used as reference catalyst.

Activity of titania fibers is first investigated in flake form. The mat of calcined fibers was broken off into large pieces and suspended in MB solution. The system was kept in the dark for 1 h to minimize the effect of MB absorption, before UV light irradiation. The results for MB photodegradation using titania fibers doped with different amount of silicon are shown in Figure 4.31-4.33. Generally, it can be seen that the highest extent and the fastest rate of the decomposition is achieved when titania fibers doped with 2 wt.% TEOS is employed. The higher the silicon content in fibers, the better the MB decomposition. As shown in Figure 4.31, where all fibers are calcined at  $500^\circ\text{C}$ , titania fibers doped with 2 wt.% TEOS results in 85% decomposition within 6 h, while about 78% decomposition is achieved by undoped fibers. It is believed to be the results from the higher fraction of anatase phase in fibers, the increase specific surface area, high crystallinity, smaller grain size and the formation of Ti-O-Si, which acts as an active site for reaction.

For fibers calcined at  $600^\circ\text{C}$ , as shown in Figure 4.32, the extents of the MB decomposition from titania fibers with 1 and 2 wt.% TEOS still remain in relatively high level, i.e. 74% and 78% decomposition after 6 h, respectively. On the other hand, decomposition rate of the undoped titania fibers is dramatically decreased (34% decomposition), comparing to the same fibers calcined at  $500^\circ\text{C}$ . This result is due to the formation of rutile phase in titania fibers, as witnessed from XRD analysis, which has been recognized as inactive phase of titania. Formation of rutile phase also leads to increased size and decreased specific surface area of fibers. At calcinations temperature of  $800^\circ\text{C}$ , majority of titania in undoped and 1 wt.% TEOS doped fibers transforms to rutile phase, which consequently results in very low MB decomposition

rate achieved, as seen in Figure 4.33. On the contrary, for fibers doped with 2 wt.% TEOS which has been proved to contain significant fraction of anatase phase, the achievable extent of MB decomposition is still high.

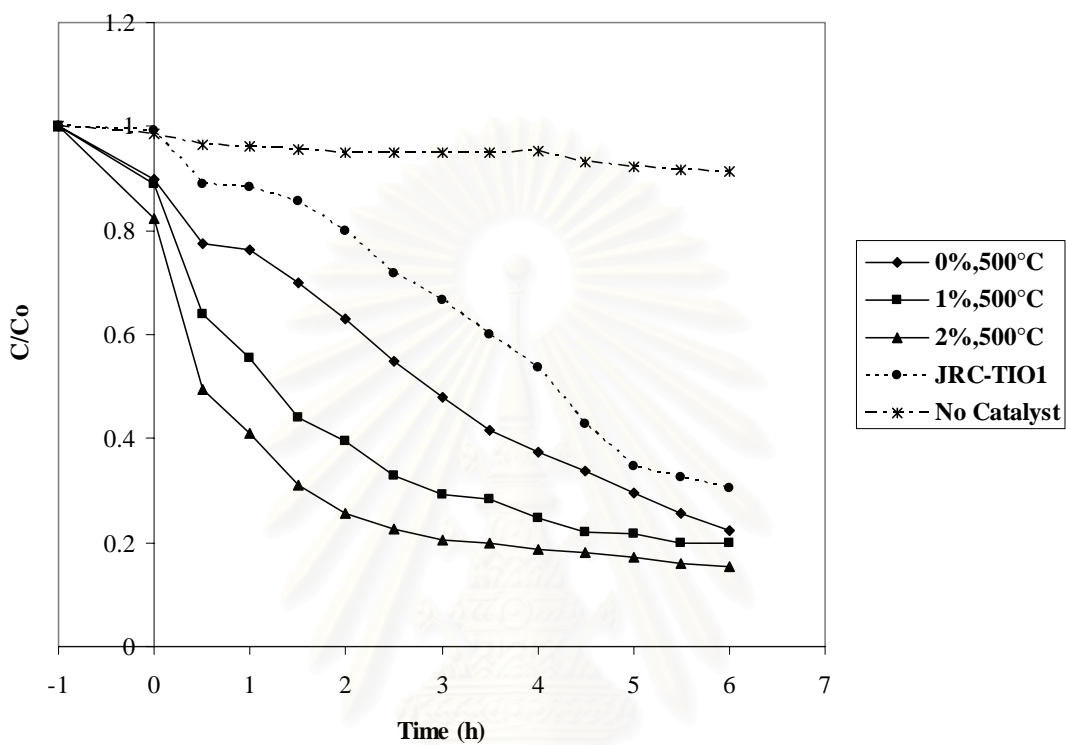


Figure 4.31 Degradation of methylene blue solution on titania fibers photocatalysts (in flake form) calcined at 500°C with different silicon content under UV irradiation.

สถาบันวิทยบริการ  
จุฬาลงกรณ์มหาวิทยาลัย

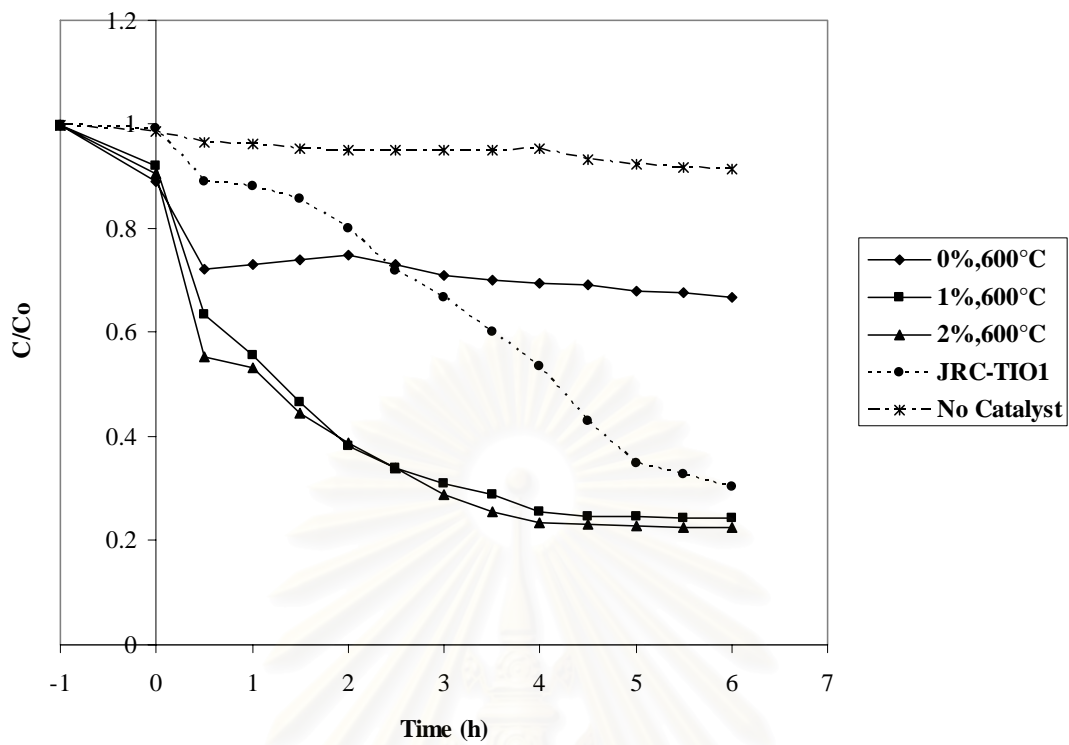


Figure 4.32 Degradation of methylene blue solution on titania fibers photocatalysts (in flake form) calcined at 600°C with different silicon content under UV irradiation.

สถาบันวิทยบริการ  
จุฬาลงกรณ์มหาวิทยาลัย

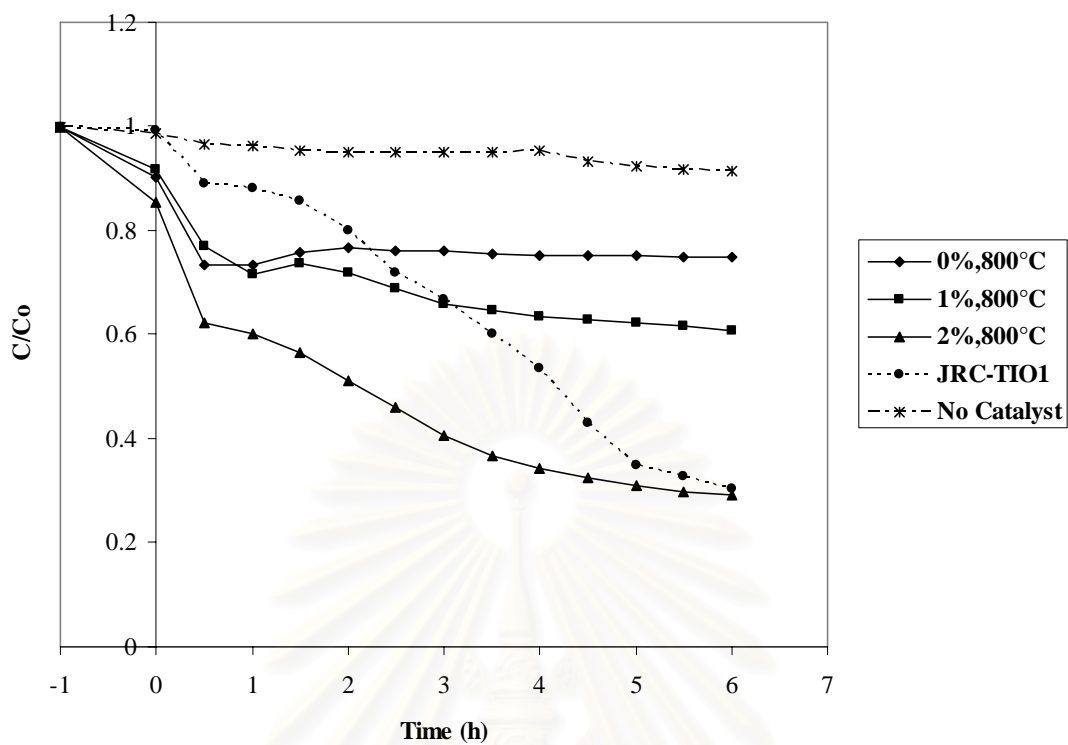


Figure 4.33 Degradation of methylene blue solution on titania fibers photocatalysts (in flake form) calcined at 800°C with different silicon content under UV irradiation.

สถาบันวิทยบริการ  
จุฬาลงกรณ์มหาวิทยาลัย

Although catalyst in form of flake is easier to handle and separate than powder, especially for the reaction in liquid, it is still unpractical for actual applications. However, because of great versatility of the electrospinning process, the fibers can be fabricated onto any kind of surface. In this work, titania fibers were fabricated on 3 cm x 3 cm stainless steel mesh and put in MB solution under UV light irradiation to test its photocatalytic activity. The results shown in Figure 4.34 reveal that no significant degradation of MB is observed from all titania fibers fabricated, while 70% decomposition of MB within 6 h is achieved from the reference catalyst in powder form.

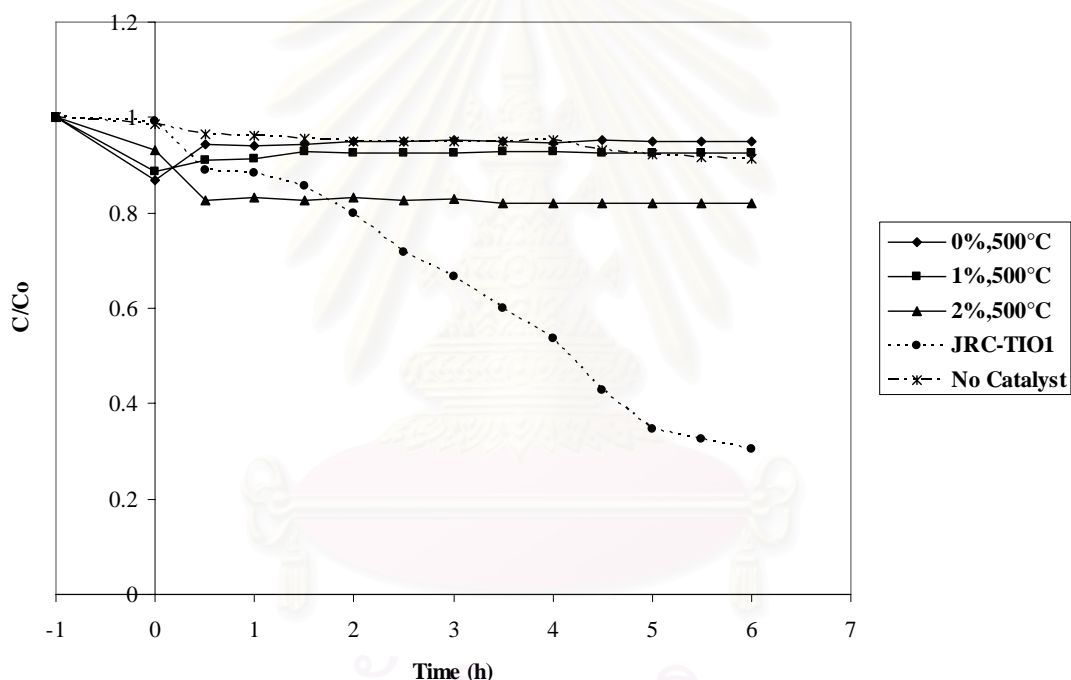


Figure 4.34 Degradation of methylene blue solution on titania fibers photocatalysts (packed with 3x3 stainless steel mesh) calcined at 500°C with different silicon content under UV irradiation.

Since titania fiber itself has been proved to have much higher photocatalytic activity than the reference titania, low rate of MB degradation observed, when stainless steel mesh is used, is the results from other factors besides the properties of titania fibers. It is suggested to be the results from lower intensity of UV light irradiated on the mesh, comparing to the case of reference catalyst. In this study, 6 UV lamps were fixed around the reaction system, in circular manner. However, UV light from only 2 lamps shined directly to the mesh. On the contrary, reference catalyst in powder form was irradiated from all directions. Therefore, further study was conduct under solar radiation, which could be considered as point source of high intensity UV light. The results are shown in Figure 4.35. It can be seen that titania fibers with 2 wt.% TEOS has the highest photoactivity comparing to the other ones. Titania fibers with 2 wt.% TEOS results in 87% decomposition after 6 h, while the reference catalyst achieves only 76% decomposition. For comparison, photodegradation of MB using titania fibers in flake form under solar radiation was also conducted. It can be seen from Figure 4.36 that titania fibers with 2 wt.% TEOS still has the highest photoactivity. The MB decomposition rate is dramatically enhanced (about 90% decomposition after 2 h) from much higher intensity of UV light from sun light. These results confirm that the intensity of UV rays significantly affects the decomposition of MB, especially in case of fibers packed within stainless steel mesh.

The results presented above reveal that the addition of silicon by suitable amount into titania fibers can effectively suppress phase transformation of titania from anatase to rutile and prevent the growth of titania grains. The addition of silicon also promotes the formation of Si-O-Ti cross-linking bonds in titania fibers. Furthermore, the higher photoactivity of silicon-doped titania fibers is the results from anatase phase of high specific surface area and high crystallinity, which effectively suppresses the electron-hole recombination. All of these effects contribute to the higher photoactivity of silicon-doped titania fibers.

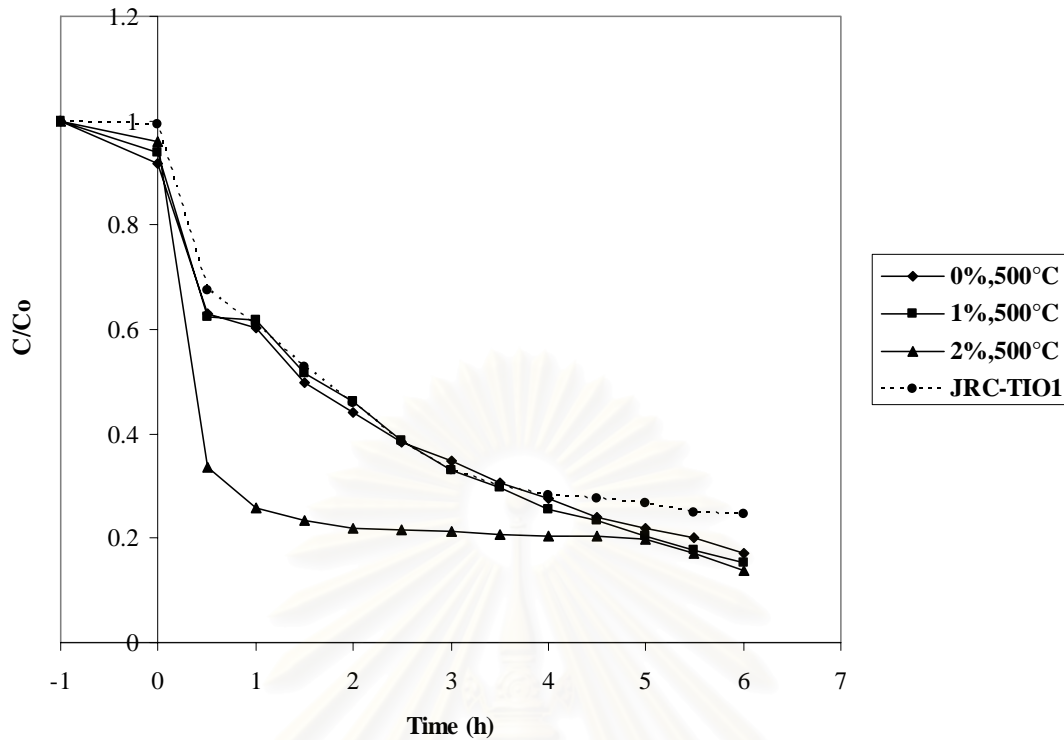


Figure 4.35 Degradation of methylene blue solution on titania fibers photocatalysts (packed with 3x3 stainless steel mesh) calcined at 500°C with different silicon content under solar radiation.

สถาบันวิทยบริการ  
จุฬาลงกรณ์มหาวิทยาลัย

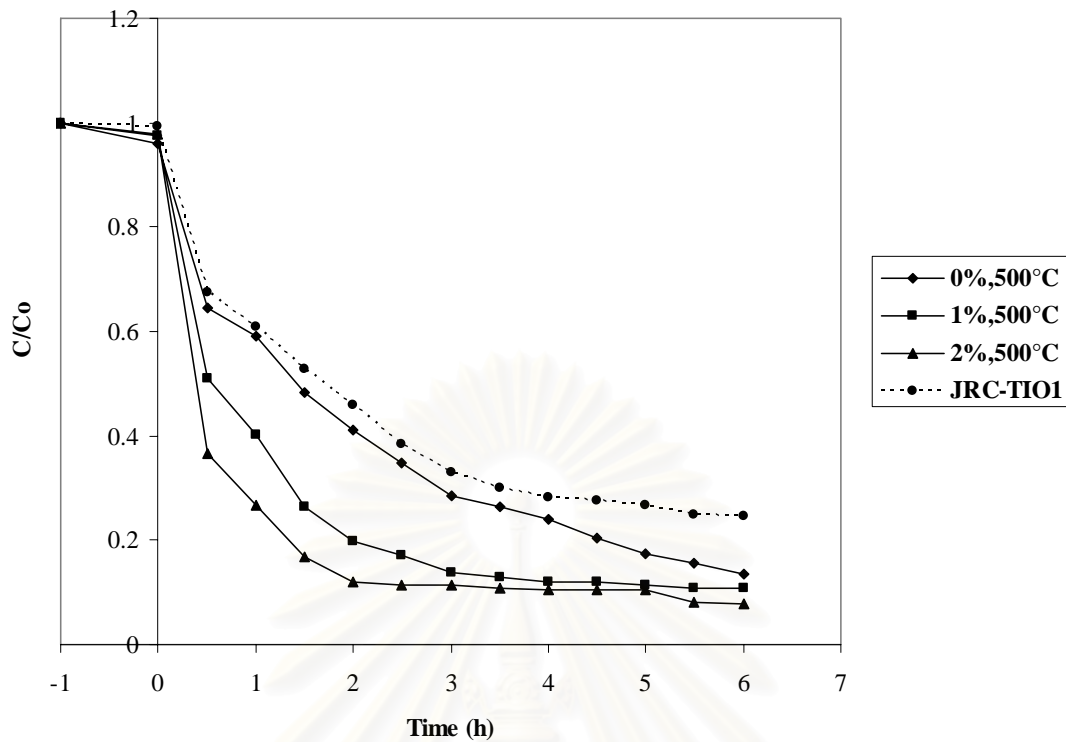


Figure 4.36 Degradation of methylene blue solution on titania fibers photocatalysts (in flake form) calcined at 500°C with different silicon content under solar radiation.

## CHAPTER V

### CONCLUSIONS AND RECOMMENDATIONS

#### 5.1 Conclusions

The conclusions of the present research are the following:

1. Titania and silicon-doped titania nanofibers were successfully prepared from combination of sol-gel and electrospinning techniques.

2. Morphology and size distribution of titania nanofibers can be controlled by PVP concentration, applied electric field strength and calcination conditions. Average diameters of titania fibers obtained in the range of 145 to 78 nm.

3. Silicon doped into titania fibers increases thermal stability by suppressing the phase transformation from anatase to rutile. It is evident that silicon is incorporated into crystal structure of titania.

4. The addition of silicon into titania fibers enhances the photocatalytic activity of titania fibers by increasing crystallinity and surface area of titania. Addition of 2 wt.% TEOS can significantly improve the activity of titania fibers in photodegradation of methylene blue.

#### 5.2 Recommendations for the Future Studies

From the previous conclusions, the following recommendations for the future studies are proposed.

1. Effect of the other metal alkoxide precursors in spinning solution on physical and chemical properties of titania nanofibers should be investigated.

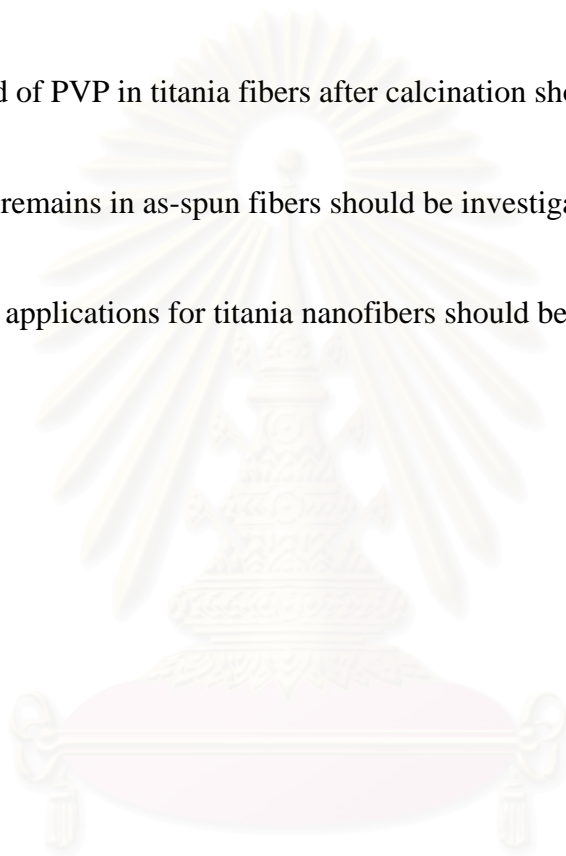
2. Although it is found that an addition of silicon as secondary metal doping can improve thermal stability and photocatalytic activity of titania fibers, the effects of the other secondary metal dopant on physical and chemical properties of titania nanofibers should be also investigated.

3. The optimum composition of silicon in titania for the maximum thermal stability and photocatalytic activity should be investigated.

4. Char yield of PVP in titania fibers after calcination should be investigated.

5. Alkoxide remains in as-spun fibers should be investigated.

6. The other applications for titania nanofibers should be also investigated.



สถาบันวิทยบริการ  
จุฬาลงกรณ์มหาวิทยาลัย

## REFERENCES

- Ammar, H., Hinda, L., Mohamed, K., Elimame, E., Chantal, G. and Jean-Marie, H. (2001). "Photocatalytic degradation pathway of methylene blue in water." Applied Catalysis B: Environmental 31: 145-157.
- Baumgarten, P. K. (1971). "Electrostatic spinning of acrylic microfibers." Journal of Colloid and Interface Science 36: 71.
- Bornat, A. (1982). U.S. Patent, 4,323,525.
- Bornat, A. (1987). U.S. Patent, 4,689,186.
- Cheng, P., Zheng, M., Jin, Y., Huang, Q. and Gu, M. (2003). "Preparation and characterization of silica-doped titania photocatalyst through sol-gel method." Materials Letters 57: 2989-2994.
- Chun, I., Reneker, D. H., Fong, H., Fang, X., Deitzel, J., Tan, N. B. and Kearns, K. (1999). "Carbon nanofibers from polyacrylonitrile and mesophase pitch." Journal of Advanced Materials 31(1): 36-41.
- Dagan, G. and Tomkiewicz, M. (1994). "Preparation and Characterization of TiO<sub>2</sub> Aerogel for Use as Photocatalysis." Journal of Non-Crystalline Solids 175(2-3): 294-302.
- De Gennes, P. G. (1974). "Coil-strech transition of dilute flexible polymers under ultrahigh velocity gradients." Journal of Chemical Physics 60: 5030.
- Ding, Z., Hu, X., Lu, G. Q., Yue, P.-L. and Greenfield, P. F. (2000). "Novel Silica gel Supported TiO<sub>2</sub> Photocatalyst Synthesized by CVD Method." Langmuir 16: 6216-6222.

- Doshi, J. and Reneker, D. H. (1995). "Electrospinning process and applications of electrospun fibers." Journal of Electrostatics 35(2-3): 151-160.
- Ertl, G., Knozinger, H. and Weitkamp, J. (1999). Preparation of solid catalysts, Wiley\_VCH.
- Fang, X. and Reneker, D. H. (1997). "DNA fibers by electrospinning." Journal of Macromolecular Science and Physics B36: 169-173.
- Fong, H., Chun, I. and Reneker, D. H. (1999a). the 24th Biennial Conference on Carbon, 380.
- Fong, H., Chun, I. and Reneker, D. H. (1999b). "Beaded nanofibers formed during electrospinning." Polymer 40: 4585-4592.
- Fong, H. and Reneker, D. H. (1999). "Elastomeric nanofibers of styrene-butadiene-styrene triblock copolymer." Journal of Polymer Science Part B: Polymer Physics 37(24): 3488-3493.
- Formhals, A. (1934). U.S. Patent, 1,975,504.
- Formhals, A. (1937). U.S. Patent, 2,077,373.
- Formhals, A. (1939a). U.S. Patent, 2,158,416.
- Formhals, A. (1939b). U.S. Patent, 2,160,962.
- Formhals, A. (1940a). U.S. Patent, 2,187,306.
- Formhals, A. (1940b). U.S. Patent, 2,323,025.
- Formhals, A. (1944). U.S. Patent, 2,349,950.

- Fox, M. A. and Dulay, M. T. (1993). "Heterogeneous Photocatalysis." Chemical Reviews 93: 341-357.
- Frenot, A. and Chronakis, I. S. (2003). "Polymer nanofibers assembled by electrospinning." Current Opinion in Colloid and Interface Science 8: 64-75.
- Fujishima, A., Hashimoto, K. and Watanabe, T. (1999a). TiO<sub>2</sub> Photocatalysis Fundamentals and Applications, BKC, Inc.
- Gladding, E. K. (1939). U.S. Patent, 2,168,027.
- Herrmann, J.-M., Tahiri, H., Ait-Icho, Y., Lassaletta, G., Gonzalez-Elipe, A. R. and Fernandez, A. (1997). "Characterization and Photocatalytic Activity in Aqueous Medium of TiO<sub>2</sub> and Ag-TiO<sub>2</sub> Coatings on Quartz." Applied Catalysis B 13: 219-228.
- Hirano, M., Nakahara, C., Ota, K. and Inagaki, M. (2002). "Direct Formation of Zirconia-Doped Titania with Stable Anatase-Type Structure by Thermal Hydrolysis." Journal of the American Ceramic Society 85(5): 1333-1335.
- Hirano, M. and Ota, K. (2004). "Direct Formation and Photocatalytic Performance of Anatase (TiO<sub>2</sub>)/Silica (SiO<sub>2</sub>) Composite Nanoparticles." Journal of the American Ceramic Society 87(8): 1567-1570.
- Hoffmann, M. R., Martin, S. T., Choi, W. and Bahnemann, D. W. (1995). "Environmental Applications of Semiconductor Photocatalysis." Chemical Reviews 95: 69-96.
- Hong, S. S., Lee, M. S., Park, S. S. and Lee, G. D. (2003). "Synthesis of nanosized TiO<sub>2</sub>/SiO<sub>2</sub> particles in the microemulsion and their photocatalytic activity on the decomposition of *p*-nitrophenol." Catalysis Today 87: 99-105.

- Huang, Z. M., Zhang, Y. Z., Kotaki, M. and Ramakrishna, S. (2003). "A review on polymer nanofibers by electrospinning and their applications in nanocomposites." Composites Science and Technology 63: 2223-2253.
- Iwamoto, S., Tanakulrungsank, W., Inoue, M., Kagawa, K. and Praserttham, P. (2000). "Synthesis of large-surface area silica-modified titania ultrafine particles by the glycothermal method." Journal of Materials Science Letter 19: 1439-1443.
- Jayesh, D. and Reneker, D. H. (1995). "Electrospinning Process and Applications of Electrospun Fibers." Journal of Electrostatics 35: 151-160.
- Jung, K. Y. and Park, S. B. (2000). "Enhanced Photoactivity of silica-embedded titania particles prepared by sol-gel process for the decomposition of trichloroethylene." Applied Catalysis B: Environmental 25: 249-256.
- Jung, K. Y. and Park., S. B. (1999). "Anatase-phase titania: preparation by embedding silica and photocatalytic activity for the decomposition of trichloroethylene." Journal of Photochemistry and Photobiology. A: Chemistry 127: 117-122.
- Kamat, P. V. and Dimitrijevic, N. M. (1990). "Colloidal Semiconductors as Photocatalysts for Solar Energy Conversion." Solar Energy 44(2): 83-98.
- Keesmann, I. (1966). "Hydrothermal Synthesis of Brookite." Zeitschrift fur Anorganische und Allgemeine Chemie 346: 30-43.
- Kim, J. and Reneker, D. H. (1999). Polymer Engineering Science 39(5): 849-854.
- Kim, J. and Reneker, D. H. (1999a). "Mechanical properties of composites using ultrafine electrospun fibers." Polymer Composites 20(1): 124-131.
- Kim, J. and Reneker, D. H. (1999b). "Polybenzimidazole nanofiber produced by electrospinning." Polymer Engineering & Science 39(5): 849-854.

- Kim, S.-J., Park, S.-D. and Jeong, Y. H. (1999). "Homogeneous Precipitation of TiO<sub>2</sub> Ultrafine Powders from Aqueous TiOCl<sub>2</sub> Solution." Journal American Ceramic Society 82(4): 927-932.
- Ko, F. K., Laurencin, C. T., Borden, M. D. and Reneker, D. H. (1998). 24th Annual Meeting of the Society for Biomaterials, San Diego, CA.
- Kominami, H., Kato, J., S.Murakami, Kera, Y., Inoue, M., Inui, T. and Ohtani, B. (1999). "Synthesis of Titanium (IV) Oxide of Ultra-High Photocatalytic Activity: High Temperature Hydrolysis of Titanium Alkoxides with Water Liberated Homogeneously from Solvent Alcohols." Journal of Molecular Catalysis A: Chemical 144: 165-171.
- Kwon, C. H., Shin, H., Kim, J. H., Choi, W. S. and Yoon, K. H. (2004). "Degradation of methylene blue via photocatalysis of titanium dioxide." Materials Chemistry and Physics 86: 78-82.
- Larrondo, L. and Manley, R. S. J. (1981a). "Electrostatic fiber spinning from polymer melts. I. and Experimental observations on fiber formation and properties." Journal of Polymer Science: Polymer Physics Edition 19: 909.
- Larrondo, L. and Manley, R. S. J. (1981b). "Electrostatic fiber spinning from polymer melts. II. Examination of the flow field in an electrically driven jet." Journal Polymer Science: Polymer Physics Edition 19: 921.
- Larrondo, L. and Manley, R. S. J. (1981c). "Electrostatic fiber spinning from polymer melts. III. Electrostatic deformation of pendant drop of polymer melt." Journal Polymer Science: Polymer Physics Edition 19: 933.
- Larson, S. A. and Falconer, J. L. (1994). "Characterization of TiO<sub>2</sub> Photocatalysts Used in Trichloroethene Oxidation." Applied Catalysis B: Environmental 4: 325-342.

- Lee, J. E., Oh, S. M. and Park, D. W. (2004). "Synthesis of nano-sized Al doped TiO<sub>2</sub> powders using thermal plasma." Thin Solid Films 457: 230-234.
- Li, D. and Xia, Y. (2003). "Fabrication of Titania Nanofibers by Electrospinning." Nano Letters 3(4): 555-560.
- Madhugiri, S., Sun, B., Smirniotis, P. G., Ferraris, J. P. and Jr., K. J. B. (2004). "Electrospun mesoporous titanium dioxide fibers." Microporous and Mesoporous Materials 69: 77-83.
- Mit-uppatham, C., Nithitannakul, M. and Supaphol, P. (2004). "Ultrafine electrospun polyamide-6 fibers: effect of solution condition on morphology and average fiber diameter." Macromolecular Chemistry and Physics, 205: 2327-2338.
- Montoya, I. A., Viveros, T., Dominguez, J. M., Canales, L. A. and Schifer, I. (1992). "On the Effect of the Sol-Gel Synthesis Parameters on Textural and Structural Characteristics of TiO<sub>2</sub>." Catalysis Letter 15: 207-217.
- Oh, S. M., Kim, S. S., Lee, J. E., Ishigaki, T. and Park, D. W. (2003). "Effect of additives on photocatalytic activity of titanium dioxide powders synthesized by thermal plasma." Thin Solid Films 435: 252-258.
- Othmer, K. (1999). Encyclopedia of Chemical Technology, Wiley interscience.
- Payakgul, W. (2002). Crystallization and precipitation mechanism of titanium(IV) oxide under the solvothermal condition and the effect of second element on titanium(IV) oxide. Chemical Engineering. Bangkok, Chulalongkorn University.
- Popielaski, S. (1998). "Photocatalysis on Nano-Sized Semiconductors." Rensselaer[Online]. Available from: [http://www.rpi.edu/locker/25/001225/public\\_html/ New%20Folder/ popielarski/](http://www.rpi.edu/locker/25/001225/public_html/New%20Folder/popielarski/).
- Rayleigh, F. R. S. (1882). Philosophical Magazine. 44: 184.

- Reneker, D. H. and Chun, I. (1996). "Nanometre diameter fibres of polymer, produced by electrospinning." Nanotechnology 7: 216-223.
- Reneker, D. H., Yarin, A. L., Fong, H. and Koombhongse, S. (2000). "Bending instability of electrically charged liquid jets of polymer solutions in electrospinning." Journal of Applied Physics 87: 4531-4547.
- Salem, D. R. (2001). Structure formation in polymeric fibers. Munich, Carl Hanser Verlag.
- Simons, H. L. (1966). U.S. Patent, 3,280,229.
- Smith, D. H. and Chu, S. (1998). "Response of flexible polymers to a sudden elongational flow." Science 281: 1335-1340.
- Soult, A. S., Carter, D. F., Schreiber, H. D., Burgt, L. J. v. d. and Stiegman, A. E. (2002). "Spectroscopy of Amorphous and Crystalline Titania-Silica Materials." Journal of Physics Chemistry B 106: 9266-9273.
- Srinivasan, G. and Reneker, D. H. (1995). "Structure and morphology of small diameter electrospun aramid fibers." Polymer International 36(2): 195-201.
- Taylor, G. I. (1964). "Disintegration of water drops in an electric field." Proceedings of the Royal Society of London A280: 383.
- Taylor, G. I. (1965). "The stability of a horizontal fluid interface in a vertical electric field." Journal of Fluid Mechanics 22: 1-15.
- Taylor, G. I. (1966). "The circulation produced in a drop by an electric field." Proceedings of the Royal Society of London A291: 159.
- Taylor, G. I. (1969). "Electrically driven jets." Proceedings of the Royal Society of London A313: 453.

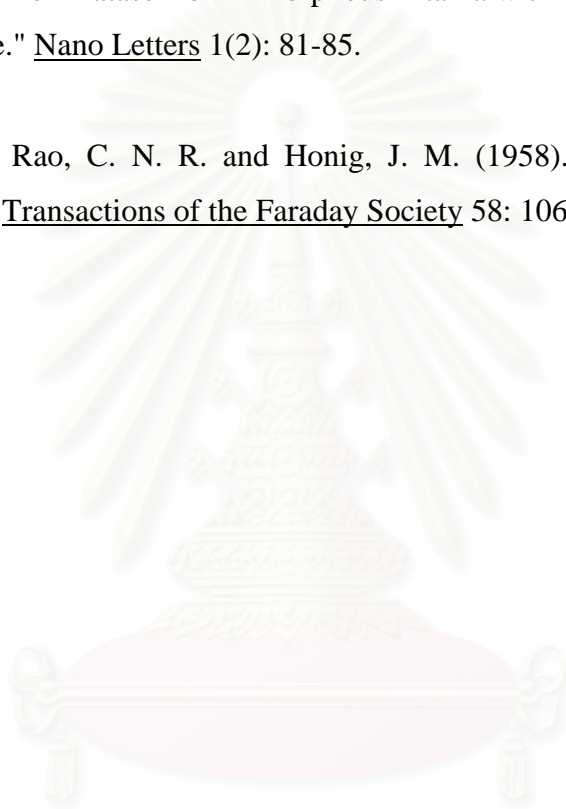
- Viswanath, R. N. and Ramasamy, S. (1998). "Study of TiO<sub>2</sub> nanocrystallites in TiO<sub>2</sub>/SiO<sub>2</sub> composites." Colloids and Surfaces A: Physicochemical and Engineering Aspects 133: 49-56.
- Viswanathamurthi, P., Bhattarai, N., Kim, C. K., Kim, H. Y. and Lee, D. R. (2004). "Ruthenium doped TiO<sub>2</sub> fibers by electrospinning." Inorganic Chemistry Communications 7: 679-682.
- Vonnegut, B. and Neubauer, R. L. (1952). "Production of monodisperse liquid particles by electrical atomization." Journal of Colloid Science 7(6): 616-622.
- Watchel, R. E. and LaMer, V. K. (1962). "The preparation and size distribution of some monodisperse emulsions." Journal of Colloid Science 17(6): 531-564.
- Yang, J., Mei, S. and Ferreira, J. M. F. (2001). "Hydrothermal Synthesis of Nanosized Titania Powders: Influence of tetraalkyl Ammonium Hydroxides on Particle Characteristics." Journal of the American Ceramic Society 84(8): 1696-1702.
- Yogarasimhan, S. R. and Rao, C. N. (1962). "Mechanism of Crystal Structure Transformations." Transactions of the Faraday Society 58: 1579-1589.
- Yoshinaka, M., Hirota, K. and Yamaguchi, O. (1997). "Formation and Sintering of TiO<sub>2</sub> (Anatase) Solid Solution in the System TiO<sub>2</sub>-SiO<sub>2</sub>." Journal of the American Ceramic Society 80(10): 2749-2753.
- Zaharescu, M., Crisan, M., Simionescu, L., Crisan, D. and Gartner, M. (1997). "TiO<sub>2</sub>-Based Porous Materials obtained from Gels, in Different Experimental Conditions." Journal of Sol-Gel Science and Technology 8(1-3): 249-253.
- Zeleny, J. (1914). "The electrical discharge from liquid points and a hydrostatic method of measuring the electric intensity at their surfaces." Physical Review 3: 69-91.
- Zeleny, J. (1915). Proceedings of the Cambridge Philosophical Society 18: 71.

Zeleny, J. (1917). "Instability of electrified liquid surfaces." Physical Review 10: 1-6.

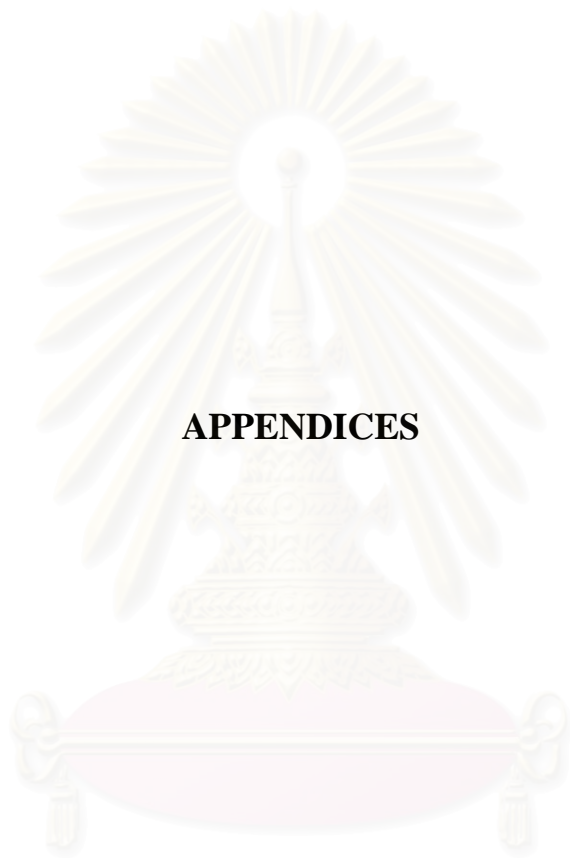
Zeleny, J. (1935). "The role of surface instability in electrical discharges from drops of alcohol and water in air at atmospheric pressure." Journal of the Franklin Institute 219(6): 659-675.

Zhang, H., Finnegan, M. and Banfield, J. F. (2001). "Preparing Single-Phase Nanocrystalline Anatase from Amorphous Titania with Particle Size Tailed by Temperature." Nano Letters 1(2): 81-85.

Zzanderna, A. W., Rao, C. N. R. and Honig, J. M. (1958). "The Anatase-Rutile Transition." Transactions of the Faraday Society 58: 1069-1073.



สถาบันวิทยบริการ  
จุฬาลงกรณ์มหาวิทยาลัย



**APPENDICES**

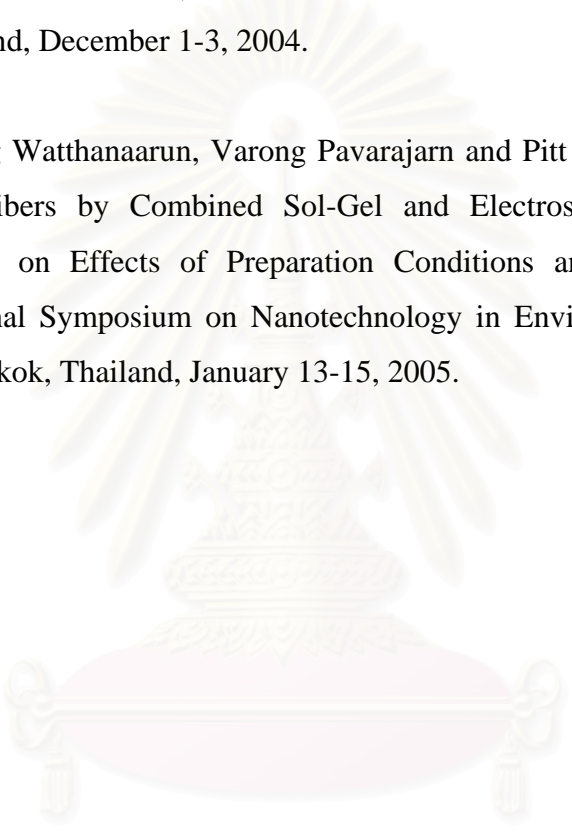
สถาบันวิทยบริการ  
จุฬาลงกรณ์มหาวิทยาลัย

## APPENDIX A

### LIST OF PUBLICATIONS

1. Jeerapong Watthanaarun, Varong Pavarajarn and Pitt Supaphol. “Effects of Preparation Parameters and secondary Metal Doping on Properties of Electrospun Titanium (IV) Oxide Nanofibers”, The International Conference on Smart Materials, Chiang Mai, Thailand, December 1-3, 2004.

2. Jeerapong Watthanaarun, Varong Pavarajarn and Pitt Supaphol. “Titanium (IV) Oxide Nanofibers by Combined Sol-Gel and Electrospinning Techniques: Preliminary Report on Effects of Preparation Conditions and Secondary Metal Dopant” International Symposium on Nanotechnology in Environmental Protection and Pollution, Bangkok, Thailand, January 13-15, 2005.



สถาบันวิทยบริการ  
จุฬาลงกรณ์มหาวิทยาลัย

## EFFECTS OF PREPARATION PARAMETERS AND SECONDARY METAL DOPING ON PROPERTIES OF ELECTROSPUN TITANIUM (IV) OXIDE NANOFIBERS

**Jeerapong Watthanaarun,<sup>1</sup> Varong Pavarajarn,<sup>1\*</sup> and Pitt Supaphol<sup>2\*</sup>**

<sup>1</sup> Department of Chemical Engineering, Faculty of Engineering, Chulalongkorn University, Bangkok 10300, Thailand.

<sup>2</sup> Technological Center for Electrospun Fibers and The Petroleum and Petrochemical College, Chulalongkorn University, Bangkok 10300, Thailand.

\* E-mails: fchvpv@eng.chula.ac.th, pitt.s@chula.ac.th

### Abstract

Titanium oxide/poly(vinyl pyrrolidone) (PVP) composite nanofibers were prepared from the combination of electrospinning and sol-gel techniques using solution precursors containing PVP and titanium tetraisopropoxide. Diameters of the obtained composite fibers were in the range of 60 to 300 nm. Calcination of these fibers resulted in pure anatase TiO<sub>2</sub> nanofibers without contamination with other phases. The effects of various parameters such as PVP concentration, applied electrostatic field strength (i.e. applied potential to collection distance ratio), calcination temperature and time on physical appearance and properties of the obtained TiO<sub>2</sub> nanofibers were investigated. The effect of addition of a secondary metal dopant, i.e. silicon, to TiO<sub>2</sub> fibers on surface morphology, crystallinity, grain growth, and thermal stability of the doped TiO<sub>2</sub> nanofibers obtained was also investigated.

**Key-words:** Electrospinning; Titania; Nanofiber

### Introduction

Titanium (IV) oxide or titania (TiO<sub>2</sub>) is one of the most common materials for a variety of applications such as catalytic devices, sensors, solar cells and other optoelectronic devices [1, 2]. Titania is a wide bandgap semiconductor with many interesting properties, such as transparency to visible light, high refractive index and low absorption coefficient. Other than these properties, it has been known to be an excellent catalyst in the field of photocatalytic decomposition of organic materials. Therefore, titania has been employed for organic pollutant treatment in the environmental applications [3]. Titania is known to have three natural polymorphs, i.e. rutile, anatase, and brookite. However, only anatase is generally accepted to have significant photocatalytic activity.

Titania can be synthesized by various techniques, such as precipitation [4], chemical vapor deposition [5], hydrothermal method [6], glycothermal method [7], and sol-gel method, which is among the techniques that results in titania with extremely high surface area [8]. In this work, it is intended to combine the sol-gel method

with electrospinning technique to produce titania nanofibers.

Electrospinning technique is a relatively simple and versatile method for fabricating nanofibers. In typical electrospinning process, polymer solution or polymer melt is injected from a small nozzle under the influence of strong electric field, as high as several kV/cm. Electrostatic charges built up on the surface of a droplet induces the formation of a jet, which is subsequently stretched to form a continuous ultrathin fiber. In the continuous operation, the number of fibers can be formed within short period of time, as short as a few seconds. Fibers are often collected on the surface of a conductor to form non-woven mat that has high surface area and relatively small pore size [1, 2, 9]. Amorphous titania nanofibers have been preliminarily produced by electrospinning technique from the mixture of titanium isopropoxide, acetic acid and high molecular weight poly(vinyl pyrrolidone) (PVP) [1].

Anatase is the unstable polymorph of titania. Phase transformation from anatase to rutile, which is less active, takes place at temperature as low as 300°C, depending upon the the synthesis method [10]. Anatase titania that transforms to rutile at high temperature is considered having high thermal stability. It is generally recognized that large surface area and reasonable thermal stability are often desirable in catalytic applications. Therefore, many studies have devoted to improve the thermal stability of titania using additives such as silicon [7] and aluminum [11]. Furthermore, it has been reported that addition of a secondary metal can enhance the photocatalytic activity of titania. Anatase/silica composite nanoparticles have shown much higher photocatalytic activity than the pure anatase phase [8, 12]. It is therefore the objective of this study to investigate an incorporation of the secondary metal doping into the electrospun titania nanofibers.

### Materials and methods

In a typical procedure, 1.5 g of titanium tetraisopropoxide (TIP) was mixed with 3 ml of acetic acid and 3 ml of ethanol. After being aged for 10 min, the as-prepared solution was added into 7.5 ml solution of poly(vinyl pyrrolidone) (PVP,  $M_w \approx 1,300,000$ ) in ethanol

under constant stirring for 10 min. The concentration of PVP solution was in the range of 7-13 % by mass. Finally, 2% by mass of tetraethyl orthosilicate (TEOS) was added into the mixture and stirred for 1 h. The amount of TEOS was varied to investigate the effect of silicon loading on the morphology of the electrospun fibers. The resulting solution is referred as the electrospinning solution.

The electrospinning solution was immediately loaded into a plastic syringe equipped with a 20 gauge stainless steel needle. The needle was connected to a high-voltage supply that is capable of generating DC voltages up to 30 kV. A piece of aluminum foil was placed approximately 7 cm below the tip of the needle to collect the nanofibers produced. Upon the application of a high voltage, in the range of 9-22.5 kV, to the needle, a fluid jet was ejected from the capillary. As the jet accelerated towards the collector, the solvent evaporated and the charged fiber was deposited on the collector. The synthesized fibers were left exposing to moisture for approximately 5 h to allow complete hydrolysis of TIP. The as-spun fibers were consequently subjected to high temperature calcination to remove residual PVP. The calcination was done at the temperature in the range of 500-800°C for 3 h.

Morphology and size of fibers were observed by a JEOL-JSM 5800 scanning electron microscope (SEM). Crystalline phase was identified by X-ray diffraction (XRD), using a Siemens D5000 diffractometer with a Cu K $\alpha$  radiation. The functional group in the fibers were also characterized by FT-IR using a Nicolet model Impact 400.

## Results and discussion

### Effects of Electrospinning Conditions on As-Spun Fibers

Nanofibers were successfully produced using electrospinning technique. SEM micrographs of as-spun fibers prepared from different PVP concentration are shown in Figure 1. It can be seen that all fibers were smooth fibers with diameters in nanometer scale. Very thin fibers, as thin as 100 nm in diameter, were obtained when solution with low PVP concentration (7% wt.) was employed. With increasing the PVP concentration, diameter of fibers increased, but more importantly, fibers obtained had broader size distribution. This observation could be explained by the fact that the electrospinning solutions of high PVP concentration had high viscosity, which resulted in the formation of non-uniform jet.

The effects of applied electrostatic field strength on the fiber structure are shown in Figure 2. The higher the electrostatic field strength, the smaller the fibers and the narrower the size distribution. This is the reverse effect from the effect of PVP concentration. High electrostatic field strengths caused the jet of electrospinning solution to be stretched with higher force. Therefore, the size of the resulting fibers were small and uniform. The summary of effects from PVP concentration and field strength are shown in Figure 3. Noted that the

error bars in the figure represents standard deviation of the data.

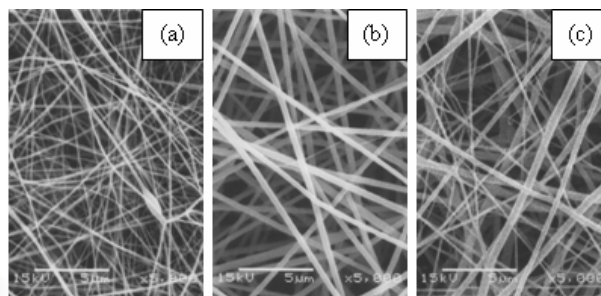


Figure 1. SEM micrographs of as-spun fibers with different PVP concentrations: (a) 7% PVP; (b) 10% PVP; (c) 13% PVP.

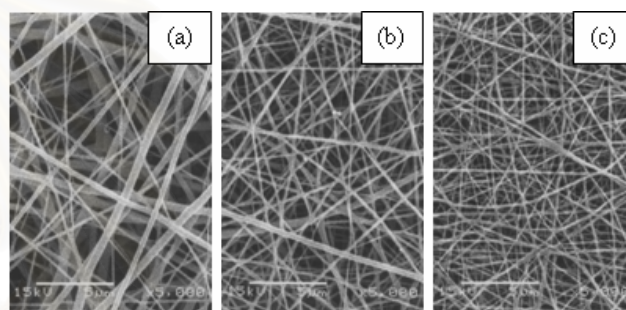


Figure 2. SEM micrographs of as-spun fibers with different applied electrostatic field strengths: (a) 9 kV; (b) 15 kV; (c) 22.5 kV.

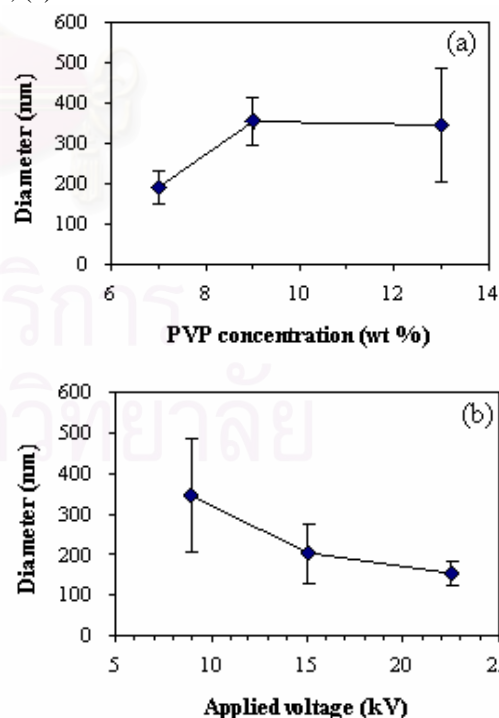


Figure 3. Effects of the electrospinning conditions on size of as-spun fibers: (a) PVP concentration; (b) electrostatic field strength.

### Properties of Titania Nanofibers

Although as-spun fibers were amorphous, crystallization took place during the calcination. All XRD analysis confirmed that the calcined fibers were anatase titania without contamination of other phases. After calcination, significant shrinkage as well as surface roughness were observed from SEM micrographs (Figure 4). Higher calcination temperature resulted in more shrinkage, as shown in Figure 5. This is expected to be the result from sintering of crystalline particles in fiber structure. The calcined fibers appeared distorted and no longer straight fibers. Nevertheless, each thread still remained as very long fibers. The shrinkage of the fibers was also the result from the removal of organic contents, i.e. PVP matrix, from PVP/titania composite fibers during the calcination. This was also supported by the IR spectroscopy analysis (Figure 6). For as-spun fibers, strong absorption bands in the range of 1000-2000  $\text{cm}^{-1}$ , which are corresponding to bending and stretching frequencies of PVP, were detected. After calcination, all of these strong features from organic substance were removed. The band associated with vibrational mode of O-Ti-O bonding of anatase at wave number around 470  $\text{cm}^{-1}$  was clearly observed. No sign of hydrocarbon impurity was detected.

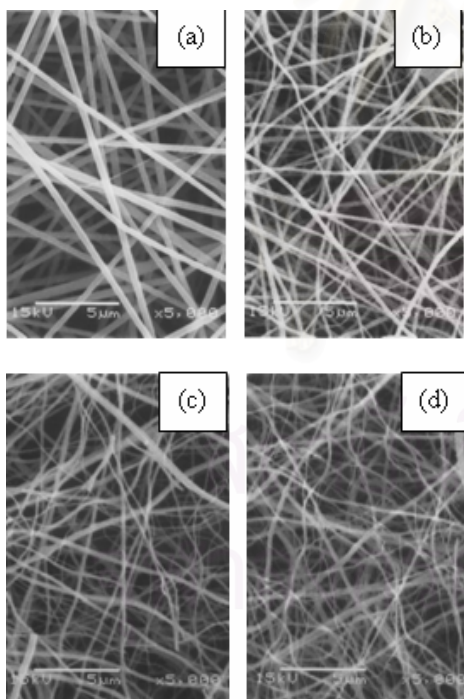


Figure 4. SEM micrographs of titania fibers:  
 (a) as-spun fibers;  
 (b) calcined at 500°C;  
 (c) calcined at 600°C;  
 (d) calcined at 800°C.

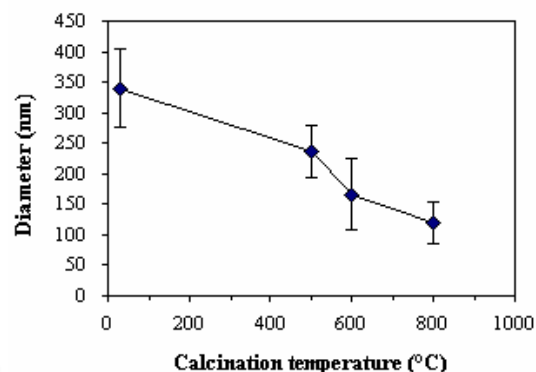


Figure 5. Effects of calcination temperature on size of titania fibers.

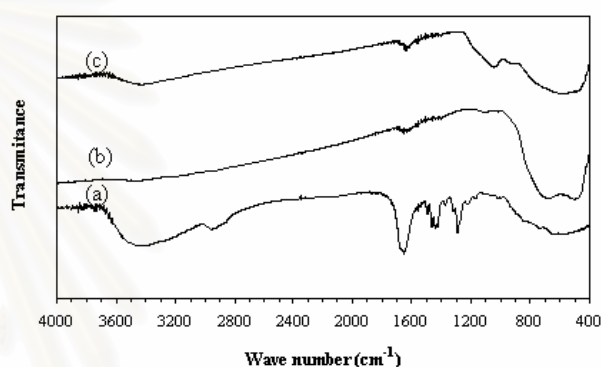
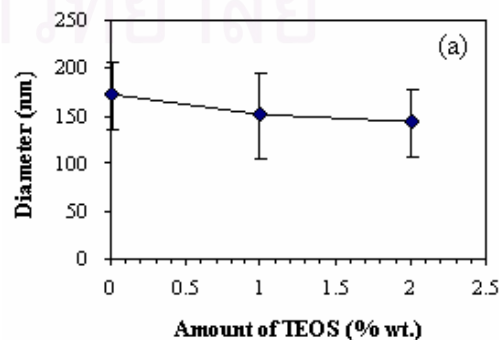


Figure 6. FTIR spectra of titania fibers:  
 (a) as-spun fibers; (b) fibers calcined at 500°C; (c) fibers doped with 2% wt. TEOS and calcined at 500°C.

### Addition of Silicon as Secondary Metal into Titania Nanofibers

Silicon was added to the electrospinning solution in the form of TEOS, as previously described. Figure 7 shows the effect of TEOS addition on the size of fibers obtained after calcination at 500°C. It can be seen that the diameters of the calcined fibers were significantly reduced by silicon addition. This agreed with a previous finding that silicon doping into titania results in smaller crystallite size, which is evidence that silicon atoms are incorporated into the lattice of titania [13].



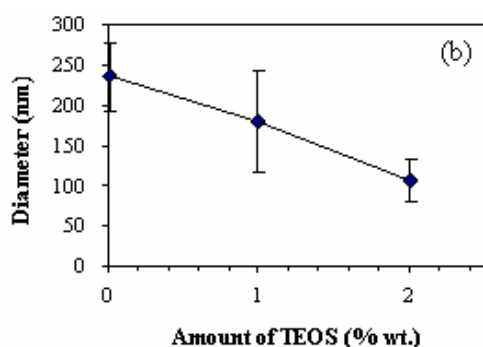


Figure 7. Effects of the TEOS addition on size of: (a) as-spun fibers; (b) calcined fibers.

The XRD analysis of silicon doped titania showed no sign of crystalline silica. However, FTIR spectra (Figure 6c) indicated the presence of silicon in the titania fibers from the band corresponding to the vibrational mode of O-Si-O bonding at wave number around  $1100\text{ cm}^{-1}$ .

### Conclusion

Titanium (IV) oxide nanofibers and silicon-doped titanium (IV) oxide nanofibers have been successfully prepared by using an electrospinning method. The obtained products are smooth and uniform fibers with diameter in range of 60 to 300 nm. It has been observed that PVP concentration, electric field strength, calcination temperature, as well as silicon content affect morphology and crystallinity of the fibers. We can control the properties of fibers for use in many suitable application.

### Acknowledgement

The authors would like to acknowledge the financial support from the Graduate School, Chulalongkorn University.

### Reference

- [1] Li, D. and Xia, Y. Fabrication of Titania Nanofibers by Electrospinning, *Nano Letters*, 2003; 3: 555-560.
- [2] Viswanathamurthi, P., Bhattarai, N., Kim, C.K., Kim, H.Y. and Lee, D.R. Ruthenium Doped  $\text{TiO}_2$  Fibers by Electrospinning, *Inorganic Chemistry Communications*, 2004; 7: 679-682.
- [3] Kwon, C.H., Shin, H., Kim, J.H., Choi, W.S. and Yoon, K.H. Degradation of Methylene Blue Via Photocatalysis of Titanium Dioxide, *Materials Chemistry and Physics*, 2004; 86: 78-82.
- [4] Kim, S.-J., Park, S.-D. and Jeong, Y.H. Homogeneous Precipitation of  $\text{TiO}_2$  Ultrafine Powders from Aqueous  $\text{TiOCl}_2$  Solution, *J. Am. Ceram. Soc.*, 1999; 82: 927-932.
- [5] Ding, Z., Hu, X.J., Lu, G.Q., Yue, P.L. and Greenfield, P.F. Novel Silica Gel Supported  $\text{TiO}_2$  Photocatalyst Synthesized by Cvd Method, *Langmuir*, 2000; 16: 6216-6222.
- [6] Yang, J., Mei, S. and Ferreira, J.M.F. Hydrothermal Synthesis of Nanosized Titania Powders: Influence of Tetraalkyl Ammonium Hydroxides on Particle Characteristics, *Journal of the American Ceramic Society*, 2001; 84: 1696-1702.
- [7] Iwamoto, S., Tanakulrungsank, W., Inoue, M., Kagawa, K. and Praserttham, P. Synthesis of Large-Surface Area Silica-Modified Titania Ultrafine Particles by the Glycothermal Method, *Journal of Materials Science Letters*, 2000; 19: 1439-1443.
- [8] Jung, K.Y. and Park, S.B. Enhanced Photoactivity of Silica-Embedded Titania Particles Prepared by Sol-Gel Process for the Decomposition of Trichloroethylene, *Applied Catalysis B-Environmental*, 2000; 25: 249-256.
- [9] Jayesh, D. and Reneker, D.H. Electrospinning Process and Applications of Electrospun Fibers, *Journal of Electrostatics*, 1995; 35: 151-160.
- [10] Jung, K.Y. and Park, S.B. Anatase-Phase Titania: Preparation by Embedding Silica and Photocatalytic Activity for the Decomposition of Trichloroethylene, *Journal of Photochemistry and Photobiology A: Chemistry*, 1999; 127: 117-122.
- [11] Lee, J.E., Oh, S.M. and Park, D.W. Synthesis of Nano-Sized Al Doped  $\text{TiO}_2$  Powders Using Thermal Plasma, *Thin Solid Films*, 2004; 457: 230-234.
- [12] Hirano, M. and Ota, K. Direct Formation and Photocatalytic Performance of Anatase ( $\text{TiO}_2$ )/Silica ( $\text{SiO}_2$ ) Composite Nanoparticles, *Journal of the American Ceramic Society*, 2004; 87: 1567-1570.
- [13] Viswanath, R.N. and Ramasamy, S. Study of  $\text{TiO}_2$  Nanocrystallites in  $\text{TiO}_2$ - $\text{SiO}_2$  Composites, *Colloids and Surfaces A: Physicochemical and Engineering Aspects*, 1998; 133: 49-56.

# TITANIUM (IV) OXIDE NANOFIBERS BY COMBINED SOL-GEL AND ELECTROSPINNING TECHNIQUES: PRELIMINARY REPORT ON EFFECTS OF PREPARATION CONDITIONS AND SECONDARY METAL DOPANT

Jeerapong Watthanaarun,<sup>1</sup> Varong Pavarajarn,<sup>1\*</sup> and Pitt Supaphol<sup>2\*</sup>

<sup>1</sup> Department of Chemical Engineering, Faculty of Engineering, Chulalongkorn University, Bangkok 10300,  
THAILAND

<sup>2</sup> Technological Center for Electrospun Fibers and the Petroleum and Petrochemical College,  
Chulalongkorn University, Bangkok 10300, THAILAND

## ABSTRACT

Sol-gel and electrospinning techniques were incorporated to produce titanium (IV) oxide/polyvinylpyrrolidone (PVP) composite nanofibers from solutions containing PVP and titanium tetraisopropoxide. Diameters of the obtained composite fibers were in the range of 120 to 350 nm. The effects of PVP concentration and electrostatic field strength on size and size distribution of the as-spun fibers were investigated. Calcination of these composite fibers at 500°C resulted in pure anatase titania nanofibers without contamination of the other phases. The effects of calcination temperature and time on phase and size of the as-spun titania fibers were also investigated in this study. Moreover, the effect of silicon secondary metal dopant on morphology, crystalline phase, and thermal stability of the resulting titania fibers was also discussed.

**Keywords:** Titania, Electrospinning, Nanofibers, Doping

---

\* Author to whom correspondence should be addressed (E-mail: fchvpv@eng.chula.ac.th)

\* Author to whom correspondence should be addressed (E-mail: pitt.s@chula.ac.th)

## 1. INTRODUCTION

Titanium (IV) oxide or titania ( $\text{TiO}_2$ ) is one of the most common materials for a variety of applications such as catalytic devices, sensors, solar cells, and other optoelectronic devices [1, 2]. Titania is a wide bandgap semiconductor with many interesting properties, such as transparency to visible light, high refractive index and low absorption coefficient. Other than these properties, it has been known to be an excellent catalyst in the field of photocatalytic decomposition of organic materials. Therefore, titania has been employed for organic pollutant treatment in the environmental applications [3]. Titania is known to have three natural polymorphs, i.e. rutile, anatase, and brookite. Only anatase is generally accepted to have significant photocatalytic activity.

Titania can be synthesized by various techniques, such as precipitation [4], chemical vapor deposition [5], hydrothermal method [6], and glycothermal method [7]. Another common technique that can result in titania with extremely high surface area is sol-gel method [8]. In this preliminary work, the sol-gel method was combined with the electrostatic spinning or electrospinning technique to produce titania nanofibers.

Electrospinning technique is a relatively simple and versatile method for fabricating ultrafine fibers with diameters ranging from tens of nanometers to sub-micrometers. Typically in this technique, a polymer solution or melt is ejected from a small opening or a nozzle under the influence of a strong electrostatic field. Electrostatic charges built up on the surface of a droplet induces the formation of a jet, which is subsequently stretched to form a continuous ultrathin fiber. During its flight to a collective target, the ejected, charged jet dries out, leaving ultrathin fibers on the target. The non-woven mat has a high surface area with relatively small pore size [1, 2, 9]. Amorphous titania nanofibers were successfully prepared by the electrospinning of a mixture of titanium isopropoxide, acetic acid, and a high molecular weight polyvinylpyrrolidone (PVP) [1].

Anatase is an unstable polymorph of titania. Phase transformation from anatase to rutile, the less chemically active polymorph, takes place at temperatures as low as  $300^\circ\text{C}$ . However, the transformation temperature strongly depends upon how titania is synthesized [10]. Anatase titania that transforms to rutile at a high temperature is considered to exhibit good thermal stability. In catalytic application, large surface area and reasonably good thermal stability is often desired. Therefore, many studies have been

devoted to improving the thermal stability of titania using additives such as silicon [7] and aluminum [11]. Furthermore, it has been also reported that the addition of a secondary metal dopant can enhance the photocatalytic activity of the resulting titania. Anatase/silica composite nanoparticles exhibited a much better photocatalytic activity than that of the pure anatase [8, 12].

The main objectives of this study are to investigate the effects of solution, spinning, and calcination conditions on morphological appearance and crystal structure of the resulting titania fibers. The effect of the addition of silicon as the secondary metal doping on the thermal stability of the resulting titania fibers was also investigated.

## 2. EXPERIMENTAL

In a typical procedure, 1.5 g of titanium tetraisopropoxide (TIP) was mixed with 3 ml of acetic acid and 3 ml of ethanol. The solution was rest for 10 min before being added into 7.5 ml of polyvinylpyrrolidone (PVP,  $M_w \approx 1,300,000$  Da) solution in ethanol. The concentration of the PVP solution was varied between 7 and 13 wt.% and the resulting mixture was constantly stirred for 10 min. Tetraethyl orthosilicate (TEOS) was finally added to the as-prepared mixture. The amount of TEOS was typically 2 wt.% (unless stated otherwise) based on the total amount of the final mixture and the mixture was constantly stirred for another hour. The as-prepared solution was referred to as the spinning solution.

The spinning solution was immediately loaded into a plastic syringe. A blunt-ended 20-gauge stainless steel needle was used as the nozzle. The emitting electrode from a Gamma High Voltage Research ES30P power supply capable of generating DC voltages up to 30 kV was attached to the needle. The grounding electrode from the same power supply was attached to a piece of aluminum foil which was used as the collector plate and was placed approximately 7 cm below the tip of the needle. Upon the application of a high voltage ranging between 9 and 22.5 kV across the needle and the collective plate, a fluid jet was ejected from the nozzle. As the jet accelerated towards the collector, the solvent evaporated, leaving only ultrathin fibers on the collector. The obtained fibers were left exposed to moisture for approximately 5 hours to allow complete hydrolysis of TIP and consequently subjected to calcination at a high temperature ranging between 500 and 800°C for 3 hours to remove residual PVP.

Morphology and size of the as-prepared titania fibers were observed by a JEOL JSM 5800 scanning electron microscope (SEM). Crystalline phase of the fibers was identified by a Siemens D5000 X-ray diffractometer with a Cu K $\alpha$  radiation and the functional groups by a Nicolet Impact 400 Fourier-transformed infrared spectroscopy (FT-IR).

### 3. RESULTS AND DISCUSSION

#### 3.1. Effects of spinning conditions

By applying a high electrical potential across the syringe needle and the collector plate, fibers were spun and deposited as a non-woven mat on the collector plate. SEM images of these fibers confirm that the obtained products were indeed a collection of ultrafine fibers with smooth surface.

The effects of PVP concentration of the spinning solutions on morphology of the pre-calcined as-spun fibers are shown in **Figure 1**. It should be noted that the applied electrostatic field strength was fixed at 9 kV/7 cm. Clearly, ultrathin fibers with average diameter being as low as about 200 nm were produced from the spinning solution with PVP concentration of 7 wt.%. Increasing PVP concentration led to an increase in the fiber diameters with broader distribution. The increase in the fiber diameters with increasing PVP concentration should be a result of the increase in the viscosity of the spinning solutions [9]. However, the increase in the viscosity of the spinning solutions could lead to non-uniform ejection of the jet, when the viscosity becomes too great.

The effect of applied electrostatic field strength on the pre-calcined fiber structure is shown in **Figure 2**. It should be noted that the PVP concentration in the spinning solution was fixed at 13 wt.%. Apparently, with increasing electrostatic field strength, the fibers obtained appeared to be smaller in diameter with narrower distribution. This is in contrast to what was observed on the effect of PVP concentration. Increasing electrostatic field strength resulted in an increase in both the electrostatic force, which is responsible for the transport of the charged jet to the collective target, and the Coulombic repulsion force, which is responsible for the stretching of an ejected jet segment [9]. The increased electrostatic force could lead an increase in the mass throughput of the material from the nozzle, while the increased Coulombic stretching force could lead to a decrease in the fiber diameters.

It is evident from [Figure 2](#) that the diameters of the fibers obtained appeared to be smaller with increasing electrostatic field strength. Such an observation should be due solely to the increase in the Coulombic repulsion force. [Figure 3](#) summarizes the relationships of the diameters of the pre-calcined fibers with respect to PVP concentration of the spinning solutions and applied electrostatic field strength. Noted that the error bars in the figure represents standard deviation of the fiber diameter data.

### 3.2. Properties of titania nanofibers

XRD analysis revealed that all of the as-spun fibers prior to calcination were amorphous (results not shown). Crystallization, however, took place during the calcination. The as-calcined fibers were anatase titania without contamination of the other phases. As evidently shown in [Figure 4](#), significant shrinkage occurred during calcination. Furthermore, the as-calcined fibers appeared to be more distorted and the surface appeared to be more rough, even though calcination did not affect much the fibrous nature of the fibers. [Figure 5](#) shows the relationship between the diameters of the as-calcined titania fibers and the calcination temperature in comparison with the diameters of the pre-calcined ones. Apparently, the higher the calcination temperature, the greater the shrinkage. The shrinkage mainly resulted from the removal of organic contents, i.e. PVP matrix, from PVP/titania composite fibers during the calcination process. This was supported by the IR spectroscopic analysis (see [Figure 6](#)) that the absorption bands in the range of 1000-2000  $\text{cm}^{-1}$ , which corresponds to the bending and stretching frequencies of PVP, diminished after calcination. Instead, the band associated with the vibrational mode of O-Ti-O bonding of the anatase phase at the wave number of around 470  $\text{cm}^{-1}$  was clearly observed. In addition, no sign of other hydrocarbon impurities was detected in the as-calcined fibers.

### 3.3. Effect of silicon as secondary metal dopant

Silicon was added into titania fibers by doping the spinning solution with TEOS, as previously described. The resulting fibers were calcined and analyzed. The presence of silicon in the as-calcined titania fibers was evident from the infrared absorption band at the wave number of around 1100  $\text{cm}^{-1}$ , which corresponds to the vibrational mode of O-Si-O bonding [see curve (c) in [Figure 6](#)].

The effect of silicon doping content on the morphology of titania fibers was also observed. **Figure 7** shows SEM images of silicon-doped titania fibers (doped with either 1 or 2 wt.% TEOS; the PVP concentration was 13 wt.%, the spinning condition was 9 kV/7 cm, and the calcination temperature was 600°C) in comparison with the undoped titania fibers. Interestingly, the diameters of the resulting titania fibers were significantly reduced by silicon addition. These observation was in agreement with the finding by Viswanath and Ramasamy [13] that incorporation of silicon atoms into titania lattice resulted in a smaller crystallite size.

The thermal stability of the as-prepared doped and undoped titania fibers was assessed by monitoring the crystalline phase of the fibers as a function of calcination temperatures. According to XRD patterns shown in **Figures 8 and 9**, it was found that the obtained titania fibers doped with 2 wt.% TEOS remained in pure anatase phase even when the calcination temperature was 600°C, while the obtained undoped titania fibers showed an evident of the transformation into the rutile phase. At 800°C, only rutile phase was found in the undoped titania fibers, while the silicon-doped titania ones still contained appreciable amount of the anatase phase. As previously mentioned, titania that transforms from anatase to the other phases at a higher calcination temperature is considered to exhibit better thermal stability, which is very desirable for catalytic applications. Consequently, addition of silicon was proved beneficial to increasing the thermal stability of the resulting titania fibers.

#### 4. CONCLUSION

In the present contribution, pure titanium (IV) oxide and silicon-doped titanium (IV) oxide nanofibers were successfully prepared by combined sol-gel and electrospinning techniques from solutions containing polyvinylpyrrolidone (PVP) and titanium tetraisopropoxide after calcination at elevated temperatures. The average diameters of the pre-calcined as-spun fibers were in the range of about 120 to 350 nm, while those of the post-calcined ones were in the range of about 100 to 230 nm. The appearance of both pre-calcined and post-calcined fibers was regular, with that of the post-calcined fibers exhibiting rougher surface. The choice of the calcination temperature had a strong influence on the crystalline phase formation of the as-prepared titania fibers, with the transformation from anatase to rutile

occurring more readily with increasing calcination temperature. Addition of silicon as the second metal dopant helped increase the thermal stability of the resulting titania nanofibers.

## 5. ACKNOWLEDGEMENT

The authors wish to acknowledge partial supports received from the Graduate School, Chulalongkorn University and the National Research Council of Thailand (contract grant number: 03009582-0002).



สถาบันวิทยบริการ  
จุฬาลงกรณ์มหาวิทยาลัย

**REFERENCES**

- [1] D. Li and Y. Xia, Fabrication of titania nanofibers by electrospinning, *Nano Letters* 3 (2003) 555-560.
- [2] P. Viswanathamurthi, N. Bhattarai, C.K. Kim, H.Y. Kim, D.R. Lee, Ruthenium-doped TiO<sub>2</sub> fibers by electrospinning, *Inorganic Chemistry Communications* 7 (2004) 679-682.
- [3] C.H. Kwon, H. Shin, J.H. Kim, W.S. Choi, K.H. Yoon, Degradation of methylene blue via photocatalysis of titanium dioxide, *Materials Chemistry and Physics* 86 (2004) 78-82.
- [4] S.J. Kim, S.D. Park, Y.H. Jeong, S. Park, Homogeneous precipitation of TiO<sub>2</sub> ultrafine powders from aqueous TiOCl<sub>2</sub> solution, *Journal of the American Ceramic Society* 82 (1999) 927-932.
- [5] Z. Ding, X.J. Hu, G.Q. Lu, P.L. Yue, P.F. Greenfield, Novel silica gel-supported TiO<sub>2</sub> photocatalyst synthesized by CVD method, *Langmuir* 16 (2000) 6216-6222.
- [6] J. Yang, S. Mei, J.M.F. Ferreira, Hydrothermal synthesis of nanosized titania powders: influence of tetraalkyl ammonium hydroxides on particle characteristics, *Journal of the American Ceramic Society* 84 (2001) 1696-1702.
- [7] S. Iwamoto, W. Tanakulrungsank, M. Inoue, K. Kagawa, P. Praserttham, Synthesis of large-surface area silica-modified titania ultrafine particles by the glycothermal method, *Journal of Materials Science Letters* 19 (2000) 1439-1443.
- [8] K.Y. Jung, S.B. Park, Enhanced photoactivity of silica-embedded titania particles prepared by sol-gel process for the decomposition of trichloroethylene, *Applied Catalysis. B: Environmental* 25 (2000) 249-256.
- [9] C. Mit-uppatham, M. Nithitanakul, P. Supaphol, Ultrafine electrospun polyamide-6 fibers: effect of solution condition on morphology and average fiber diameter, *Macromolecular Chemistry and Physics* 205 (2004) 2327-2338.
- [10] K.Y. Jung, S.B. Park, Anatase-phase titania: preparation by embedding silica and photocatalytic activity for the decomposition of trichloroethylene, *Journal of Photochemistry and Photobiology. A: Chemistry* 127 (1999) 117-122.
- [11] J.E. Lee, S.M. Oh, D.W. Park, Synthesis of nano-sized Al-doped TiO<sub>2</sub> powders using thermal plasma, *Thin Solid Films* 457 (2004) 230-234.

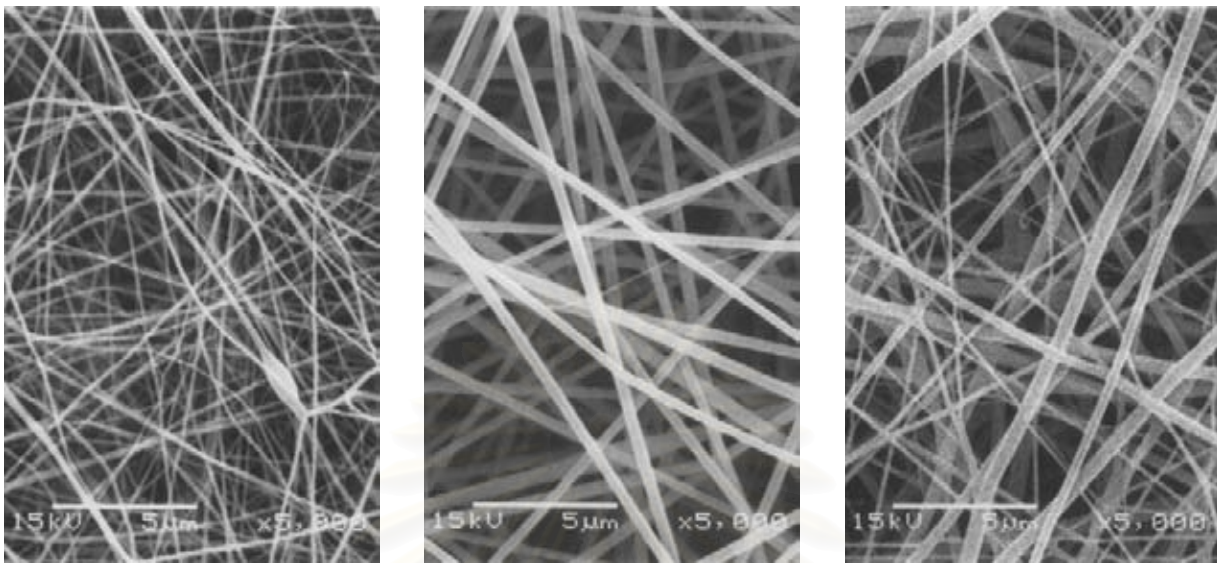
- [12] M. Hirano, K. Ota, Direct formation and photocatalytic performance of anatase (TiO<sub>2</sub>)/silica (SiO<sub>2</sub>) composite nanoparticles, *Journal of the American Ceramic Society* 87 (2004) 1567-1570.
- [13] R.N. Viswanath, S. Ramasamy, Study of TiO<sub>2</sub> nanocrystallites in TiO<sub>2</sub>-SiO<sub>2</sub> composites, *Colloids and Surfaces. A: Physicochemical and Engineering Aspects* 133 (1998) 49-56.



สถาบันวิทยบริการ  
จุฬาลงกรณ์มหาวิทยาลัย

**CAPTION OF FIGURES**

- Figure 1 SEM images of pre-calcined as-spun fibers from spinning solutions containing (a) 7, (b) 9, or (c) 13 wt.% PVP solution. The applied electrostatic field strength was 9 kV/7 cm.
- Figure 2 SEM images of pre-calcined as-spun fibers from spinning solution containing 13 wt.% PVP solution under various applied electrostatic field strengths: (a) 9 kV/7 cm, (b) 15 kV/7 cm, and (c) 22.5 kV/7 cm.
- Figure 3 Diameters of pre-calcined as-spun fibers as a function of (a) PVP concentration and (b) applied electrostatic potential (across a fixed collection distance of 7 cm).
- Figure 4 SEM images of (a) pre-calcined as-spun fibers and titania fibers after calcination at various temperatures: (b) 500, (c) 600, and (d) 800°C. The PVP concentration of the spinning solution was 13 wt.% and the applied electrostatic field strength was 9 kV/7 cm.
- Figure 5 Diameters of as-calcined titania fibers as a function of calcination temperature.
- Figure 6 FTIR spectrum of (a) pre-calcined as-spun fibers and (b) titania fibers calcined at 500°C and (c) titania fibers doped with 2 wt.% TEOS and calcined at 500°C. The PVP concentration of the spinning solution was 13 wt.% and the applied electrostatic field strength was 9 kV/7 cm.
- Figure 7 SEM images of (a) undoped titania fibers and titania fibers doped with TEOS in various amounts: (b) 1 and (c) 2 wt.% after being calcined at 600°C. The PVP concentration of the spinning solution was 13 wt.% and the applied electrostatic field strength was 9 kV/7 cm.
- Figure 8 XRD pattern of undoped titania fibers calcined at various temperatures: (a) 500, (b) 600, and (c) 800°C. The PVP concentration of the spinning solution was 13 wt.% and the applied electrostatic field strength was 9 kV/7 cm.
- Figure 9 XRD patterns of titania fibers doped with 2 wt.% TEOS and calcined at various temperatures: (a) 500, (b) 600, (c) 800°C. The PVP concentration of the spinning solution was 13 wt.% and the applied electrostatic field strength was 9 kV/7 cm.



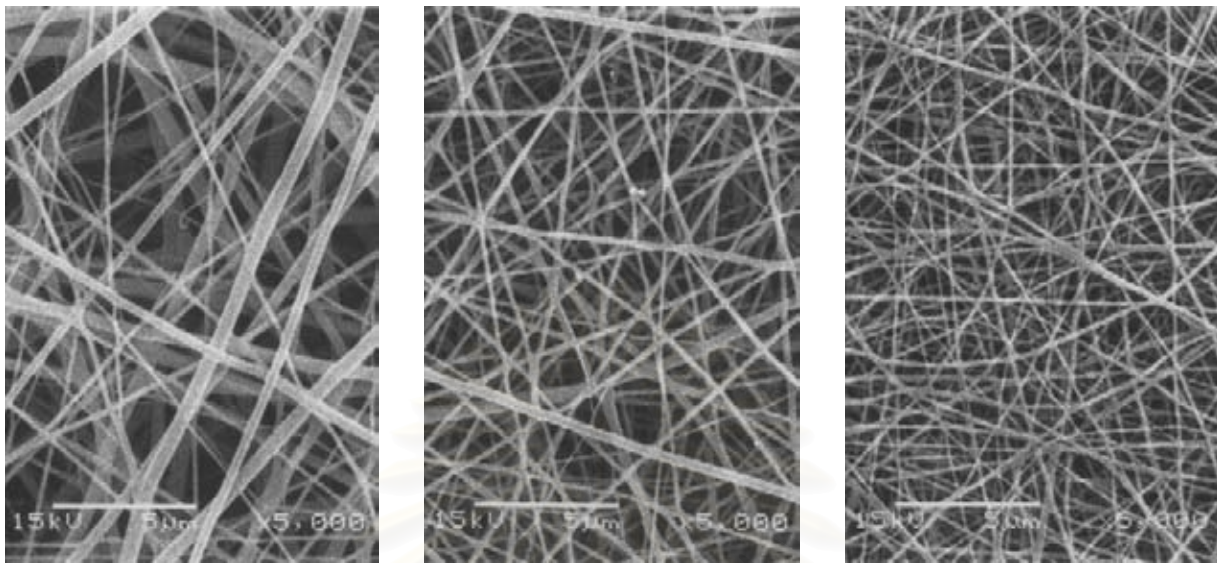
(a)

(b)

(c)

Figure 1

สถาบันวิทยบริการ  
จุฬาลงกรณ์มหาวิทยาลัย



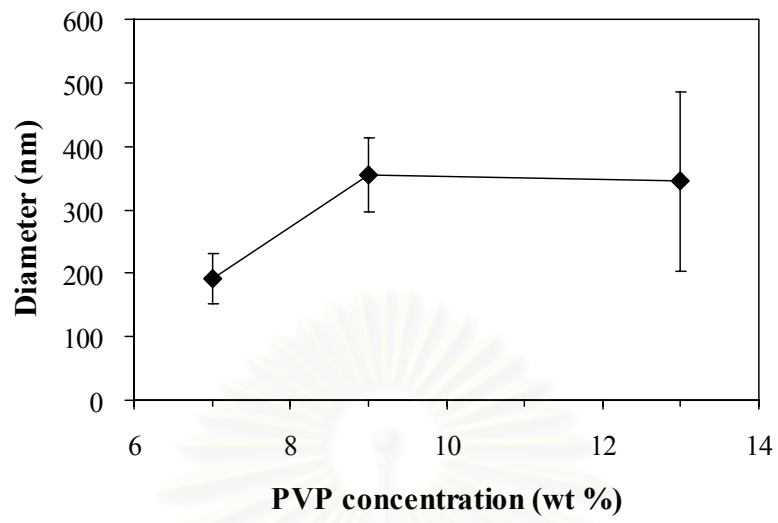
(a)

(b)

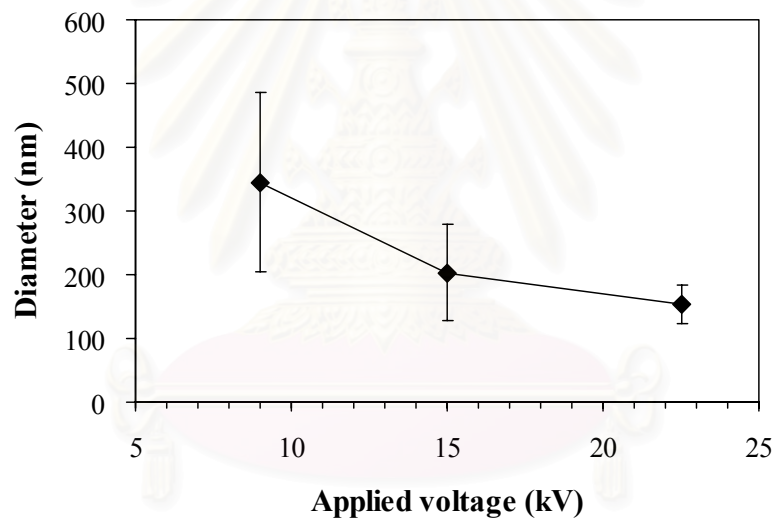
(c)

Figure 2

สถาบันวิทยบริการ  
จุฬาลงกรณ์มหาวิทยาลัย

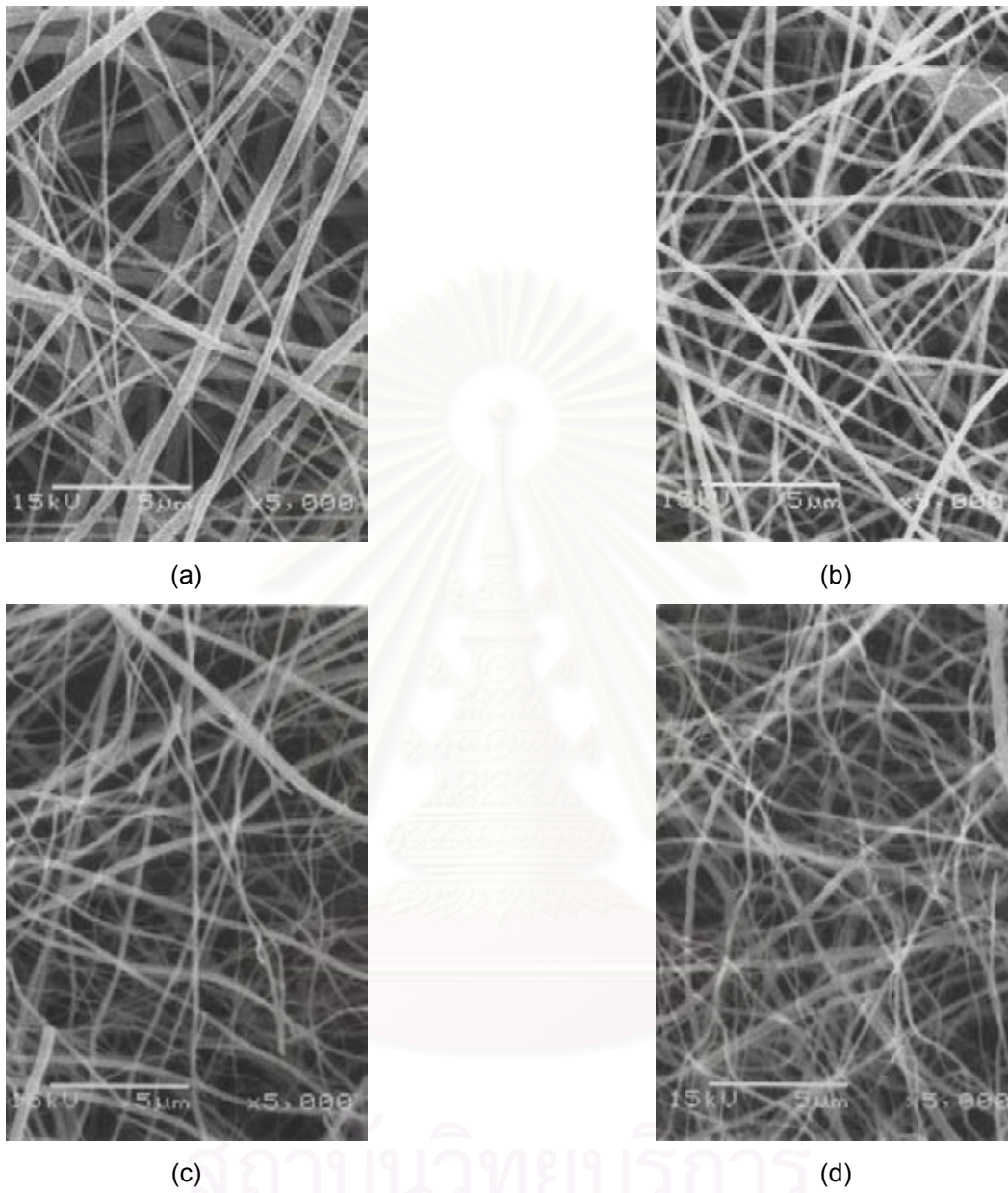


(a)



(b)

Figure 3  
สถาบันวิทยบริการ  
จุฬาลงกรณ์มหาวิทยาลัย



สถาบันวิทยบริการ  
จุฬาลงกรณ์มหาวิทยาลัย  
Figure 4

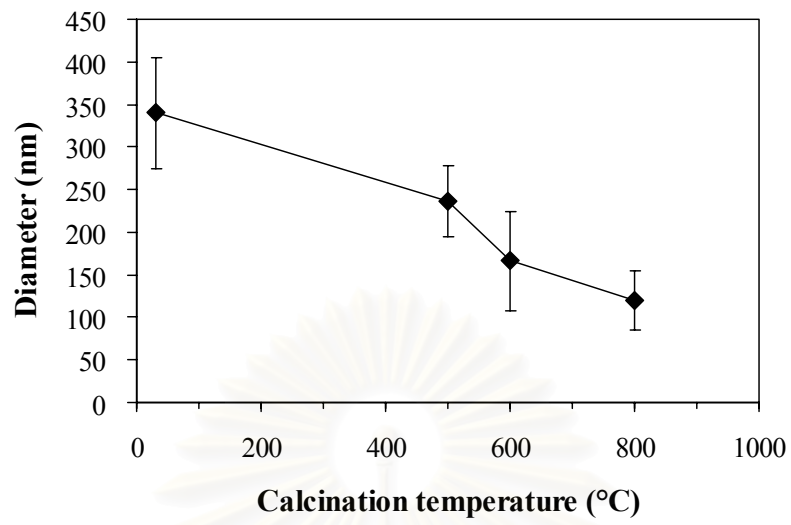


Figure 5

สถาบันวิทยบริการ  
จุฬาลงกรณ์มหาวิทยาลัย

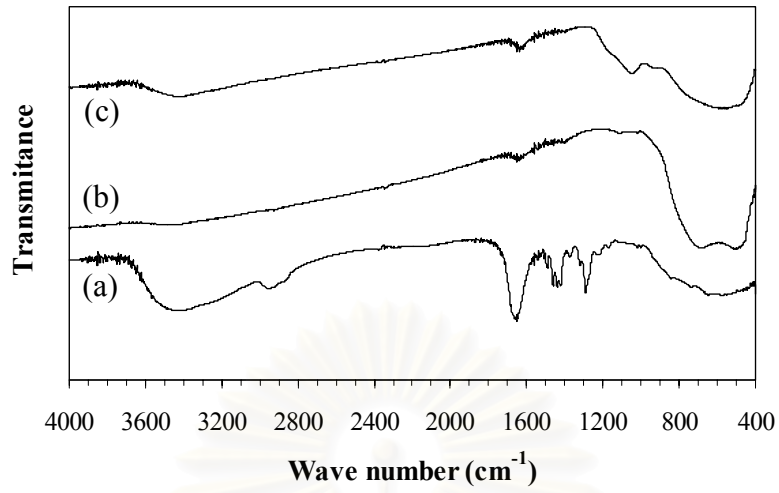
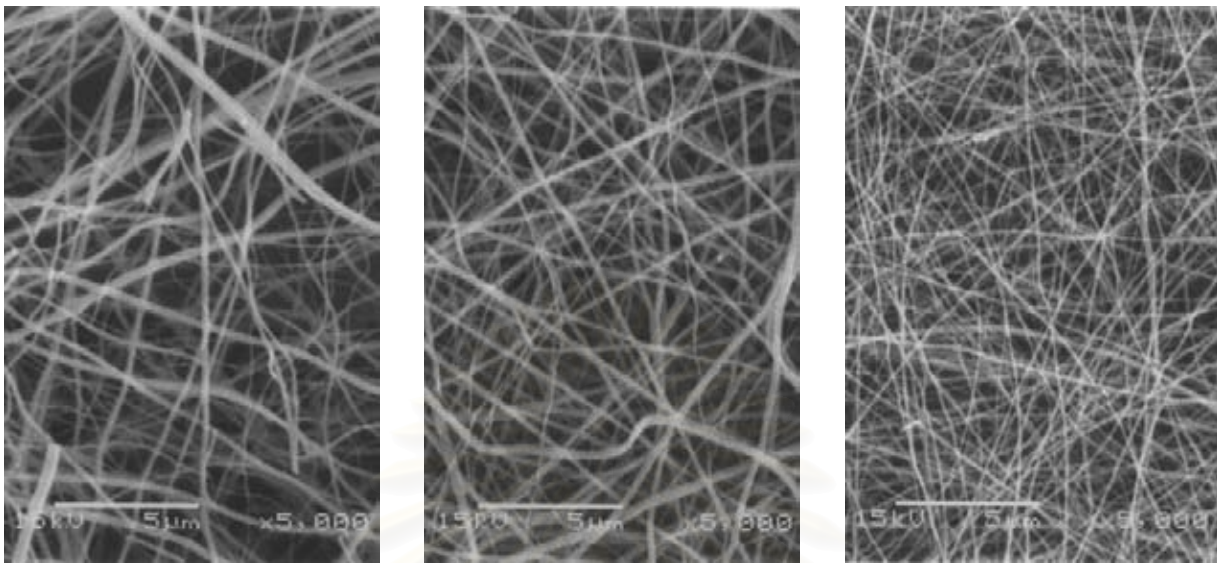


Figure 6

สถาบันวิทยบริการ  
จุฬาลงกรณ์มหาวิทยาลัย



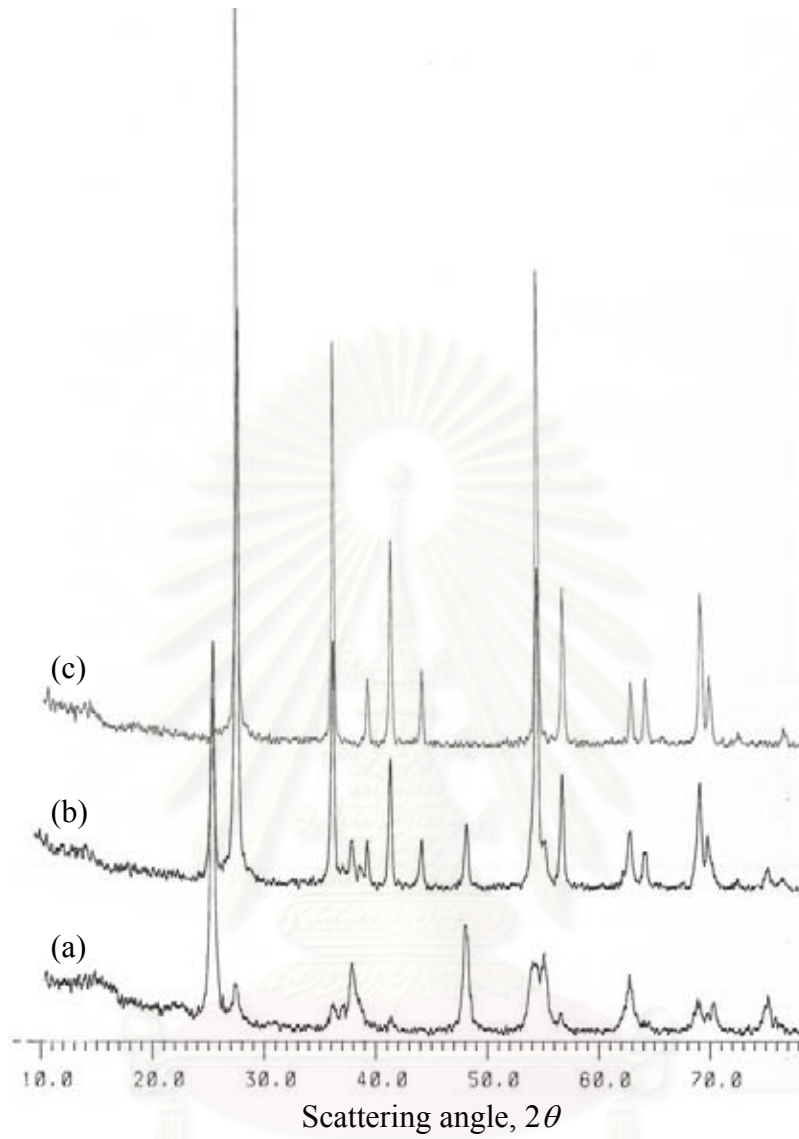
(a)

(b)

(c)

Figure 7

สถาบันวิทยบริการ  
จุฬาลงกรณ์มหาวิทยาลัย



สถาบันวิทยบริการ  
จุฬาลงกรณ์มหาวิทยาลัย  
Figure 8

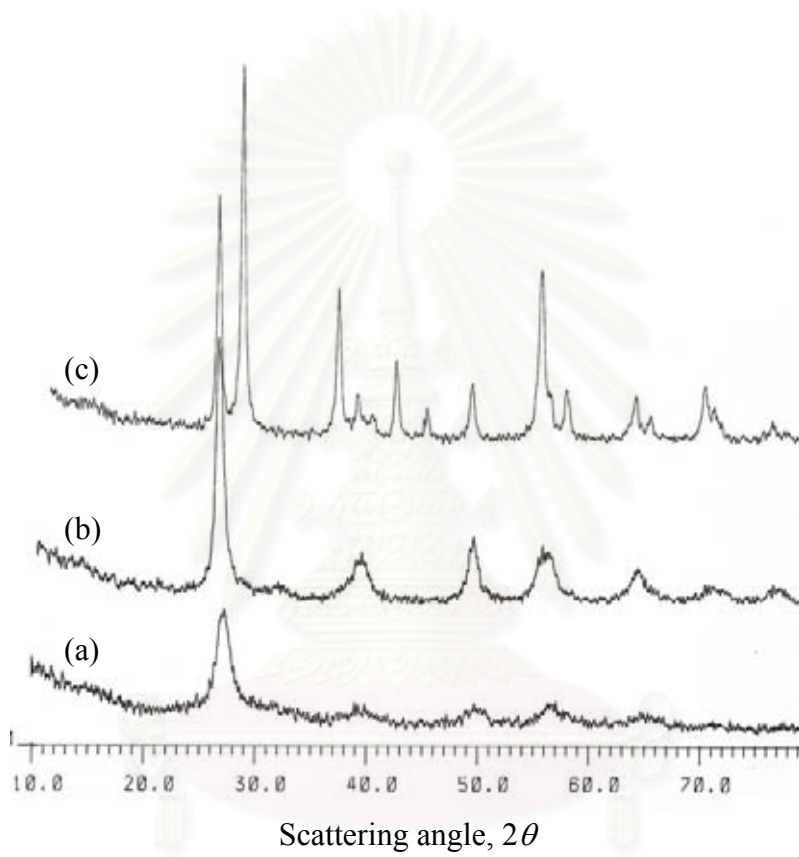


Figure 9

สถาบันวิทยบริการ  
จุฬาลงกรณ์มหาวิทยาลัย

## VITA

Mr. Jeerapong Watthanaarun was born on March 9, 1980 in Bangkok, Thailand. He received the Bachelor Degree of Chemical Engineering from Faculty of Engineering, Kasetsart University in 2002. He continued his Master's study at Chulalongkorn University in June, 2003.



สถาบันวิทยบริการ  
จุฬาลงกรณ์มหาวิทยาลัย